DETECTION OF BROKEN ROTOR BARS IN INDUCTION
MOTORS USING STATOR CURRENT MEASUREMENTS

by

MARK STEVEN WELSH

Courses 6 and 13A   May 1988

DETECTION OF BROKEN ROTOR BARS IN INDUCTION MOTORS
USING STATOR CURRENT MEASUREMENTS

by

MARK STEVEN WELSH

B.S.E.E., University of Missouri-Columbia, 1982

SUBMITTED IN PARTIAL FULFILLMENT OF THE
REQUIREMENTS FOR THE DEGREES OF
NAVAL ENGINEER
and
MASTER OF SCIENCE
in
ELECTRICAL ENGINEERING AND COMPUTER SCIENCE
at the
MASSACHUSETTS INSTITUTE OF TECHNOLOGY
May, 1988

DETECTION OF BROKEN ROTOR BARS IN INDUCTION MOTORS
USING STATOR CURRENT MEASUREMENTS

by

MARK STEVEN WELSH

ABSTRACT

Broken rotor bars are a common cause of induction motor failures. In the past, the detection of broken rotor bars has primarily been limited to non-operating, and typically, disassembled machines. The ability to detect broken rotor bars while the machine is operating at normal speed and load is desirable. In support of the ongoing development of a failure analysis system for electrical machines, this thesis evaluates the method of using stator currents and voltages to detect the presence of broken rotor bars in squirrel-cage induction motors. The hypothesis of this method is that, given a sinusoidally applied voltage, the presence of certain harmonics in the stator currents could be used to detect the presence of broken rotor bars.

To support the evaluation, a system of first-order differential equations describing the electrical performance of a three-phase, squirrel-cage induction motor was developed using stator phase currents and rotor loop currents as state variables. A FORTRAN simulation program was developed to solve the system of equations for a motor with or without a broken rotor bar. Using an "off-the-shelf" 3-HP motor, numerical and physical experiments were conducted to test the failure detection hypothesis. Although the results of the numerical experiments indicated that the hypothesis was plausible, the experimental results showed that distinguishing between a manufacturing asymmetry and a broken rotor bar was impossible due to the existence of inter-bar currents.

The existence of inter-bar currents in a squirrel-cage induction motor of the type tested in this thesis effectively "masks" the effects of a broken rotor bar. Thus, detection of broken rotor bars based upon a technique using only stator current measurements appears highly improbable.

Thesis Supervisor: Jeffrey H. Lang
Title: Associate Professor of Electrical Engineering

Thesis Supervisor: Stephen D. Umans
Title: Principal Research Engineer

ACKNOWLEDGMENTS

I am grateful to my thesis advisors, Professor Jeffrey Lang and Dr. Stephen Umans, for their patience, encouragement, and timely guidance.

I express my thanks to Fred Barber and Glenn Hottel for their time and effort to produce the drawings included in Chapter 2. I also thank Ricky Powell for his time-saving advice on numerical methods.

For their support, love, and understanding during the past three years, I am deeply indebted to my wife Katherine and our two daughters, Heather and Holly.

TABLE OF CONTENTS

LIST OF FIGURES

LIST OF TABLES

CHAPTER 1

INTRODUCTION

1.1 **Thesis** **Objectives**

In recent surveys [1,2,3] on the reliability of electric motors, three kinds of faults have been identified as constituting the majority of failures in induction motors. These are bearing-related (41%), stator-related (37%), and rotor-related (10%). Table 1-1 shows a summary of failures for these areas by components. The remaining failures (12%) are scattered among a variety of effects. As shown in Table 1-1, of the rotor-related failures, cage faults in the form of broken rotor bars or end rings are the cause of half of the machine failures. Cage faults occur due to design and manufacturing defects, misoperation and misapplication of the machine, lack of preventive maintenance, and aging/fatigue failure. Rotor cage defects result in machine failure due to increased frame vibrations, localized temperature increases on the rotor, and the "domino" effect in which one broken bar leads to another broken bar and so on.

The purpose of this thesis is to present the results of research investigating the detection of broken rotor bars using stator current and voltage measurements. This research effort supports the ongoing development of a

failure analysis system for electric machines by the M.I.T. Laboratory for Electromagnetic and Electronic Systems [4,5].

Bearing-Related (41%)		Stator-Related (37%)		Rotor-Related (10%)	
Sleeve Bearings	16%	Ground Insulation	23%	Cage	5%
Anti-friction Bearings	8%	Turn Insulation	4%	Shaft	2%
Seals	6%	Bracing	3%	Core	1%
Thrust Bearing	5%	Wedges	1%	Other	2%
Oil Leakage	3%	Frame	1%		
Other	3%	Core	1%		
		Other	4%		

Table 1-1. Motor Failures by Components [1].

1.2 Condition Monitoring of Electric Machines

The unexpected and sometimes catastrophic failure of electric machines can result in the reduction or total loss of production and operational safety, expensive repairs and extended downtime, and in most cases, large capital losses. In the case of military applications, these failures can result in the degradation of mission effectiveness and perhaps even the inability to perform a primary mission.

11

For many years, private industry and the military have used planned maintenance strategies to minimize electric machine failures. One major drawback of this strategy is that the need for corrective maintenance cannot be determined without removing the machine from service, disassembling it, and inspecting it. Without a method to externally determine the condition of an operating machine, a machine in perfect condition may be removed from service while a machine on the verge of failure maybe ignored. Obviously, a more efficient and cost-effective maintenance strategy would be to schedule maintenance and repairs based on a continuous assessment of the machine's condition while it is operating at normal speed and load.

There are currently two methods being used and/or developed to assess the condition of an operating electric machine [6]. The first method involves the analysis of vibration data and historical performance records. This method is commonly referred to as signature trend analysis. In signature trend analysis, sensor measurements (typically accelerations) are collected and processed through Fourier Transform at regular intervals. Each data collection is compared to previous data and known "good" baseline data in order to expose signature trends. Based on experience, these signature trends can be related to specific defects and failures. Thus, signature trend analysis is essentially a heuristic method used to assess the condition of a

machine. Although signature trend analysis is a viable and widely used monitoring system, the requirement for a database of historical performance and the experience required to relate a signature trend to a specific defect or failure are major disadvantages. The second method is more theoretical by nature and seeks to identify the fundamental causes of failures and predict their effects. In this method, a detailed understanding of the machine response for various operating scenarios including normal operation as well as for various fault conditions is required. Thus, for any given operating condition, the theoretical response of the machine is calculated and compared to the actual response of the machine. By comparing these responses an estimate or prediction of the machine's condition can be made. Although both of these methods typically require the use of a processor such as a microcomputer for continuous monitoring, each can be used both to prevent catastrophic failures by early detection and to aid in the preparation of routine maintenance schedules.

A failure analysis system for electrical machines is currently being developed by the Laboratory of Electromagnetic and Electronic Systems (LEES) at the Massachusetts Institute of Technology. The development of this system is a major task of the Ship Service Power System Development research sponsored by the Department of the Navy's Naval

Sea Systems Command [5]. The ultimate goal of the proposed failure analysis system is to provide a tool which can be used onboard naval ships to prevent, predict, and detect electric machine failures, and to suggest the corresponding maintenance. The system is intended for retrofit onto existing electrical machines or incorporation into future electrical machines and for implementation with inexpensive sensors and processors [4]. The following paragraphs, extracted from the research proposal [5], briefly describe the proposed failure analysis system. The system will use a combination of both methods described above to assess the condition of a machine.

The underlying principle of the system is that failure prevention, prediction, and detection should be based on the estimation of states and parameters in relevant physical models of electrical machines. These models should include failure modes, mechanisms, or symptoms that are expressed in terms of the electrical machine states and parameters. The models, coupled with state and parameter estimation, then provide a means of directly and justifiably connecting measured data to impending or existing failures. Thus, the reliability of the failure analysis is enhanced. The models also provide a means by which measured data from a variety of sensors can be processed

together in a consistent manner.

A (one-line) diagram of the proposed failure analysis system is shown in Figure 1-1. Measurements from sensors on the electrical machine are processed by a model reference state and parameter estimator. State and parameter estimates are then passed to a rule based evaluator which suggest the corresponding maintenance. Initially, the system will be developed using information readily available from terminal voltage and current sensors. The system can be expanded later to include information from other sensors such as thermocouples, accelerometers, acoustic sensors, and gas analyzers.

The development of the failure analysis system is broken down into four subtasks. These are:

    1. Develop physical models which include failure modes, mechanisms, and symptoms expressed in terms of the model states and parameters.

    2. Develop estimators for the model states and parameters.

    3. Develop state and parameter evaluators that act on the estimated quantities so as to prevent, predict, or detect electrical machine failures and suggest corresponding

maintenance.

4. Demonstrate and evaluate the results of theoretical work through numerical and physical experimentation.

The results presented in this thesis directly support the physical model development of subtask (1) above. In particular, this thesis is concerned with the development and demonstration of models which include rotor bar failures in induction motors.
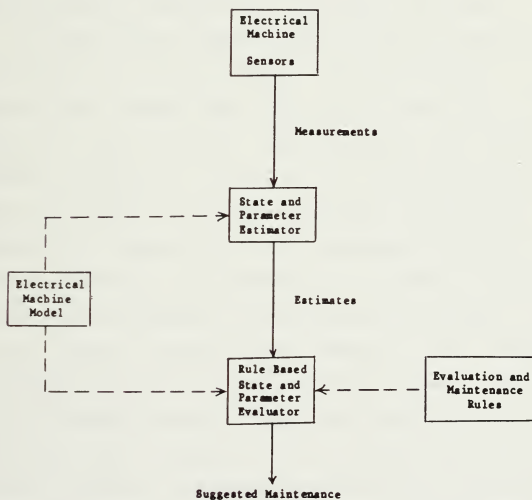
Figure 1-1. Proposed failure analysis system [5].

1.3 Detection of Rotor Bar Defects

In order to detect broken rotor bars, several methods have been employed. Visual inspection and bench test methods such as the "growler" and related probe techniques applied to disassembled motors have been used for many years [7]. The "single phase" test has also been used as a standard test for assembled but non-operating motors [7]. Recently, there have been a number of studies [7,8,9,10,11] to develop theories of the response of induction motors in the presence of broken rotor bars and/or end rings.

A common result found in each of these studies is the existence of a lower sideband frequency component in the stator phase current when the motor is driven by a single harmonic stator voltage. This component of the stator current, which is at a frequency of $(1-2s)f$, where s is the rotor slip and f is the line frequency, is a result of the fundamental component of the backwards-rotating airgap field produced by the induced rotor currents. This field, which rotates backwards at slip speed with respect to the rotor, rotates forward with respect to the stator at $(1-2s)N_s$, where N_s is the synchronous speed. Thus, this field induces currents of frequency $(1-2s)f$ in the stator windings. This component of the stator current causes torque pulsations and speed oscillations at twice the slip frequency. In addition to these effects, it has been shown

17

by Kliman et al. [7] and Penman et al. [11] that axially directed fluxes arise due to the asymmetry of the rotor magnetic circuit with a broken rotor bar.

Based on these results, there have been a number of instruments developed to give an indication of a broken rotor bar while the motor is running at normal speed and load. These instruments detect broken rotor bars using measurements of one or more of the following parameters:

- stator current
- mechanical speed
- frame vibration (i.e., acceleration)
- air gap flux
- axial leakage flux

The most successful of these instruments has been an instrument based on detecting the twice slip frequency speed oscillations via a shaft position measurement [8]. However the sensitivity of the speed variation method is highly dependent on knowledge of the load inertia and torque, and results may be confused by other asymmetries.

Recently, two new instruments have been used to successfully detect broken rotor bars in operating induction machines. Although both instruments are still in the "field test" stage of development, they appear quite promising. The first instrument, developed by Kliman et al. [7], uses stator current measurements to detect broken rotor bars. The second instrument, developed by Penman et

al. [11], uses axial flux measurements to detect broken rotor bars as well as several other fault conditions such as phase imbalances and short-circuited turns on a stator winding. The following paragraphs summarize the operating theory and experimental results for these new instruments.

1.3.1 Broken Bar Detector (BBD)

The BBD being developed by Kliman et al. is based on existing theories for the performance of induction motors with broken bars. A broken rotor bar is modeled by superimposing a fault current, a current equal and opposite to the normal current, on the rotor bar. The magnetic field in the airgap caused by the fault current is always two-pole and rich in harmonics. This field anomaly rotates at the mechanical frequency of the rotor since it is attached to the broken bar. The field can be resolved, using Fourier analysis, into an infinite series of counter-rotating, slip-frequency waves of smaller and smaller wavelength on the rotor. In addition to broken rotor bars, other fault conditions such as cage misalignment (rotor out of round), bearing misalignment (rotating eccentricity), and non-uniform magnetic orientation of the rotor laminations create airgap field anomalies with a fundamental component on the same order as that of a broken bar. However, the higher-order harmonic components of the airgap field due to these other fault conditions are predicted to be much smaller than

19

those due to a broken bar. Figure 1-2 (from [7]) shows a comparison of the airgap flux spectra predicted for these various asymmetries and a broken rotor bar.
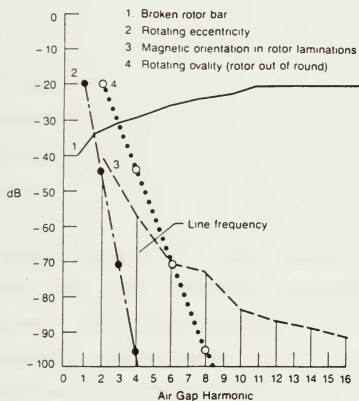
Figure 1-2. Airgap flux spectra for asymmetries [7].

Based on this spectra, two conclusions can be drawn. First, with sensitivity sufficient to detect a broken bar, these other asymmetries may give rise to a false broken bar indication. Second, by examination of the higher order harmonic amplitudes, broken bars can be distinguished from asymmetries. The analytical expression for the frequencies present in the airgap flux is [7]

$$f_k = f_o \left[\left(\frac{k}{p} \right) (1-s) \pm s \right] \qquad (1-1)$$

where

f_o = line frequency
k = harmonic index (1,2,3...)
p = number of pole-pairs
s = rotor slip

For a typical motor, due to the design of the stator windings, only the odd, non-triplet harmonics of airgap flux couple with the stator windings. Thus, only those harmonic frequencies where k/p is 1,5,7,11,13, etc. appear in the stator currents. Table 1-2 (from [7]) shows these predictable stator current harmonics and relative amplitudes (as a percentage of the input current amplitude) due to an open rotor bar.

21

HARMONIC	FREQUENCY (Hz)	AMPLITUDE ($\%I_{in}$)
FUNDAMENTAL	60	4
LSB 1	60(1-2s)	4
USB 5	60(5-4s)	0.5
LSB 5	60(5-6s)	0.5
USB 7	60(7-6s)	0.05
LSB 7	60(7-8s)	0.05
LSB = LOWER SIDEBAND USB = UPPER SIDEBAND		

Table 1-2. Current harmonics due to broken rotor bars [7].

Based on the above theory, Kliman et al. developed the computer-based instrument in Figure 1-3. The instrument performs two basic functions: signal processing and the implementation of a decision algorithm. The signal processing involves sampling the external leakage flux and current signals and transforming these time functions via the fast Fourier transform into frequency spectra. Since the harmonic frequencies of interest shown in Table 1-2 are slip dependent, a precise measurement of the rotor speed is necessary. This is accomplished using an externally mounted coil which picks up a strong axial leakage flux from the rotor end ring at the slip frequency

(sf). Combining this with a measurement of the line frequency from the current signal, rotor speed is determined to within 0.2 rpm. The spectral windows of interest are computed and a narrow search around the predicted frequencies is performed. The amplitudes and frequencies of the broken bar signals are stored in computer memory, and if desired, can be printed out in a tabular form. The spectral windows can also be viewed on the computer screen. Figure 1-4 shows the experimental results (line current spectra in the vicinity of 60 Hz) presented in [7] for a test motor with varying degrees of fault. The increase in the amplitude of the lower sideband signal with increasing fault is quite evident.
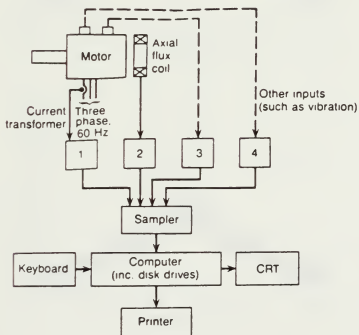
Figure 1-3. BBD one-line diagram [7].
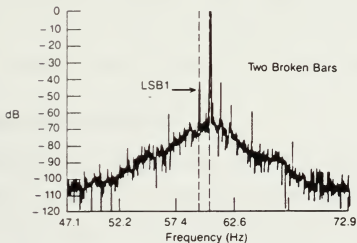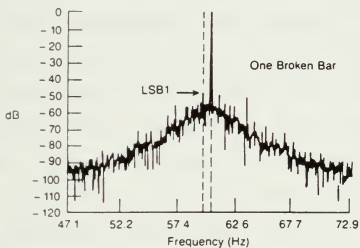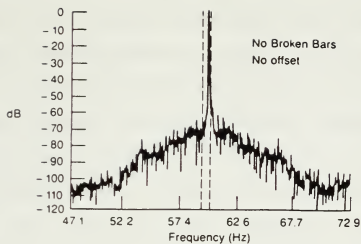
Figure 1-4. BBD experimental results for s=0.01 [7].

Two decision algorithms may be implemented in the BBD. The first is a "trend" algorithm that recognizes the change from a healthy motor to a motor with a cage defect. Two sets of line-current frequency spectra are compared to detect any changes in the harmonic sidebands. If a significant change (>20dB) occurs in the first harmonic lower sideband, the higher-harmonic sidebands are examined. If any of these harmonics have changed significantly, a broken bar is declared. Otherwise it is concluded than an asymmetry other than a broken bar is present. The second algorithm is a single-test diagnostic. Based on experimental data gathered from 23 power plant motors, "good" motors exhibit a first harmonic lower sideband of -60dB or less relative to the line frequency component. Thus if the first harmonic lower sideband is less than -60dB there is probably no fault. If the first harmonic sideband is greater than -50dB there is probably a broken rotor bar. These thresholds will be updated, if necessary, based on the results of further field tests.

1.3.2 Leakage Flux Detector

The leakage flux monitoring system developed by Penman et al. [11] is based on theories describing the harmonic content of the axial flux produced by an electric machine for various fault conditions. Ideally, with no faults, an electric machine will not produce a net axial flux. However, due to small asymmetries in both the material and

geometry of a machine, a small, axial leakage field is produced and can be detected by an externally mounted coil. Under the assumption that fault conditions represent a gross change in the electric and/or magnetic circuit behavior of a machine, the faults can be identified by the effect these changes produce in the axial leakage field. In order to use this technique, a master table of all possible axial flux harmonic components for a given machine type must be generated. Once this is done, certain groups of these harmonics can be identified with various fault conditions.

For an induction motor, the harmonic components of the airgap flux produced by a balanced 3-phase stator winding is given by

$$B = B_1 \cos(\omega t - p\theta) + B_5 \cos(\omega t + 5p\theta)$$
$$+ B_7 \cos(\omega t - 7p\theta) + B_{11} \cos(\omega t + 11p\theta)... \qquad (1-2)$$

where

p = number of pole pairs

θ = angle from a reference point on the stator

To determine the harmonic components of the induced rotor currents, a transformation to the rotor reference frame is necessary. The transformation is made using the relation

$$\theta = \frac{\omega(1-s)}{p} t + \phi \qquad (1-3)$$

where

$\dfrac{\omega(1-s)}{p} =$ rotor angular velocity

$\phi =$ angle between the stator and rotor at t=0

Thus, in the rotor frame of reference, the airgap flux density is given by

$$B = B_1 \cos(s\omega t - p\phi) + B_5 \cos((6-5s)\omega t + 5p\phi)$$
$$+ B_7 \cos((7s-6)\omega t - 7p\phi) + B_{11} \cos((12-11s)\omega t + 11p\phi)\ldots \quad (1-4)$$

The harmonic frequencies of the currents induced in the rotor bars by this field are slip dependent. The small axial leakage flux, which is produced by the rotor currents and minor asymmetries in the machine, will contain these same frequency components. If a fault condition exists, the expressions for the airgap flux

density given above are no longer valid. For example, a phase asymmetry on the stator winding will result in the airgap flux density

$$B = \frac{1}{2} \sum_{n \, odd} B_n [\cos(\omega t - np\theta) + \cos(\omega t + np\theta)] \qquad (1-5)$$

which, in the rotor frame of reference, becomes

$$B = \frac{1}{2} \sum_{n \, odd} B_n \cos[(1 \pm n(1-s))\omega t \pm np\phi] \qquad (1-6)$$

Thus, additional frequency components are present in the induced rotor currents and axial leakage flux.

Using the same methodology, a table of axial flux frequencies (or harmonics) can be developed for various fault conditions. Table 1-3 (from [11]) shows the predicted axial flux harmonics for a 4-pole induction motor at a slip of 0.02. In the table, stator and rotor faults are grouped as either symmetrical (related to a phase) or unsymmetrical (related to a pole). The table includes effects due to the fundamental (f_1) and third harmonic (f_3) components of the supply current. The numbers in each column represent the component of the airgap flux wave that produces the associated axial flux

harmonic (i.e., 1 is the forward traveling first harmonic and -3 is the backward traveling third harmonic component).

By monitoring the spectral components of the axial leakage flux, a fault group can be identified by comparing the spectra to the master table. This is the philosophy incorporated into the leakage flux monitoring system. A one-line diagram of this system is shown in Figure 1-5. The transducer (a printed-circuit split coil) is externally mounted on a machine. The transducer signal (induced voltage by the leakage flux) is processed and transferred to the diagnostic unit. The diagnostic unit analyzes the spectra and identifies any fault conditions present using the master spectrum table. As stated previously, this system has successfully detected various faults imposed on a 4KW squirrel-cage induction motor. Figures 1-6, 1-7, 1-8 are samples of the experimental results presented in [11] for various fault conditions. Figure 1-6 is the axial flux spectra for a healthy motor. Figure 1-7 shows the large amplitude increase in the fundamental (50 Hz) component for a short-circuited stator winding. For a broken rotor bar, increased amplitudes in the fundamental as well as third (150 Hz) and fifth (250 Hz) components are evident in Figure 1-8.

Number	Frequency factor	Frequency at s = 0.02 Hz	Stator harmonics				Rotor harmonics			
			Phase		Pole		Phase		Pole	
			f_1	f_3	f_1	f_3	f_1	f_3	f_1	f_3
1	s	1.0	1		2					
2	$3s$	3.0		3		6				
3	$(7s-1)/2$	21.5				7				-1
4	$(3s-1)/2$	23.5			3				-1	
5	$(1+s)/2$	25.5			1				1	
6	$(1+5s)/2$	27.5				5				1
7	$4s-1$	46.0						-1		-2
8	$2s-1$	48.0					-1		-2	
9	1	50.0					1		2	
10	$2s-1$	52.0						1		2
11	$(9s-3)/2$	70.5				9				-3
12	$(5s-3)/2$	72.5			5				-3	
13	$(3-s)/2$	74.5			-1				3	
14	$(3-3s)/2$	76.5				3				3
15	$5s-2$	95.0		5		10				
16	$3s-2$	97.0	3		6					
17	$2-s$	99.0	-1		-2					
18	$2-s$	101.0		1		2				
19	$(11s-5)/2$	119.5				11				-5
20	$(7s-5)/2$	121.5			7				-5	
21	$(5-3s)/2$	123.5			-3				5	
22	$(5+s)/2$	125.5				1				5
23	$6s-3$	144.0						-3		-6
24	$4s-3$	146.0					-3		-6	
25	$3-2s$	148.0					3		6	
26	3	150.0						3		6
27	$(13s-7)/2$	168.5				13				-7
28	$(9s-7)/2$	170.5			9				-7	
29	$(7-5s)/2$	172.5			-5				7	
30	$(7-s)/2$	174.5				-1				7
31	$7s-4$	193.0		7		14				
32	$5s-4$	195.0	5		10					
33	$4-3s$	197.0	-3		-6					
34	$4-s$	199.0		-1		-2				
35	$(15s-9)/2$	217.5				15				-9
36	$(11s-9)/2$	219.5			11				-9	
37	$(9-7s)/2$	221.5			-7				9	
38	$(9-3s)/2$	223.5				-3				9
39	$8s-5$	242.0						-5		-10
40	$6s-5$	244.0					-5		-10	
41	$5-4s$	246.0					5		10	
42	$5-2s$	248.0						5		10
43	$(17s-11)/2$	266.5				17				-11
44	$(13s-11)/2$	268.5			13				-11	
45	$(11-9s)/2$	270.5			-9				11	
46	$(11-5s)/2$	272.5				-5				11
47	$9s-6$	291.0		9		18				
48	$7s-6$	293.0	7		14					
49	$6-5s$	295.0	-5		-10					
50	$6-3s$	297.0		-3		-6				

Table 1-3. Axial flux harmonics [11].
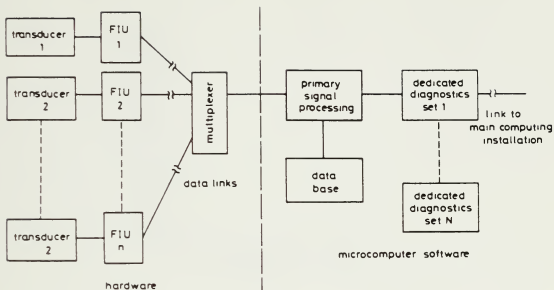
Figure 1-5. Leakage flux monitoring system [11].
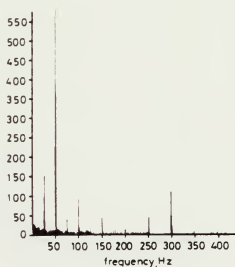
Figure 1-6. Healthy motor [11].
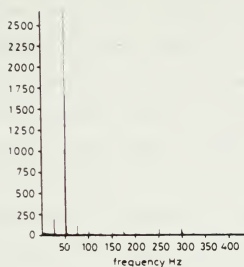
Figure 1-7. Short-circuited stator winding turn [11].
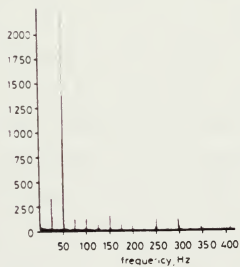
Figure 1-8. Broken rotor bar [11].

1.4 Significance of Thesis

From the discussions presented in the previous sections, one can see that broken rotor bars can be (or have been) detected using stator current measurements. Thus, the results presented in this thesis confirm existing theories and experimental results [7,8,9,10,11]. However, several contributions are made to the field of electrical-machine fault analysis.

First, a more general approach is taken to develop the system of equations describing the electrical performance of an induction motor. If desired, the system of equations and computer simulation can be used to analyze other fault conditions as well as broken rotor bars (subject to the limitations resulting from the assumptions discussed in Chapter 2). Although the system of equations and computer simulation developed consider only fundamental space harmonics, both can be easily modified to include additional space harmonics. In order to analyze other fault conditions and/or include additional space harmonics, the expressions for the appropriate matrix elements must be modified. This flexibility is not possible using the method presented by Williamson and Smith [10], where the equations were derived for a specific fault condition using specific stator current harmonics. In order to analyze other fault conditions or to include additional space harmonics, an entire new set of equations must be developed.

Second, a relationship between the standard single-phase, equivalent-circuit model of an induction motor and the system of equations has been derived. With this relationship, the electrical parameters, for example rotor bar resistance, rotor bar leakage inductance, and stator phase leakage inductance needed to solve the system of equations can be easily calculated from the single-phase circuit model values. Instead of disassembling the machine and measuring these parameters or requesting the design data from the manufacturer, the standard no-load, locked-rotor, and DC tests can be used to determine the required parameters.

Finally, the experimental results provide another "data point" or quantitative comparison between motors with and without broken rotor bars. Combination of this data with the previous data collected and presented by others may aid in determining threshold values for fault analysis system decision algorithms. The experimental results presented show that the existence of inter-bar currents (currents which flow through the rotor iron) in squirrel-cage induction motors mask the existence of a broken rotor bar and thus, severely limit the ability to detect a broken rotor bar using stator current measurements. This finding confirms the analysis of inter-bar currents presented by Kerszenbaum and Landy [9].

1.5 <u>Outline</u> <u>of</u> <u>Thesis</u>

The material presented in the following chapters is organized in the same fashion in which the research was conducted. Chapter 2 starts out with the development of the system of equations describing the electrical performance of an induction motor. The assumptions used to develop the equations are discussed in detail. In addition, the relationship between the single-phase, equivalent-circuit model and the system of equations is presented. The solution to the system of equations is addressed in Chapter 3. The numerical technique and computer simulation program used to solve the equations are described. Simulation results (using the parameters of the experimental test motor) with and without a broken rotor bar are presented. In Chapter 4, the experimental results using an "off-the-shelf" 3-HP motor with and without a broken rotor bar are presented, analyzed, and compared to the simulation results. Finally, Chapter 5 summarizes the results of the research, discusses the limitations of the analysis, and provides some recommendations for follow-on research.

CHAPTER 2

THEORETICAL DEVELOPMENT OF SYSTEM

2.1 Discussion of Approach

In order to meet the primary objective of this research which is to detect broken rotor bars using stator current and voltage measurements, the system of equations describing the electrical performance of an induction motor is developed using stator phase currents and rotor loop currents as state variables. Each stator phase and rotor loop is described in terms of resistances and inductances. The forcing functions for the system are the stator phase voltages. The rotor is described in terms of loops in order to facilitate the determination of stator and rotor coupling.

Using classical field theory and a coupled-circuit viewpoint in which stator phases and rotor loops are regarded as circuit elements whose inductances depend on the angular position of the rotor, flux linkages are expressed in terms of stator phase and rotor loop currents and inductances. The stator phase voltages are related to these flux linkages using Faraday's law. The result is a system of first-order differential equations describing the electrical performance of an induction motor. The form of this system of equations is

$$[v(t)] = \frac{d}{dt}[\lambda(t)] + [R][i(t)] \qquad (2-1)$$

where

$[v(t)]$ = voltage vector

$[\lambda(t)]$ = flux linkage matrix = $[L(\theta(t))][i(t)]$

$[R]$ = resistance matrix

$[i(t)]$ = current vector

$[L(\theta(t))]$ = inductance matrix

$\theta(t)$ = rotor position

This approach is quite general and can be used to describe the electrical performance of any induction motor, healthy or failed. In this analysis, a transformation matrix will not be used to eliminate the rotor-position-dependent elements of the inductance matrix. The use of a transformation matrix requires the transformation of rotor currents as well. Since a broken rotor bar will be simulated by setting the rotor bar current to zero, the use of a transformation matrix is undesirable.

2.1.1 Assumptions

Several assumptions are made in order to reduce the complexity of the analysis. Although each assumption reduces the generality of the analysis, the goal of understanding the effect of a broken rotor bar on stator

currents can still be achieved. It should be noted that each assumption can be relaxed and the system of equations can be developed using the method presented. The following paragraphs summarize the assumptions used and their consequences.

1.) The stator windings are balanced and sinusoidally distributed. Thus, the airgap field produced by stator phase currents consists of a fundamental space component only. In addition, only the fundamental space component of the airgap field produced by rotor currents will couple with the stator windings.

2.) With the exception of a fault, the rotor cage is symmetrical. This dictates that the spacing between adjacent rotor bars, as well as the rotor radius, is constant over the surface of the rotor. In addition, rotor skew is neglected.

3.) The rotor cage end rings are perfectly conducting disks. Thus, no axial flux is produced and the sum of the rotor loop currents is zero. Thus, end effects are neglected.

4.) The rotor bars are insulated from the rotor iron. Current flows only in the rotor bars and thus, inter-bar currents which flow through the rotor iron laminations are neglected.

5.) The airgap dimension is small compared to the mean rotor radius. Thus, the airgap magnetic field is assumed to be only radially directed and to be only a function of azimuthal angle.

6.) Only the fundamental space component of the airgap field produced by rotor currents will be considered. Higher order space harmonics will be neglected since the stator windings couple with the fundamental component only.

7.) The mechanical speed of the rotor is constant. The system of equations describe the electrical performance of the motor and the mechanical dynamics are not included. Rotor speed will be considered an input to the system.

8.) The magnetic backing material on the rotor and stator has infinite permeability. Thus, the magnetic field intensity is confined to the airgap region. In addition, saturation effects are neglected.

2.2 Development of Equations for an N-bar Rotor

Before proceeding with the development of the system of equations some background information is necessary. The following paragraphs describe the nomenclature used, the geometry and coordinate system, and the definition of a rotor loop.

Wherever possible, an attempt has been made to use "standard" symbols for parameters throughout this thesis. The following list of symbols is provided to avoid confusion which may arise due to the numerous variations of "standard" symbols. The appropriate MKS units are included in brackets following the definition of each symbol.

List of Symbols

r, θ, z	=	cylindrical coordinates for stator reference frame
r', θ', z'	=	cylindrical coordinates for rotor reference frame
$\bar{B}$	=	magnetic flux density [Wb/m²]
B_r	=	radial component of flux density [Wb/m²]
d	=	active length of machine [m]
$\bar{E}$	=	electric field intensity [V/m]
g	=	airgap length [m]
$\bar{H}$	=	magnetic field intensity [A/m]
H_r	=	radial component of magnetic field intensity [A/m]
$[i]$	=	electrical current vector [A]
I	=	electrical current [A]
$i_{a,b,c}$	=	current in stator phase a,b, or c [A]
i_{rn}	=	current in rotor loop n [A]
$i_{bar\,n}$	=	current in rotor bar n [A]
J	=	current density [A/m²]
$\bar{K}$	=	surface current density [A/m]
K_z	=	axial component of surface current density [A/m]

$[L]$	=	inductance matrix [H]
L_{Lrbn}	=	leakage inductance of rotor bar n [H]
L_{Ls}	=	leakage inductance of a stator phase winding [H]
$L_{mn} = L_{nm}$	=	mutual inductance between windings m and n [H]
M	=	mutual inductance coefficient for a rotor loop and stator phase winding [H]
N_s	=	total number of turns of a stator phase winding [turns]
$n_{a,b,c}$	=	stator winding azimuthal turns density [turns per unit azimuthal length]
N_{RB}	=	number of rotor bars
p	=	number of machine pole-pairs
$[R]$	=	resistance matrix [Ohms]
$[RR]$	=	effective resistance matrix [Ohms]
R_0	=	mean rotor radius [m]
R_{rbn}	=	resistance of rotor bar n [Ohms]
R_s	=	resistance of a stator phase winding [Ohms]
s	=	rotor slip
t	=	time [sec]
$[v]$	=	voltage vector [V]
$v_{a,b,c}$	=	stator phase a,b, or c voltage [V]
θ_e	=	electrical angle [radians]
θ_0	=	angular displacement between stator and rotor reference frames at t=0 [radians]
$[\lambda]$	=	flux linkage matrix [Wb]
$\lambda_{a,b,c}$	=	stator phase winding a,b, or c flux linkage [Wb]
λ_{rn}	=	rotor loop n flux linkage [Wb]
μ_0	=	permeability of free space [H/m]

$$\omega \quad = \quad \text{stator electrical frequency [rad/sec]}$$

$$\omega_m \quad = \quad \text{rotor angular velocity [rad/sec]}$$

$$\omega_r \quad = \quad \text{rotor electrical frequency [rad/sec]}$$

The standard definitions for electrical angle, rotor slip, and rotor electrical frequency are shown below. Unless otherwise specified all angles will be given in mechanical degrees.

electrical angle: $\quad \theta_e = p\theta$ $\qquad (2-2)$

rotor slip: $\quad s = \dfrac{\omega - p\omega_m}{\omega}$ $\qquad (2-3)$

rotor frequency: $\quad \omega_r = \omega - p\omega_m = s\omega$ $\qquad (2-4)$

The coordinate system chosen to describe the stator and rotor is a cylindrical system. The stator is described using a fixed coordinate system (r,θ,z). The rotor is described using a moving coordinate system (r',θ',z') which travels at an angular velocity of ω_m with respect to the fixed coordinate system. Defining θ_0 as the angular separation between fixed and moving systems at $t=0$, a point on the rotor in terms of the stator reference frame is described by

$$r = r'$$
$$z = z'$$
$$\theta = \theta' + \omega_m t + \theta_0$$

<div align="right">(2-5)</div>
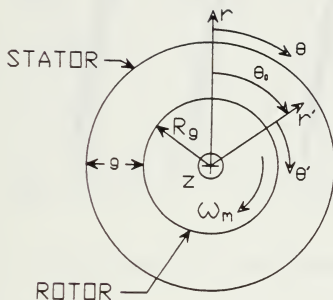
Figure 2-1. Coordinate system.

As stated previously, the rotor is described in terms of loops. Figure 2-2 shows a section of the rotor cage. A rotor loop can be thought of as a current path which includes two adjacent rotor bars and the portions of the end rings connecting the bars. Thus for an N_{RB}-bar rotor, there are N_{RB} rotor loops (N_{RB} adjacent single-turn coils). Since the rotor is symmetric, the separation between adjacent rotor bars is $2\pi/N_{RB}$ radians.
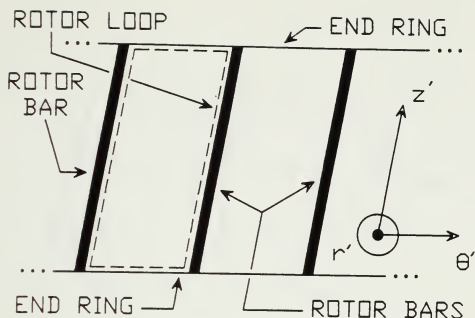
Figure 2-2. Rotor loop description.

Rotor loop current is defined as the current flowing in the single-turn coil (see Figure 2-3). The actual rotor bar current can be expressed in terms of rotor loop currents. For example, the current in rotor bar n is given by

$$i_{bar\ n} = i_{rn} - i_{r(n-1)} \tag{2-6}$$

Each rotor loop current produces an airgap flux which couples with each stator phase winding and every other rotor loop. In addition to this coupling, every rotor loop couples with the two adjacent rotor loops due to the resistance and leakage inductance of the common rotor bars as shown in Figure 2-3.

44
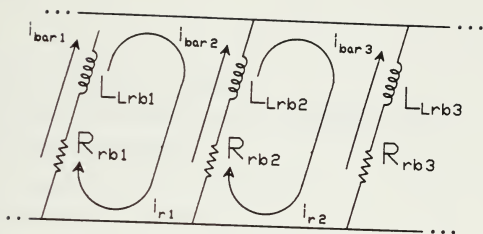
Figure 2-3. Coupling between adjacent rotor loops.

In order to derive the system of equations, two steps are required. First, the flux linkage of each winding (stator phases and rotor loops) must be expressed in terms of stator phase and rotor loop currents and inductances. Second, a relationship between the flux linkages and forcing functions (stator phase voltages) is required. The flux linkage of each winding will be determined using the principle of superposition. That is, the total flux linked by a winding is simply the sum of the flux linkages due to each current flowing in the system. The flux linkages can be related to terminal voltages using Faraday's law. In mathematical terms for a system with m windings we have

$$\lambda_n = \sum_m L_{nm} i_m \tag{2-7}$$

$$v_n = \frac{d}{dt}\lambda_n + R_n i_n \tag{2-8}$$

where

λ_n = flux linkage of winding n

L_{nm} = mutual inductance between windings n and m

i_m = current in winding m

v_n = terminal voltage of winding n

R_n = resistance of winding n

i_n = current in winding n

For an induction motor with N_{RB} rotor bars, there are N_{RB} +3 windings (N_{RB} rotor loops plus 3 stator phase windings). Since there is no net axial flux, the sum of the rotor loop currents is zero and the system of equations can be reduced from N_{RB}+3 to N_{RB}+2. The following sections detail the calculation of inductances for each winding. The calculations are broken down into three sections; stator relations (involving stator terms only), rotor relations (involving rotor terms only), and stator-rotor relations (coupling between the rotor and stator).

2.2.1 Stator Relations

Each stator phase winding is assumed to be represented by a sinusoidally distributed surface winding, separated

by 120 electrical degrees from the adjacent phases. For a p pole-pair machine, the stator winding azimuthal turns density is given by

$$n_a(\theta) = \frac{N_s}{2R_s}\cos p\theta$$

$$n_b(\theta) = \frac{N_s}{2R_s}\cos\left(p\theta - \frac{2\pi}{3}\right) \tag{2-9}$$

$$n_c(\theta) = \frac{N_s}{2R_s}\cos\left(p\theta + \frac{2\pi}{3}\right)$$

Open-circuiting phases b and c and exciting phase a with a current I, a surface current is produced on the stator according to

$$K_z = \frac{N_s I}{\cdot 2R_s}\cos p\theta \tag{2-10}$$

Choosing a contour that crosses the airgap at $\theta = \phi$ and $\theta = \phi + \pi/p$, the radial magnetic flux density can be determined using Ampere's law; see Figure 2-4. Thus,

$$\oint_c \vec{H} \cdot dl = \int\int_s J \cdot \bar{n} \, da \tag{2-11}$$

$$H_r(\phi)g - H_r(\phi + \pi/p)g = \int_\phi^{\phi+\pi/p} K_z R_s \, d\theta = \frac{-N_s I}{p}\sin p\phi \tag{2-12}$$
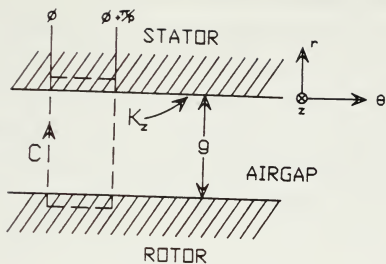
Figure 2-4. Integration contour on stator.

Using the symmetry relation $H_r(\phi) = -H_r(\phi + \pi/p)$,

$$H_r(\phi) = \frac{-N_s I}{2gp} \sin p\phi \qquad (2-13)$$

$$B_r(\phi) = \frac{-\mu_0 N_s I}{2gp} \sin p\phi \qquad (2-14)$$

Since ϕ is an arbitrary angle, the radial flux density in terms of θ is

$$B_r(\theta) = \frac{-\mu_0 N_s I}{2gp} \sin p\theta \qquad (2-15)$$

The flux linked by a full-pitch, single-turn coil can be calculated by integrating over the surface enclosed by the coil. Note that the surface enclosed by a coil for all flux linkage calculations is obtained by traversing the coil in the direction of positive current flow, i.e., current flows in the z direction at ϕ and in the -z direction at $\phi + \pi/p$. For the coordinate system being used, the normal component of this surface is in the -r direction. In this case,

$$
\begin{aligned}
\phi(\phi) &= \int_0^d \int_\phi^{\phi + \pi/p} \overline{B} \cdot \overline{n}\, da \\
&= d \int_\phi^{\phi + \pi/p} \frac{\mu_o N_s I}{2gp} \sin p\theta R_g\, d\theta \\
&= \frac{\mu_o N_s dR_g I}{gp^2} \cos p\phi
\end{aligned}
\tag{2-16}
$$

Again, since ϕ is an arbitrary angle, the flux linked by a coil extending from angle θ to angle $\theta + \pi/p$ is

$$
\phi(\theta) = \frac{\mu_o N_s dR_g I}{gp^2} \cos p\theta
\tag{2-17}
$$

The total flux linked by the stator phase windings can be calculated by integrating the number of turns times this flux linkage over the winding surface. This results in

49

$$\lambda_a = p \int_0^{\pi/p} n_a(\theta) \Phi(\theta) R_g \, d\theta$$

$$= \frac{\mu_o \pi N_s^2 d R_g I}{4gp^2} \tag{2-18}$$

$$\lambda_b = p \int_{2\pi/3p}^{5\pi/3p} n_b(\theta) \Phi(\theta) R_g \, d\theta$$

$$= \frac{-\mu_o \pi N_s^2 d R_g I}{8gp^2} \tag{2-19}$$

$$\lambda_c = p \int_{4\pi/3p}^{7\pi/3p} n_c(\theta) \Phi(\theta) R_g \, d\theta$$

$$= \frac{-\mu_o \pi N_s^2 d R_g I}{8gp^2} \tag{2-20}$$

From these flux linkages, the inductances of the stator phase windings due to a current in the phase a winding are

$$L_{aa} = \frac{\lambda_a}{I} = \frac{\mu_o \pi N_s^2 R_g d}{4gp^2} + L_{Ls} \tag{2-21}$$

$$L_{ba} = \frac{\lambda_b}{I} = \frac{-\mu_o \pi N_s^2 R_g d}{8gp^2} \tag{2-22}$$

$$L_{ca} = \frac{\lambda_c}{I} = \frac{-\mu_o \pi N_s^2 R_g d}{8gp^2} \tag{2-23}$$

where L_{Ls} is the leakage inductance of phase a representing additional phase a flux linkages not accounted for by the space fundamental component of the airgap flux.

Defining the inductance due to the space fundamental component of the airgap flux produced by a stator phase current as the stator phase airgap inductance (L_s), the following relations are obtained

$$L_{aa} = L_{bb} = L_{cc} = L_S + L_{Ls} \tag{2-24}$$

$$L_{ab} = L_{ac} = L_{ba} = L_{bc} = L_{ca} = L_{cb} = -\frac{L_S}{2} \tag{2-25}$$

where

$$L_s = \frac{\mu_o \pi N_s^2 R_g d}{4 g p^2} \tag{2-26}$$

2.2.2 Rotor Relations

Applying a current I to rotor loop 1 and open-circuiting all other rotor loops, the radial magnetic flux density can be determined using Ampere's law and Gauss's law. From Ampere's law, it can be shown that the radial flux density is a constant (B_1) in the region $0 \leq \theta' \leq 2\pi/N_{RB}$ and that the radial flux density is a constant (B_2) in the region $2\pi/N_{RB} \leq \theta' \leq 2\pi$ (see Figure 2-5). Using Gauss's law and noting that there is no axial flux, a relation between these constants can be calculated. In this case

51

$$\int_0^d \left(\int_0^{2\pi/N_{RB}} B_1 R_g \, d\theta' + \int_{2\pi/N_{RB}}^{2\pi} B_2 R_g \, d\theta' \right) dz = 0 \qquad (2-27)$$

$$B_1 = -(N_{RB} - 1) B_2 \qquad (2-28)$$

Choosing a contour which crosses the airgap and encloses rotor bar 1 (see Figure 2-5), the radial flux density can be determined from Ampere's law. Following this analysis,
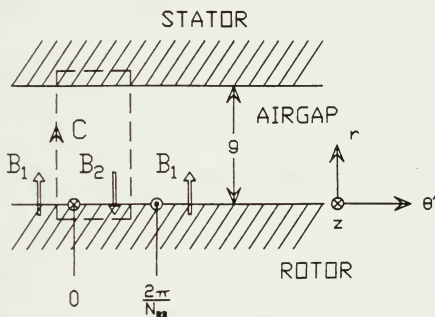
Figure 2-5. Integration contour on rotor.

$$H_2 - H_1 = \frac{I}{g} \qquad (2-29)$$

Using $B = \mu_c H$ and equations 2-28 and 2-29, B_1 can be found as

52

$$B_1 = \frac{-\mu_o I (N_{RB} - 1)}{g N_{RB}} \tag{2-30}$$

Since each rotor loop is a single-turn coil, the flux linkages can easily be determined. In general,

$$\lambda_{rn} = \int_0^d \int_{2\pi(n-1)/N_{RB}}^{2\pi n/N_{RB}} B_r(\theta')(-R_g) d\theta' dz \tag{2-31}$$

for rotor loop 1, this yields

$$\lambda_{r1} = \frac{2\pi\mu_o d R_g I (N_{RB} - 1)}{g N_{RB}^2} \tag{2-32}$$

and for all other rotor loops this yields

$$\lambda_{rb} = \frac{-2\pi\mu_o d R_g I}{g N_{RB}^2} \tag{2-33}$$

From these flux linkage values the rotor loop inductances are determined to be

$$L_{r1r1} = \frac{\lambda_{r1}}{I} = \frac{2\pi\mu_o R_g d (N_{RB} - 1)}{g N_{RB}^2} + L_{Lrb1} + L_{Lrb2} \tag{2-34}$$

$$L_{rN_{RB}r1} = \frac{\lambda_{rN_{RB}}}{I} = \frac{-2\pi\mu_o R_g d}{g N_{RB}^2} - L_{Lrb1} \tag{2-35}$$

53

$$L_{r2r1} = \frac{\lambda_{r2}}{1} = \frac{-2\pi\mu_0 R_g d}{g N_{RB}^2} - L_{Lrb2} \qquad (2-36)$$

where L_{Lrb1} and L_{Lrb2} are leakage inductances of the rotor bars accounting for flux linkages not accounted for by the airgap flux distribution.

For the other rotor loops ($n=3,4,5....N_{RB}-1$)

$$L_{rnr1} = \frac{\lambda_{rn}}{1} = \frac{-2\pi\mu_0 R_g d}{g N_{RB}^2} \qquad (2-37)$$

From equations 2-34, 2-35, and 2-36 one can see how the leakage inductance of each rotor bar is associated with the two adjacent rotor loops. Thus, for each rotor loop, the leakage inductances of the two rotor bars which make up the rotor loop are included in the "self inductance" term. For the two adjacent rotor loops, the leakage inductance of the common rotor bar is included in the "mutual inductance" term.

Defining the inductance due to the airgap flux produced by a rotor loop current as the rotor loop airgap inductance (L_R), the relations

$$L_{rara} = L_R + L_{Lrba} + L_{Lrb(a+1)} \qquad (2-38)$$

$$L_{rar(a+1)} = \frac{-L_R}{\left(N_{RB} - 1\right)} - L_{Lrb(a+1)} \qquad (2-39)$$

$$L_{rar(a-1)} = \frac{-L_R}{\left(N_{RB} - 1\right)} - L_{Lrba} \qquad (2-40)$$

$$L_{rarm} = -\frac{L_R}{\left(N_{RB} - 1\right)} \text{ for } m \neq n, n \pm 1 \qquad (2-41)$$

are obtained where

$$L_R = \frac{2\pi\mu_o R_s d\left(N_{RB} - 1\right)}{g N_{RB}^2} \qquad (2-42)$$

2.2.3 <u>Stator-rotor</u> <u>Mutual</u> <u>Relations</u>

From section 2.2.1, the radial flux density in the airgap due to a current I in stator phase a is

$$B_r(\theta) = \frac{-\mu_o N_s I}{2gp} \sin p\theta \qquad (2-43)$$

To determine the flux linked by a rotor loop, this flux density must be transformed to the rotor frame of reference. In the rotor reference frame the radial flux density is

$$B_r(\theta') = \frac{-\mu_o N_s I}{2gp}\sin p(\theta' + \omega_m t + \theta_o) \qquad (2-44)$$

The flux linked by a rotor loop is

$$\lambda_{rn} = \int_0^d \int_{2\pi(n-1)/N_{RB}}^{2\pi n/N_{RB}} B_r(\theta')(-R_g)d\theta'dz \qquad (2-45)$$

$$= \frac{\mu_o N_s d R_g I}{gp^2}\sin\left(\frac{\pi p}{N_{RB}}\right)\sin p\left(\frac{(2n-1)\pi}{N_{RB}} + \omega_m t + \theta_o\right)$$

The mutual inductance between phase a and rotor loop n is

$$L_{rna} = \frac{\lambda_{rn}}{I} = \frac{\mu_o N_s R_g d}{gp^2}\sin\left(\frac{\pi p}{N_{RB}}\right)\sin p\left(\frac{(2n-1)\pi}{N_{RB}} + \omega_m t + \theta_o\right) \qquad (2-46)$$

Similarly, for currents applied to stator phase b and c, the results are

$$L_{rnb} = \frac{\mu_o N_s R_g d}{gp^2}\sin\left(\frac{\pi p}{N_{RB}}\right)\sin\left(p\left(\frac{(2n-1)\pi}{N_{RB}} + \omega_m t + \theta_o\right) - \frac{2\pi}{3}\right) \qquad (2-47)$$

$$L_{rnc} = \frac{\mu_o N_s R_g d}{gp^2}\sin\left(\frac{\pi p}{N_{RB}}\right)\sin\left(p\left(\frac{(2n-1)\pi}{N_{RB}} + \omega_m t + \theta_o\right) + \frac{2\pi}{3}\right) \qquad (2-48)$$

Using the relation $L_{mn} = L_{nm}$ and defining M as the constant coefficient of the mutual inductance between a stator phase and rotor loop, the relations

56

$$L_{rna} = L_{arn} = M \sin p\left(\frac{(2n-1)\pi}{N_{RB}} + \omega_m t + \theta_o\right) \qquad (2-49)$$

$$L_{rnb} = L_{brn} = M \sin\left(p\left(\frac{(2n-1)\pi}{N_{RB}} + \omega_m t + \theta_o\right) - \frac{2\pi}{3}\right) \qquad (2-50)$$

$$L_{rnc} = L_{crn} = M \sin\left(p\left(\frac{(2n-1)\pi}{N_{RB}} + \omega_m t + \theta_o\right) + \frac{2\pi}{3}\right) \qquad (2-51)$$

are obtained where

$$M = \frac{\mu_o N_s R_g d}{g p^2} \sin\left(\frac{\pi p}{N_{RB}}\right) \qquad (2-52)$$

2.2.4 Overall System of Equations

Using the relations derived in the previous sections, the flux linkages for the system can be expressed in matrix form

$$[\lambda] = [L][\imath] \qquad (2-53)$$

where

$$[\lambda] = \begin{pmatrix} \lambda_a \\ \lambda_b \\ \lambda_c \\ \lambda_{r1} \\ \cdot \\ \cdot \\ \cdot \\ \lambda_{rN_{RB}} \end{pmatrix} \qquad (2-54)$$

57

$$[L] = \begin{pmatrix} L_{aa} & L_{ab} & L_{ac} & L_{ar1} & \cdots & L_{arN_{RB}} \\ L_{ba} & L_{bb} & L_{bc} & L_{br1} & \cdots & L_{brN_{RB}} \\ \cdot & \cdot & \cdot & \cdot & \cdot & \cdot \\ \cdot & \cdot & \cdot & \cdot & \cdot & \cdot \\ \cdot & \cdot & \cdot & \cdot & \cdot & \cdot \\ \cdot & \cdot & \cdot & \cdot & \cdot & \cdot \\ L_{rN_{RB}a} & L_{rN_{RB}b} & L_{rN_{RB}c} & L_{rN_{RB}r1} & \cdots & L_{rN_{RB}rN_{RB}} \end{pmatrix} \tag{2-55}$$

$$[i] = \begin{pmatrix} i_a \\ i_b \\ i_c \\ i_{r1} \\ \cdot \\ \cdot \\ i_{rN_{RB}} \end{pmatrix} \tag{2-56}$$

The flux linkages are related to the stator phase voltages by Faraday's law. For example, applying Faraday's law to stator phase a, the following is obtained

$$-v_a + R_s i_a = \frac{-d\lambda_a}{dt} \tag{2-57}$$

Similarly, for rotor loop n (whose net voltage is zero because it is shorted), Faraday's law yields

$$\left(R_{rbn} + R_{rb(n-1)}\right) i_{rn} - R_{rbn} i_{r(n-1)} - R_{rb(n+1)} i_{r(n+1)} = \frac{-d\lambda_{rn}}{dt} \tag{2-58}$$

Defining a resistance matrix, [R], and combining the above
results, the system of equations can be expressed as

$$[v] = [L]\frac{d[i]}{dt} + \left([R] + \frac{d[L]}{dt}\right)[i] \qquad (2-59)$$

where

$$[v] = \begin{pmatrix} v_a \\ v_b \\ v_c \\ 0 \\ . \\ . \\ . \\ 0 \end{pmatrix} \qquad (2-60)$$

$$[R] = \begin{pmatrix} [R_{Stator}] & [0] \\ [0] & [R_{Rotor}] \end{pmatrix} \qquad (2-61)$$

$$[R_{Stator}] = \begin{pmatrix} R_s & 0 & 0 \\ 0 & R_s & 0 \\ 0 & 0 & R_s \end{pmatrix} \qquad (2-62)$$

$$[R_{Rotor}] = \begin{pmatrix} R_{rb1} + R_{rb2} & -R_{rb2} & 0 & \dots & 0 & -R_{rb1} \\ -R_{rb2} & R_{rb2} + R_{rb3} & -R_{rb3} & \dots & 0 & 0 \\ . & . & . & \dots & . & . \\ . & . & . & \dots & . & . \\ -R_{rb1} & 0 & 0 & \dots & -R_{rbN_{RB}} & R_{rbN_{RB}} + R_{rb1} \end{pmatrix}$$

$$(2-63)$$

Once again defining a new matrix, the system of equations can be expressed as

$$[v] = [L]\frac{d[i]}{dt} + [RR][i] \qquad (2-64)$$

where

$$[RR] = [R] + \frac{d[L]}{dt} = \text{effective resistance matrix} \qquad (2-65)$$

The equations for the elements of the voltage, inductance, and effective resistance matrices are given in Appendix A.

The system of equations describing the electrical performance of three-phase induction motor has been developed. The elements of the inductance and effective resistance matrices are described in terms of the machine geometry (airgap active length and width, slot distribution, rotor radius, etc.) and electrical parameters (number of turns for a stator phase winding, rotor bar resistance, and leakage inductances). Thus, in order to solve the system of equations for stator phase and rotor loop currents, these quantities must be known.

2.3 Relation Between System and Single-phase Model

The object of this section is to derive a relationship between the standard single-phase, equivalent-circuit model of an induction motor (Figure 2-6) and the system of equations developed in the preceding section. From this relationship (equations 2-100 to 2-106 of this section), the values of the parameters required to solve the system of equations can be calculated using the single-phase circuit model parameters.
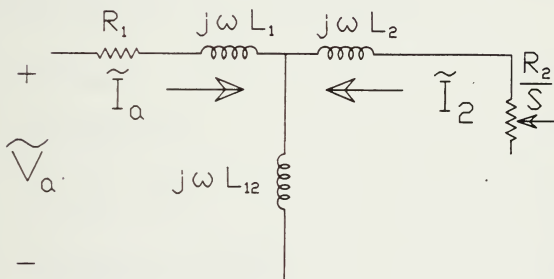
Figure 2-6. Single-phase equivalent-circuit model for an induction machine.

The parameter values of the single-phase circuit model can be obtained from the results of a no-load test, a locked-rotor test, and measurements of the DC resistances

of the stator phase windings. Section 9-6 of reference [12] provides a detailed discussion of the standard test procedure and calculations required to obtain the equivalent single-phase circuit parameters for a three-phase induction motor.

In order to derive a relationship between the system of equations and a single-phase equivalent circuit model, some basic assumptions are necessary. First, the rotor cage is symmetric. Thus, each rotor bar is assumed to have the same resistance (R_{rb}) and leakage inductance (L_{lr}). Second, balanced currents are assumed in both the stator phase windings and rotor loops and are given by

$$i_a = I_s \cos \omega t \qquad (2-66)$$

$$i_b = I_s \cos\left(\omega t - \frac{2\pi}{3}\right) \qquad (2-67)$$

$$i_c = I_s \cos\left(\omega t + \frac{2\pi}{3}\right) \qquad (2-68)$$

$$i_{rn} = I_r \cos\left(\omega_r t + \phi - \frac{(n-1)2\pi p}{N_{RB}}\right) \qquad (2-69)$$

where ϕ is the phase angle of rotor loop 1 current with respect to the stator reference frame at t=0.

Using these assumptions and the system of equations, the flux linkages for stator phase a and rotor loop 1 are given by the following relations

62

$$\lambda_a = \left(\frac{3}{2}L_s + L_{Ls}\right)I_s \cos \omega\, t$$

$$+ \frac{MI_r N_{RB}}{2}\cos\left(\omega\, t + \phi + \frac{\pi p}{N_{RB}} + p\,\theta_o - \frac{\pi}{2}\right) \qquad (2-70)$$

$$\lambda_{r1} = \frac{3MI_s}{2}\cos\left(\omega_r t - p\,\theta_o - \frac{p\pi}{N_{RB}} + \frac{\pi}{2}\right)$$

$$+ \left(\left(\frac{N_{RB}L_r}{N_{RB}-1}\right) + 4L_{Lrb}\sin^2\left(\frac{\pi p}{N_{RB}}\right)\right)I_r \cos\left(\omega_r t + \phi\right) \qquad (2-71)$$

The terminal voltage relations for stator phase a and rotor loop 1 are

$$v_a = \frac{d\lambda_a}{dt} + R_s I_s \cos \omega\, t \qquad (2-72)$$

$$0 = \frac{d\lambda_{r1}}{dt} + 4R_{rb}\sin^2\left(\frac{\pi p}{N_{RB}}\right)I_r \cos\left(\omega_r t + \phi\right) \qquad (2-73)$$

Defining the variables in complex form according to

$$\lambda_a = Re\left\{\Lambda_a \exp(j\omega\, t)\right\} \qquad (2-74)$$

$$i_a = Re\left\{I_a \exp(j\omega\, t)\right\} \qquad (2-75)$$

$$v_a = Re\left\{\nabla_a \exp(j\omega\, t)\right\} \qquad (2-76)$$

$$\lambda_{r1} = Re\left\{\Lambda_{r1} \exp(j\omega_r t)\right\} \qquad (2-77)$$

$$i_{r1} = Re\left\{I_r \exp(j\omega_r t)\right\} \qquad (2-78)$$

and also defining a new rotor loop current in order to eliminate phase shifts

$$I_{AR} = I_r \exp\left(j\left(p\theta_o + \frac{p\pi}{N_{RB}} - \frac{\pi}{2} + \phi\right)\right) \tag{2-79}$$

the terminal voltage relations become

$$\bar{V}_a = j\omega\left(\frac{3L_S}{2} + L_{Ls}\right)I_s + j\omega\frac{M N_{RB} I_{AR}}{2} + R_s I_s \tag{2-80}$$

$$0 = j\omega\frac{3 M I_s}{2} + j\omega\left(\left(\frac{N_{RB} L_r}{N_{RB} - 1}\right) + 4 L_{Lrb} \sin^2\left(\frac{\pi p}{N_{RB}}\right)\right)I_{AR}$$

$$+ \frac{4 R_{rb}}{s}\sin^2\left(\frac{\pi p}{N_{RB}}\right)I_{AR} \tag{2-81}$$

Now, in order to transform the rotor loop equation into an equivalent stator phase, a stator-equivalent rotor current, I_2, is defined. This stator-equivalent rotor current is defined to be the magnitude of the current required in the stator windings (under balanced three-phase conditions) to produce the same space fundamental component of airgap flux as is produced by rotor loop currents of magnitude I_{AR}. This corresponds to the equivalent rotor current I_2 of the single-phase, equivalent-circuit of Figure 2-6.

The flux linked by stator phase a due to the space fundamental component of airgap flux produced by balanced rotor loop currents of magnitude I_{AR} is

$$\Lambda_{ag} = \frac{M N_{RB} I_{AR}}{2} \tag{2-82}$$

64

The flux linked by stator phase a due to the space fundamental component of airgap flux produced by balanced stator phase currents of magnitude I_2 is

$$\Lambda_{ag} = \frac{3 L_s I_2}{2} \tag{2-83}$$

Since the airgap flux must be the same for these currents, the following relation between a rotor loop current and the equivalent stator phase current is obtained

$$I_{AR} = \left(\frac{3 L_s}{M\,N_{RB}} \right) I_2 \tag{2-84}$$

Using this relation to eliminate I_{AR}, equations 2-80 and 2-81 become

$$V_a = j\omega\left(\frac{3L_s}{2} + L_{Ls}\right)I_s + j\omega\,\frac{3L_sI_2}{2} + R_s I_s \tag{2-85}$$

$$0 = j\omega\,\frac{3MI_s}{2} + j\omega\left\{\left(\frac{N_{RB}\,L_r}{N_{RB}-1}\right) + 4L_{Lrb}\sin^2\left(\frac{\pi p}{N_{RB}}\right)\right\}\left(\frac{3L_s}{M\,N_{RB}}\right)I_2$$

$$+ \frac{4R_{rb}}{s}\sin^2\left(\frac{\pi p}{N_{RB}}\right)\left(\frac{3L_s}{M\,N_{RB}}\right)I_2 \tag{2-86}$$

Multiplying each term in equation 2-81 by the factor L_s/M the following result is obtained

$$0 = j\omega \frac{3L_S I_s}{2} + j\omega \left\{ \left(\frac{N_{RB} L_r}{N_{RB}-1} \right) + 4L_{Lrb} \sin^2\left(\frac{\pi p}{N_{RB}} \right) \right\} \left(\frac{3L_S^2}{M^2 N_{RB}} \right) I_2$$

$$+ \frac{4R_{rb}}{s} \sin^2\left(\frac{\pi p}{N_{RB}} \right) \left(\frac{3L_S^2}{M^2 N_{RB}} \right) I_2 \qquad (2-87)$$

The voltage relations for the single-phase, equiv-alent-circuit model shown in Figure 2-6 are given by equations 2-88 and 2-89 below

$$V_a = j\omega\left(L_1 + L_{12}\right)I_a + j\omega L_{12}I_2 + R_1 I_a \qquad (2-88)$$

$$0 = j\omega L_{12}I_a + j\omega\left(L_{12} + L_2\right)I_2 + \frac{R_2}{s}I_2 \qquad (2-89)$$

By comparing the terms in equations 2-85 and 2-87 to the terms in equations 2-88 and 2-89, the following relations are obtained

$$R_1 = R_s \qquad (2-90)$$

$$L_1 = L_{Ls} \qquad (2-91)$$

$$L_{12} = \frac{3L_S}{2} \qquad (2-92)$$

$$L_2 = \left\{ \left(\frac{N_{RB} L_r}{N_{RB}-1} \right) + 4L_{Lrb} \sin^2\left(\frac{\pi p}{N_{RB}} \right) \right\} \left(\frac{3L_S^2}{M^2 N_{RB}} \right) - \frac{3L_S}{2} \qquad (2-93)$$

66

$$R_2 = \frac{4R_{rb}}{s}\sin^2\left(\frac{\pi p}{N_{RB}}\right)\left(\frac{3L_s^2}{M^2 N_{RB}}\right) \tag{2-94}$$

From the definitions of L_s, L_R, and M given in the previous sections, the relationship between the single-phase, equivalent-circuit model parameters and the actual machine geometry and electrical parameters is

$$R_1 = R_s \tag{2-95}$$

$$L_1 = L_{Ls} \tag{2-96}$$

$$L_{12} = \left(\frac{3}{2}\right)\frac{\mu_o \pi N_s^2 R_g d}{4g p^2} \tag{2-97}$$

$$L_2 = \left(\frac{3}{2}\right)\frac{\mu_o \pi N_s^2 R_g d}{4g p^2}\left\{\left(\frac{\pi p}{N_{RB}\sin\left(\frac{\pi p}{N_{RB}}\right)}\right)^2 - 1\right\} + \left(\frac{3\pi^2 N_s^2}{4N_{RB}}\right)L_{Lrb} \tag{2-98}$$

$$R_2 = \left(\frac{3\pi^2 N_s^2}{4N_{RB}}\right)R_{rb} \tag{2-99}$$

From the equations for L_{12}, L_2, and R_2, one cannot explicitly determine the resistance and leakage inductance of a rotor bar. To determine these values the number of rotor bars and either the geometry parameters (R_s, d, and

67

g) or the number of stator winding turns are required. The number of rotor bars can be determined from visual inspection or possibly from test methods discussed by Hargis et al. [8]. For example, one could use stator frame vibration frequencies or rotor slot product frequencies present in the stator phase currents. However, determining these other parameters will require disassembling the machine, removing the rotor, and measuring the rotor diameter and length, stator diameter, and number of turns. Obviously, this is undesirable.

Because there is no requirement to determine rotor currents explicitly (i.e., they can't be measured directly), it is quite sufficient to deal with equivalent rotor currents as seen from the stator windings. This will simply result in rotor currents which are scaled by a stator-rotor turns ratio and has the effect of rendering the choice of N_s totally arbitrary. By arbitrarily choosing a value for the number stator phase winding turns, the rotor loop currents will be scaled by the ratio of the actual number of turns to the arbitrary number of turns while not affecting in any way the value of stator currents or voltages predicted by the model. Although this may not be entirely obvious, a simple example will illustrate the point.

EXAMPLE:

Given: A 3-phase, Y-connected, 100 V (line-to-neutral), 60 Hz, 2-pole induction motor with a 10-bar squirrel-cage rotor has the following single-phase, equivalent-circuit parameters

$$R_1 = 1.0\,\Omega \qquad L_1 = 0.005\,H \qquad L_{12} = 0.05\,H$$
$$L_2 = 0.005\,H \qquad R_2 = 0.5\,\Omega$$

The machine is operating at a rotor slip of 0.1

Equivalent-circuit model solution:

From equations 2-88 and 2-89, the magnitude of the stator phase and equivalent rotor currents calculated are

$$I_s = 14.961\ A \qquad I_2 = 13.222\ A$$

System of equations solution:

a. Assuming $N_s = 1$, the parameters of the system of equations are (calculated using equations 2-90 to 2-94)

$$R_s = 1.0\,\Omega \qquad L_{Ls} = 0.005\,H \qquad L_s = 0.0333\,H \qquad M = 0.0131\,H$$
$$R_{rb} = 0.676\,\Omega \qquad L_{Lrb} = 0.0045\,H \qquad L_R = 0.024\,H$$

69

The magnitude of the stator phase and rotor loop currents calculated from equations 2-80 and 2-81 are

$$I_s = 14.961 \text{ A} \qquad I_{AR} = 10.082 \text{ A}$$

Using equation 2-84, the stator-equivalent rotor current is

$$I_2 = 13.222 \text{ A}$$

b. Assuming $N_s = 10$, the parameters of the system of equations are (calculated using equations 2-85 to 2-89)

$$R_s = 1.0 \,\Omega \qquad L_{Ls} = 0.005 \text{ H} \qquad L_S = 0.0333 \text{ H} \qquad M = 0.00131 \text{ H}$$
$$R_{rb} = 0.00676 \,\Omega \qquad L_{Lrb} = 0.000045 \text{ H} \qquad L_R = 0.00024 \text{ H}$$

The magnitude of the stator phase and rotor loop currents calculated from equations 2-80 and 2-81 are

$$I_s = 14.961 \text{ A} \qquad I_{AR} = 100.82 \text{ A}$$

Using equation 2-84, the stator-equivalent rotor current is

$$I_2 = 13.222 \text{ A}$$

The results of (a) and (b) above show that the value of the stator current calculated using the system of equations is independent of the number of stator turns arbitrarily chosen. Although the rotor loop current calculated is proportional to the number of stator turns, the stator-equivalent rotor current is also independent of the number of stator turns arbitrarily chosen. Thus, the number of stator turns can be chosen arbitrarily without affecting the values of the stator currents calculated using the system of equations developed.

Finally, assuming the number of rotor bars is known and arbitrarily setting the number of stator turns to one, the parameters required for the system of equations can be calculated from the single-phase, equivalent-circuit model parameters.

$$R_s = R_1 \tag{2-100}$$

$$L_{Ls} = L_1 \tag{2-101}$$

$$L_s = \left(\frac{2}{3}\right) L_{12} \tag{2-102}$$

$$M = \left(\frac{8}{3\pi}\right) \sin\left(\frac{p\pi}{N_{RB}}\right) L_{12} \tag{2-103}$$

$$R_{rb} = \left(\frac{4 N_{RB}}{3 \pi^2}\right) R_2 \qquad (2-104)$$

$$L_{Lrb} = \left\{ L_2 - \left[\left(\frac{p \pi}{N_{RB} \sin\left(\frac{p\pi}{N_{RB}}\right)}\right)^2 - 1 \right] L_{12} \right\} \left(\frac{4 N_{RB}}{3 \pi^2}\right) \qquad (2-105)$$

$$L_R = \left(\frac{16(N_{RB} - 1) p^2}{3 N_{RB}^2}\right) L_{12} \qquad (2-106)$$

As a final check of the relationship between the system of equations and the single-phase, equivalent-circuit model, a comparison of the power transferred across the airgap will be made. The results must be identical.

The airgap power for the system of equations is given by

$$P_{AG\,sys} = N_{RB} \left| i_{bar\,n} \right|^2 \left(\frac{R_{rb}}{s}\right) \qquad (2-107)$$

$$i_{bar\,n} = i_{rn} - i_{r(n-1)}$$
$$= 2 I_r \sin\left(\frac{p\pi}{N_{RB}}\right) \sin\left(\omega_r t + \phi - \frac{(2n-3)p\pi}{N_{RB}}\right) \qquad (2-108)$$

$$\left| i_{bar\ n} \right|^2 = 4 I_r^2 \sin^2 \left(\frac{p\pi}{N_{RB}} \right)$$

$$= 4 I_{AR}^2 \sin^2 \left(\frac{p\pi}{N_{RB}} \right) \qquad (2-109)$$

$$P_{AG\ sys} = 4 N_{RB} I_{AR}^2 \sin^2 \left(\frac{p\pi}{N_{RB}} \right) \frac{R_{rb}}{s} \qquad (2-110)$$

The airgap power for the single-phase circuit model is

$$P_{AG\ model} = 3 \left| I_2 \right|^2 \left(\frac{R_2}{s} \right) \qquad (2-111)$$

$$\left| I_2 \right|^2 = \left(\frac{4 N_{RB} I_{AR}}{3\pi} \sin \left(\frac{p\pi}{N_{RB}} \right) \right)^2 \qquad (2-112)$$

$$R_2 = \left(\frac{3\pi^2}{4 N_{RB}} \right) R_{rb} \qquad (2-113)$$

$$P_{AG\ model} = 4 N_{RB} I_{AR}^2 \sin^2 \left(\frac{p\pi}{N_{RB}} \right) \frac{R_{rb}}{s} \qquad (2-114)$$

The airgap power is identical for both the circuit model and system of equations. Thus, the relationship between the system of equations and equivalent-circuit model is valid.

2.4 Summary

The system of equations describing the electrical performance of a three-phase induction motor has been developed using stator phase and rotor loop currents as state variables. Each stator phase and rotor loop is described in terms of resistances and inductances. The stator phase voltages are the driving functions for the system. The assumptions used to develop the equations impose limitations on the ability of the system to accurately model any given induction motor. However, each assumption can be relaxed and the corresponding system of equations can be developed using the method presented.

A relationship between the standard single-phase, equivalent-circuit model for an induction motor and the system of equations has been derived (equations 2-100 to 2-106). With this relationship, the electrical and geometrical parameters needed to solve the system of equations can be easily calculated from the single-phase circuit model values. This relationship is useful in that the solution to the system of equations can be obtained without disassembling the motor, removing the rotor, and physically measuring these parameters. Thus, by performing the standard no-load, locked-rotor, and DC tests and knowing the number of rotor bars, the system of equations can be used to simulate any three-phase induction motor, subject to the limitations resulting from the assumptions.

CHAPTER 3

COMPUTER SIMULATION OF SYSTEM

3.1 Requirement for a Simulation Routine

Due to the number and complexity of the system of first-order differential equations developed in Chapter 2, a numerical integration routine must be used to solve for the time-varying stator phase and rotor loop currents. In general, numerical integration methods are used to solve systems of equations which are expressed in the following form

$$\frac{d[x(t)]}{dt} = [A][x(t)] + [B] \qquad (3-1)$$

There are a variety of numerical integration procedures and computer simulation programs available which can be used to solve the above system of equations. The most widely used integration procedures are Euler's, Milne's, Runge-Kutta, and Hamming's methods. These methods, which are described in references [13,14,15,16,17], are typically used to solve initial-value problems. Initial-value problems are problems in which the values of the dependent variables and necessary derivatives are known at the point the integration begins. These various procedures can be easily implemented on computers. Several "canned" computer programs such as SIMNON, a nonlinear system simulation

program developed by the Department of Automatic Control at Lund Institute of Technology in Lund, Sweden, and PRO-MATLAB, a matrix computation software package by The MathWorks, Inc., Sherborn, MA, either use these procedures inherently or can be programmed readily to use these procedures to solve the system of equations given above.

The system of equations describing the electrical performance of an induction motor is expressed in the form

$$[L(t)]\frac{d[i(t)]}{dt} = -[RR(t)][i(t)] + [v(t)] \qquad (3-2)$$

In order to use a numerical integration procedure to solve for the time-varying stator phase and rotor loop currents, the system of equations must be expressed in the form shown in equation 3-1. Comparison of equations 3-2 and 3-3 shows that the inductance matrix in equation 3-2 must be inverted. Since some of the elements in this matrix are time-dependent, the matrix must be inverted for each value of time. This inversion is always possible unless the leakage flux is defined to be zero, in which case the inverse of the inductance matrix does not exist. With the inductance matrix inverted, the system of equations can be expressed in the required form i.e.,

$$\frac{d[i(t)]}{dt} = -[L(t)]^{-1}[RR(t)][i(t)] + [L(t)]^{-1}[v(t)] \qquad (3-3)$$

As a result of the inductance matrix inversion requirement, SIMNON could not be used to solve the system of equations. On the other hand, PRO-MATLAB could be programmed to invert the inductance matrix and numerically integrate the system of equations. For an induction motor with a 45-bar rotor, using a fourth-order Runge-Kutta integration procedure, a total CPU run time of five hours is required on the LEES Vax-750 to simulate 100 time steps using PRO-MATLAB. The major cause of this long run time is the inductance matrix inversion.

In order to reduce the CPU run time required to simulate the system, a FORTRAN program was developed. Using this program on the LEES Vax-750 for the 45-bar rotor, 100 time steps can be simulated in five minutes (approximately 60 times faster than PRO-MATLAB). In addition to the FORTRAN program, which solves the system of equations for the time-varying stator phase and rotor loop currents, a PRO-MATLAB fast Fourier transform routine is used to determine the frequency components of these currents.

3.1.1 FORTRAN Simulation Program

From the preceding discussion, the computer simulation program must be capable of performing two major steps. First, for each value of time, the inductance matrix must

77

be inverted. Second, the resulting system of equations, namely equation 3-3 above, must be numerically integrated to determine the time-varying values of the stator phase and rotor loop currents. Cholesky's method (also known as Crout's method) with partial pivoting is used to invert the inductance matrix. This method was selected over the more common Gauss elimination and Gauss-Jordan elimination methods since it is more economical with regard to computer time and memory allocation [13]. Partial pivoting is used to improve the accuracy of the matrix inversion. Section 3-4 of reference [13] describes the theory of Cholesky's method. A fixed-step, fourth-order Runge-Kutta procedure is used to numerically integrate the system of equations. This procedure was selected for several reasons. The Runge-Kutta method is a single-step, self-starting procedure (i.e., for each integration time step, only the previous value of the dependent variables is required). This procedure is relatively easy to program and has a small per-step error (on the order of the step size to the fifth power). One disadvantage of this method is the requirement to perform four function evaluations per step. Section 6-5 of reference [13] discusses the theory, implementation, and error analysis of the fourth-order Runge-Kutta integration procedure.

The FORTRAN simulation program is divided into six parts, a main program and five subroutines. Subject to the

assumptions discussed in Chapter 2, the program simulates the electrical operation of an induction motor (i.e., solves the system of equations for the time-varying stator phase and rotor loop currents) with either no broken rotor bars or one broken rotor bar. A flowchart for the program is shown in Figure 3-1. The FORTRAN source code and sample input and output data files are included in section B-1 of Appendix B. The following paragraphs describe the purpose of each part of the simulation program.

Main program: The main program performs several functions. The primary function is to act as a buffer and pass data between the subroutines. In addition, the main program keeps track of the simulation time, calculates the value of the current vector at the end of each time step, and writes the results to an external file.

Subroutine INPUT: This subroutine is called once by the main program. It performs two functions. First, it reads the data contained in an external input file. The external input file provides a description of the machine being simulated. It includes the single-phase, equivalent-circuit model values, number of rotor bars, and number of pole-pairs for the machine, the rotor slip, and the supply voltage and frequency. The

79

Figure 3-1.   FORTRAN simulation program flowchart.
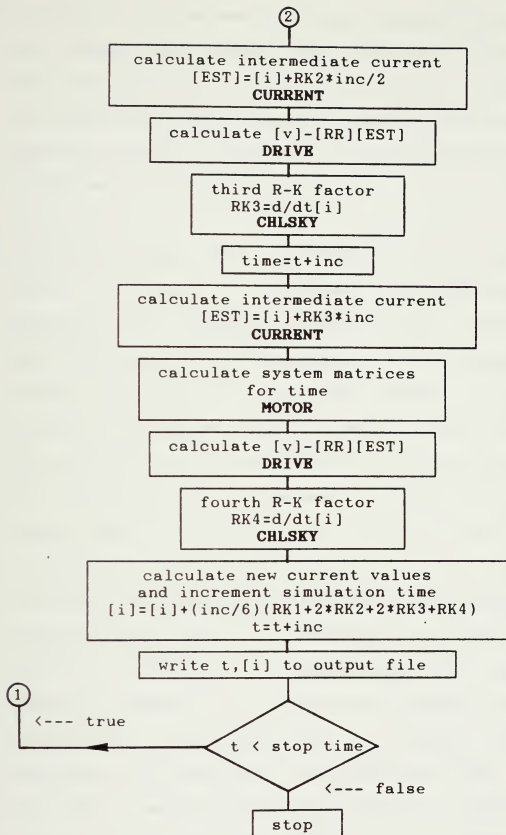
Figure 3-1.(cont.) FORTRAN simulation program flowchart.

simulation time parameters (step-size and stop time) and a broken bar flag are also included in the input file. Second, using the relations derived in section 2.3, the coefficients for the inductance and effective resistance matrix elements are calculated and passed to the main program.

Subroutine MOTOR: This subroutine is called for each value of time. It performs two functions; it calculates the elements of the voltage, inductance, and effective resistance matrices, and it reduces the system of equations. For the voltage vector, a balanced three-phase supply is assumed. The inductance and effective resistance elements are calculated using the relations given in Appendix A. For both a "no broken bar" simulation and a "one broken bar" simulation, the system of equations can be reduced from $N_{RB}+3$ to $N_{RB}+2$ since the sum of the rotor loop currents equals zero. This condition is imposed on the system of equations by eliminating rotor loop N_{RB} current. Column $N_{RB}+3$ is subtracted from columns 4 through $N_{RB}+2$ and column $N_{RB}+3$ is deleted from the inductance and effective resistance matrices. Next, row $N_{RB}+3$ is deleted from each matrix to complete the reduction. In addition, for a "one broken bar" simulation (assume rotor bar $N_{RB}-1$ is broken), the

82

system of equations can be reduced again by setting rotor loop $N_{RB}-1$ current equal to rotor loop $N_{RB}-2$ current. For this condition, column $N_{RB}+2$ is added to column $N_{RB}+1$ and column $N_{RB}+2$ is deleted from the inductance and effective resistance matrices. Faraday's law is satisfied by adding row $N_{RB}+2$ to row $N_{RB}+1$ and deleting row $N_{RB}+2$ from each matrix to complete the reduction.

Subroutine CURRENT: This subroutine is used to calculate the intermediate values of the current vector for the Runge-Kutta method.

$$[EST] = [I] + \frac{d[I]}{dt} \Delta t \qquad (3-4)$$

where

    [EST] = intermediate value of current vector

    [I] = initial current vector

Subroutine DRIVE: The purpose of this subroutine is to calculate the "driving function" for each value of time and current, i.e.,

$$\text{driving function} = [V] - [RR][I] \qquad (3-5)$$

Subroutine CHLSKY: This subroutine performs the inductance matrix inversion to calculate the derivative of the current vector for each time value. For the fourth-order Runge-Kutta procedure, this calculation is performed four times per time step.

The program can be modified, if desired, to simulate a variety of operating/fault conditions. For example, an unbalanced voltage supply can be simulated by simply changing the appropriate statements in subroutine MOTOR. Similarly, the effects of an increase or decrease in the impedance of one or more rotor bars can be simulated by modifying the appropriate statements for the elements of the inductance and effective resistance matrix in subroutine MOTOR. In addition, multiple broken rotor bars can be simulated by repeating the system reduction scheme in subroutine MOTOR for each broken bar.

3.1.2 Determining the Time Step

An appropriate time step for any simulation can be determined using a "trial and error" procedure. Basically, a series of simulations are run with increasing values of time steps and the output results are compared. The largest time step that gives "good" results (i.e., same output values as those using a smaller time step) is an appropriate time step.

Another method which provides an estimate for an appropriate time step and also provides an indication of the system stability and of the time required for the solution to reach a steady-state value is to determine the eigenvalues of the system when the rotor speed is equal to zero. From equation 3-3, the eigenvalues of interest are those of the matrix $-[L]^{-1}[RR]$. For a rotor speed of zero ($s=1.0$), this matrix is time-invariant and the system is stable if all the eigenvalues are negative. The inverse of the magnitude of the largest eigenvalue represents the "fastest" transient time for the system and thus provides an estimate for the largest time step. Similarly, the inverse of magnitude of the smallest eigenvalue represents the "slowest" transient time for the system and thus provides an estimate of the time required for the solution to reach steady-state. PRO-MATLAB, which has a built-in eigenvalue function, can be used to determine these eigenvalues. A PRO-MATLAB routine which calculates the system eigenvalues for $s=1.0$ and the eigenvalues for a 3-bar rotor and a 45-bar rotor induction motor are included in section B-2 of Appendix B.

3.1.3 Running the Simulation Program

In order to start the simulation program, the stator phase and rotor loop currents must be initialized. Since the steady-state values of the stator phase and rotor loop currents for a "one broken bar" case are not known, the

85

currents are set to zero initially and the simulation
program runs until steady-state conditions exist. For the
3-bar rotor and 45-bar rotor induction motors simulated,
steady-state conditions were reached after approximately
0.2 seconds of simulation time.

3.1.4 Processing the Simulation Output

In order to determine the harmonic content of the
time-varying stator phase and rotor loop currents, a
transformation from the time to the frequency domain is
necessary. This transformation is accomplished by taking
the fast Fourier transform (FFT) of the time-varying
stator phase and rotor loop currents. For a broken rotor
bar, the stator phase currents will contain a harmonic
component at a frequency of $(1-2s)f$ (refer to section
1.3). Most induction machines are designed to operate at
small slip values on the order of 0.02-0.05. Thus, the
frequency of this harmonic component is very near the
fundamental frequency ($0.9f$ to $0.96f$). To distinguish this
component from the fundamental frequency component using
an FFT routine, a frequency resolution on the order of
$0.02f$ is required. From reference [18], the bin width or
frequency resolution of a FFT for N samples is given by

$$\Delta f = \frac{f_s}{N} \tag{3-6}$$

where

    Δf = frequency resolution

    f_s = sample frequency

    N = number of data samples

In addition to selecting the proper frequency resolution, a weighting function, or window, can be applied to the sampled data to aid in distinguishing frequency components which are relatively close. References [18,19] provide a detailed description of the fast Fourier transform and common window functions used, their properties, and their advantages and disadvantages.

PRO-MATLAB, which has a built-in FFT function, is used to transform the stator phase and rotor loop currents from the time domain to the frequency domain. A frequency resolution of 0.3 Hz and a second-order Hanning window [18] are used to enhance the detection of the $(1-2s)f$ component of the stator phase current. A sample frequency of 153.6 Hz and a sample size of 512 data points satisfy the 0.3 Hz frequency resolution requirement and PRO-MAT-LAB's requirement for a sample size which is an integer power of two. The PRO-MATLAB FFT routine and a sample output file is included in section B-3 of Appendix B.

The relation between the magnitude of the FFT using a second-order Hanning window and the magnitude of the corresponding periodic signal in the time domain is given by [18]

$$|F(\omega)| = \frac{N}{4}|f(t)| \qquad (3-7)$$

where

$|F(\omega)|$ = magnitude of FFT at ω

$f(t) = |f(t)|\cos(\omega t + \phi)$

For the PRO-MATLAB FFT routine, the magnitude of the FFT is converted to a dB reference scale (for graphing purposes) using the relation

$$dB = 20\log|F(\omega)| \qquad (3-8)$$

3.2 "Hand" Verification of Simulation

For initial validation and "debugging" of the FORTRAN simulation program and FFT routine, a two-pole, 3-bar rotor induction motor was chosen. An exact solution for the stator phase and rotor loop currents can be calculated by

88

hand for this simple machine with either no broken rotor bars or one broken rotor bar. The exact solutions can be calculated using the method of undetermined coefficients.

<u>No broken rotor bars:</u> The system of equations for this case can be reduced from six to four by imposing the following constraints

$$i_a + i_b + i_c = 0 \qquad\qquad (3-9)$$

$$i_{r1} + i_{r2} + i_{r3} = 0 \qquad\qquad (3-10)$$

Assuming the following form for the stator phase and rotor loop currents and substituting into the system of equations, the unknown coefficients (A, B, C, D) can be determined.

$$i_a = A \cos \omega t + B \sin \omega t \qquad\qquad (3-11)$$

$$i_b = A \cos\left(\omega t - \frac{2\pi}{3} \right) + B \sin\left(\omega t - \frac{2\pi}{3} \right) \qquad\qquad (3-12)$$

$$i_{r1} = C \cos(s \omega t) + D \sin(s \omega t) \qquad\qquad (3-13)$$

$$i_{r2} = C \cos\left(s \omega t - \frac{2\pi}{3} \right) + D \sin\left(s \omega t - \frac{2\pi}{3} \right) \qquad\qquad (3-14)$$

89

The amplitude of the stator phase and rotor loop currents are given by the following relations

$$I(60 \text{ Hz}) = |i_a| = |i_b| = \sqrt{A^2 + B^2} \tag{3-15}$$

$$Ir = |i_{r1}| = |i_{r2}| = \sqrt{C^2 + D^2} \tag{3-16}$$

<u>One broken rotor bar:</u> Assuming rotor bar 2 is the broken bar, the system of equations can be reduced from six to three by imposing the constraints given by equations 3-9 and 3-10 plus the constraint

$$i_{r1} = i_{r2} \tag{3-17}$$

Again, assuming the following form for the stator phase and rotor loop currents, the unknown coefficients can be determined.

$$i_a = A \cos \omega t + B \sin \omega t + \\ C \cos((1-2s)\omega t) + D \sin((1-2s)\omega t) \tag{3-18}$$

$$i_b = A \cos\left(\omega t - \frac{2\pi}{3}\right) + B \sin\left(\omega t - \frac{2\pi}{3}\right) + \\ C \cos\left((1-2s)\omega t - \frac{2\pi}{3}\right) + D \sin\left((1-2s)\omega t - \frac{2\pi}{3}\right) \tag{3-19}$$

$$i_{r1} = E\cos(s\omega t) + F\sin(s\omega t) \qquad (3-20)$$

The amplitude of the stator phase currents (both the 60 Hz and $(1-2s)f$ components) and the rotor loop currents are given by the following relations

$$I(60\ Hz) = |i_a(60\,Hz)| = |i_b(60\,Hz)| = \sqrt{A^2 + B^2} \qquad (3-21)$$

$$I(1-2s)f = |i_a(1-2s)f| = |i_b(1-2s)f| = \sqrt{C^2 + D^2} \qquad (3-22)$$

$$Ir = |i_{r1}| = \sqrt{E^2 + F^2} \qquad (3-23)$$

3.2.1 Three-bar Rotor Simulation

To simulate a 3-bar rotor induction motor, the single-phase, equivalent-circuit model parameters from the 3-HP experimental motor are used as inputs for the FORTRAN simulation program. The parameters used for the 3-bar rotor induction motor are listed in Table 3-1.

Using the method described in the preceding paragraphs, the exact solution of the stator phase and rotor loop currents were calculated for various rotor slip values. Table 3-2 shows the results from these calculations. The results generated from the simulation program are shown in Table 3-3.

91

PARAMETER	VALUE
R_1	0.8590 ohms
L_1	0.0046 H
L_{12}	0.0704 H
L_2	0.0046 H
R_2	0.5612 ohms
$N_{R\beta}$	3
p	1
Input Frequency	60 Hz
Input Phase Voltage	169.71 V

Table 3-1. 3-bar rotor parameters.

The correlation between the exact and simulation results is extremely good. For all cases, the error between these results is less than 1%. The absolute error between the simulation and exact results is shown in Table 3-4.

The close correlation between the exact and simulation results is demonstrated graphically in Figures 3-2, 3-3, 3-4, 3-5, 3-6. Based on the results presented above, the FORTRAN simulation program and FFT routine can be seen to accurately solve the system of equations developed in Chapter 2 for the stator phase and rotor loop currents.

	NO BROKEN BARS		ONE BROKEN BAR		
SLIP	I(60 Hz)	Ir	I(60 Hz)	I(1-2s)f	Ir
	Amps	Amps	Amps	Amps	Amps
0	6.00	0	6.00	0	0
0.05	14.66	11.60	9.84	6.39	6.18
0.10	23.98	20.02	15.42	11.53	11.15
0.50	43.85	37.30	10.68	0	4.54
1.0	46.71	39.76	41.58	0	19.88

Table 3-2. 3-bar rotor exact results.

	NO BROKEN BARS		ONE BROKEN BAR		
SLIP	I(60 Hz)	Ir	I(60 Hz)	I(1-2s)f	Ir
	Amps	Amps	Amps	Amps	Amps
0	6.01	0	6.01	0	0
0.05	14.59	11.49	9.81	6.35	6.14
0.10	23.85	19.87	15.37	11.49	11.44
0.50	43.83	37.28	10.68	0	4.54
1.0	46.71	39.75	41.58	0	19.87

Table 3-3. 3-bar rotor simulation results.

	NO BROKEN BARS		ONE BROKEN BAR		
SLIP	I(60 Hz) % error	Ir % error	I(60 Hz) % error	I(1-2s)f % error	Ir % error
0	0.17	0	0.17	0	0
0.05	0.48	0.94	0.30	0.63	0.65
0.10	0.58	0.75	0.32	0.35	0.36
0.50	0.05	0.05	0	0	0
1.0	0	0.03	0	0	0.05

Table 3-4. Error between exact and simulation results.

For this simple machine, a broken rotor bar represents a significant change in the rotor magnetic circuit. As a result of this change, the stator phase current is also significantly altered. The drastic change of the stator phase current (in both the time and frequency domain) for a rotor slip of 0.05 is shown in figures 3-7, 3-8, 3-9, 3-10.

3-BAR ROTOR STATOR PHASE CURRENT
SIMULATION vs. EXACT RESULTS
NO BROKEN BARS
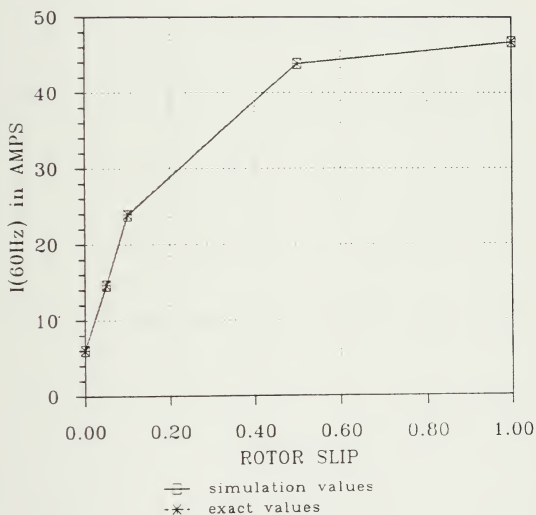
Figure 3-2. I(60 Hz) with no broken bars.

3-BAR ROTOR ROTOR LOOP CURRENT
SIMULATION vs. EXACT RESULTS
NO BROKEN BARS
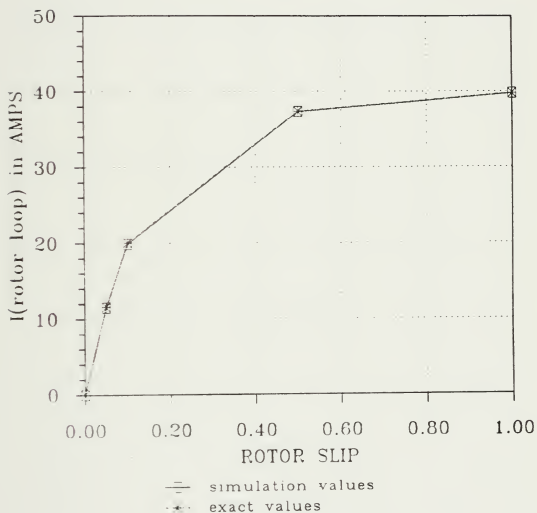
Figure 3-3. Ir with no broken bars.

3–BAR ROTOR STATOR PHASE CURRENT
SIMULATION vs. EXACT RESULTS
ONE BROKEN BAR
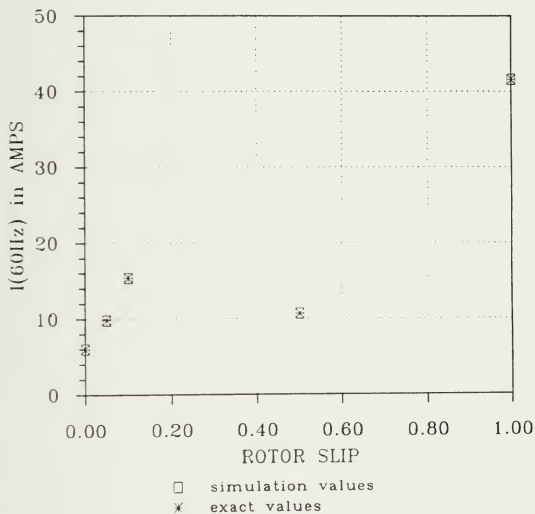
Figure 3-4. I(60 Hz) with one broken bar.

3-BAR ROTOR STATOR PHASE CURRENT
SIMULATION vs. EXACT RESULTS
ONE BROKEN BAR
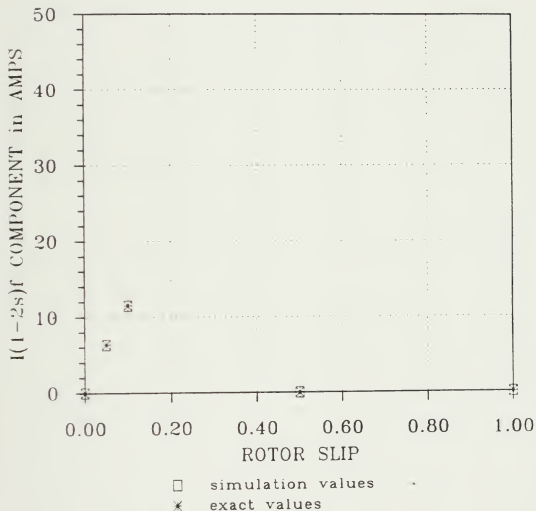
Figure 3-5. I(1-2s)f with one broken bar.

3-BAR ROTOR ROTOR LOOP CURRENT
SIMULATION vs. EXACT RESULTS
ONE BROKEN BAR
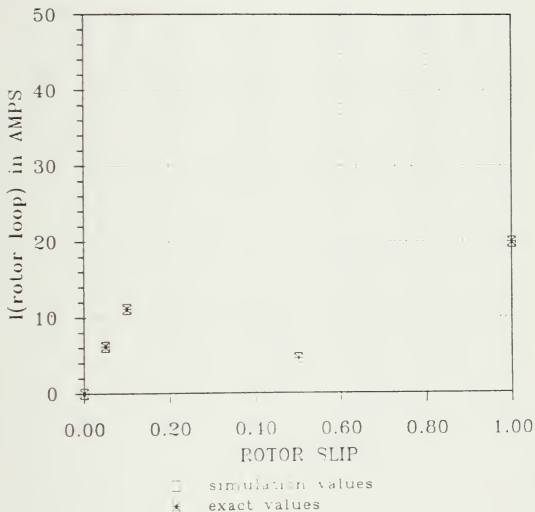
Figure 3-6. Ir with one broken bar.

99

SIMULATION STATOR PHASE CURRENT
3-BAR ROTOR slip=.05
NO BROKEN BARS
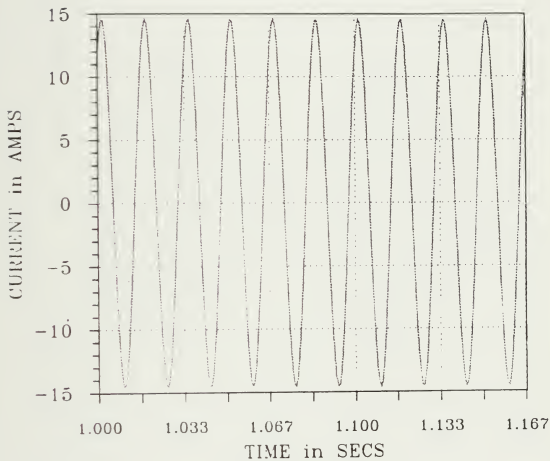
Figure 3-7. Stator phase current with no broken bars.

SIMULATION STATOR PHASE CURRENT
3-BAR ROTOR slip=.05
ONE BROKEN BAR
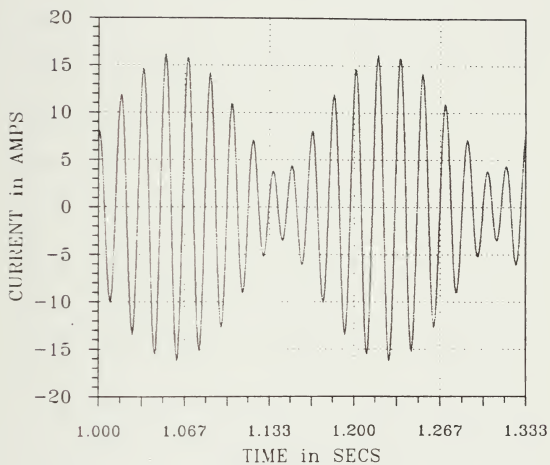
Figure 3-8. Stator phase current with one broken bar.

STATER PHASE FREQUENCY SPECTRUM
3-BAR ROTOR slip=.05
NO BROKEN BARS
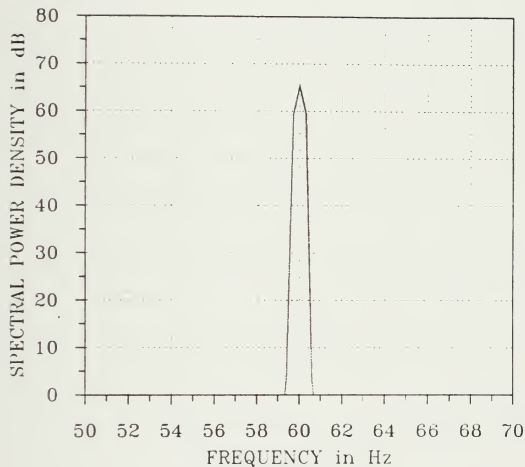
Figure 3-9. Frequency spectrum with no broken bars.
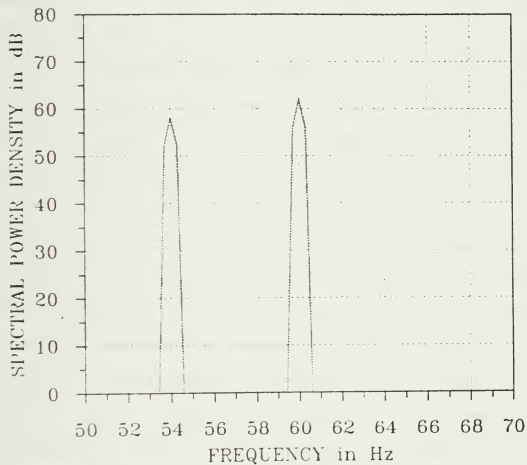
Figure 3-10. Frequency spectrum with one broken bar.

3.3 <u>Simulation</u> <u>Results</u> <u>For</u> <u>Experimental</u> <u>Motor</u>

Now that the simulation program has been initially
validated, it can be used to predict the results of a real
induction motor. These predicted results will then be
compared to actual experimental results to validate the
methodology presented in Chapter 2 and the simulation
program. A series of experiments will be conducted using a
3-phase, 3-HP, 230 V (line-to-line), 60 Hz, 1730 rpm
"off-the-shelf" induction motor. Due to testing facility
limitations (explained in Chapter 4), the experiments can
only be conducted for small values of rotor slip (0 to
0.04). Although this is a rather small range, it does cover
the full load operating range of the experimental motor. In
addition, only one rotor bar will broken. The following
sections present the simulation results for the experimen-
tal motor operating at small slip values with and without a
broken rotor bar. For the "no broken bar" simulations, the
simulation results are compared to the results calculated
using the single-phase, equivalent-circuit model for this
machine. The parameters required to simulate the
experimental motor are listed in Table 3-5. The
single-phase, equivalent-circuit model parameters were
determined using a least squares parameter estimation
routine [20].

PARAMETER	VALUE
R_1	0.8590 ohms
L_1	0.0046 H
L_{12}	0.0704 H
L_2	0.0046 H
R_2	0.5612 ohms
N_{RB}	45
p	2
Input Frequency	60 Hz
Input Phase Voltage	169.71 V

Table 3-5. Experimental motor parameters.

3.3.1 Case 1: No Broken Rotor Bars

The simulation results, equivalent-circuit model results, and the error between these results are given in Table 3-6. As expected, the error between the simulation and equivalent-circuit model results is less than 0.5% for each rotor slip value. Figure 3-11 shows the small difference between these results.

SLIP	SIMULATION I(60 Hz) Amps	EQ. CKT. MODEL I(60 Hz) Amps	% ERROR
0.0011	5.98	6.00	0.33
0.01	6.59	6.61	0.30
0.02	8.20	8.23	0.36
0.03	10.25	10.29	0.38
0.04	12.42	12.48	0.40

Table 3-6. Simulation results-no broken bars.

SIMULATION RESULTS FOR TEST MOTOR
STATOR PHASE CURRENT
NO BROKEN BARS
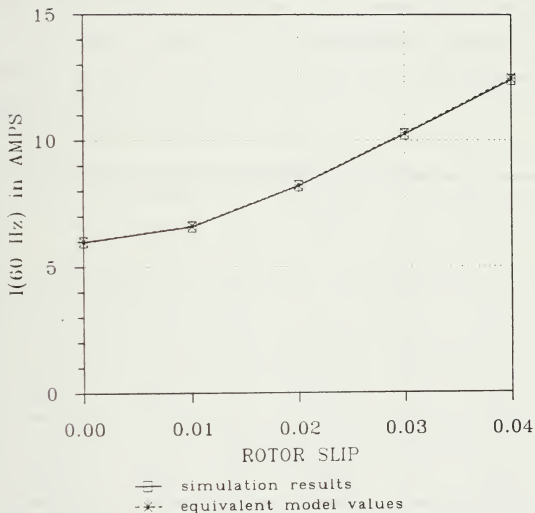
Figure 3-11. Simulation vs. equivalent circuit results.

3.3.2 Case 2: One Broken Rotor Bar

The simulation results for a one broken bar case are given in Table 3-7. Plots of the fundamental and (1-2s)f component of the stator phase current as a function of rotor slip are shown in Figures 3-12 and 3-13. The results show that the (1-2s)f component of the stator phase current increases approximately linearly with increasing rotor slip. Unlike the 3-bar rotor case above, there is only a slight change in the fundamental component with respect to the no-broken-bar case. This is demonstrated graphically in Figure 3-14.

SLIP	I(60 Hz) Amps	I(1-2s)f Amps	I(1-2s)f/I(60 Hz) %
0.0011	5.98	0	0
0.01	6.57	0.059	0.90
0.02	8.13	0.123	1.51
0.03	10.11	0.186	1.84
0.04	12.23	0.249	2.03

Table 3-7. Simulation results-one broken bar.

SIMULATION RESULTS FOR TEST MOTOR
STATOR PHASE CURRENT
ONE BROKEN BAR
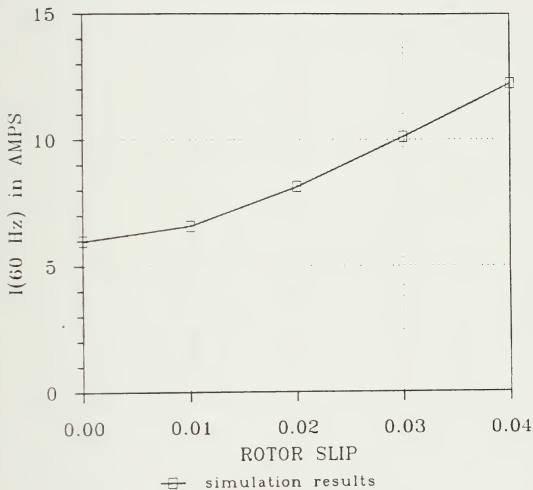
Figure 3-12. I(60 Hz) vs. slip.

SIMULATION RESULTS FOR TEST MOTOR
STATOR PHASE I(1-2s)f CURRENT
ONE BROKEN BAR
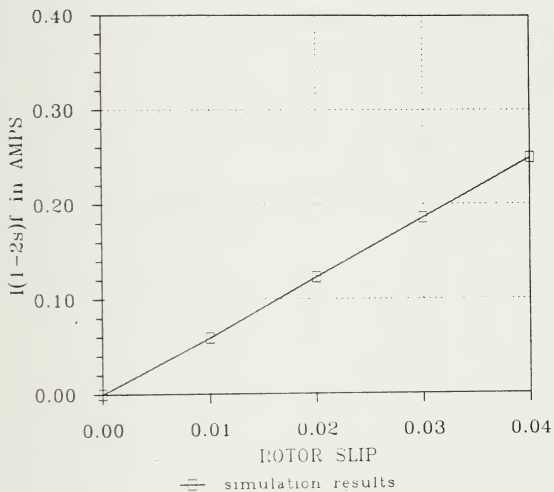
Figure 3-13. I(1-2s)f vs. slip.

SIMULATION RESULTS FOR TEST MOTOR
STATOR PHASE CURRENT
GOOD vs BAD ROTOR
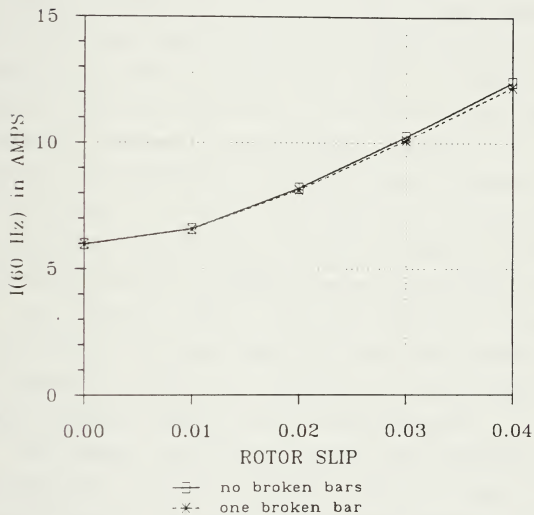
Figure 3-14. I(60 Hz) no vs. one broken bar.

3.4 Summary

A FORTRAN simulation routine has been developed to solve the system of equations describing the electrical performance of an induction motor derived in Chapter 2. The routine uses a fixed-step, fourth-order Runge-Kutta procedure to numerically integrate the system of equations. A matrix inversion routine, Cholesky's method with partial pivoting, is required to invert the time-varying inductance matrix for each value of time. The program can be used to simulate an induction motor with either no broken rotor bars or one broken rotor bar. In addition to the FORTRAN simulation program, two PRO-MATLAB routines, are also employed. The PRO-MATLAB eigenvalue routine is used to aid in determining the fixed time step for the Runge-Kutta integration. A PRO-MATLAB FFT routine is used to transform the output data of the FORTRAN program from the time domain to the frequency domain. Thus the harmonic frequency components of the stator phase and rotor loop currents can be determined. Appendix B includes the source code and sample input and output files for these routines.

The FORTRAN simulation program and PRO-MATLAB FFT routine were initially validated using a 3-bar rotor induction motor. The error between the simulation results and exact solutions for both a no-broken-bar and a

one-broken-bar case is less than 1%. The simulation program accurately solves the system of equations derived in Chapter 2 for the stator phase and rotor loop currents.

The simulation results for the experimental motor have been presented and will be compared to actual experimental results for final validation of the simulation program in Chapter 4.

CHAPTER 4

INVESTIGATION OF AN INDUCTION MOTOR

WITH A BROKEN ROTOR BAR

4.1 Introduction

A series of experiments was conducted using a set of initially identical "off-the-shelf" 3-HP squirrel-cage induction motors with various rotors modified so as to investigate their performance with and without a broken rotor bar. The magnitudes of the fundamental and $(1-2s)f$ harmonic components of the stator phase current were recorded. Two identical, "as manufactured" rotors were used to collect data corresponding to a "good" motor with no broken rotor bars. A third rotor, identical to the other two with the exception that a single rotor bar was deliberately open-circuited, was used to collect data corresponding to a "broken rotor bar" motor. A single stator was used with the rotors being swapped in and out for the various tests.

The nameplate data for the test motors is given in Table 4-1. As stated in the preceding paragraph, three rotors were alternately installed into the same stator for the experiments. Table 4-2 provides a summary for these rotors. For the broken bar rotor, one end of a single rotor bar was initially "disconnected" from the end ring by removing a small section of the rotor bar at the rotor bar-to-end ring interface with a milling machine. After the

114

initial tests were completed, the opposite end of the same
rotor bar was also "disconnected" from the other end ring
and a series of tests were again conducted using this rotor
(ROTOR #2.1).

Westinghouse Life-Long T AC Motor			
3-phase	60 Hz	3-HP	1730 rpm
230/460 V	9.4/4.7 A	182T frame	1.0 s.f.
catalog no.: 05-3H4SBFC-SKB		motor style: 773B646G41	

Table 4-1. Test motor nameplate data.

ROTOR #1	As manufactured; no broken bars.
ROTOR #2	One broken bar; one end open.
ROTOR #2.1	Same as ROTOR #2 with both ends open.
ROTOR #3	As manufactured; no broken bars.

Table 4-2. Rotor summary.

The experimental data collected for each motor serves
two primary purposes. First, comparison between the
experimental results and predicted results (presented in
Chapter 3) will be used to validate the computer simulation

program. Of interest is whether the simulation program accurately solves for the stator phase currents of an induction motor with and without a broken rotor bar. In addition, this comparison can provide an indication of the areas which must be added and/or modified, if required, in the simulation program to accurately describe the electrical performance of an induction motor with or without a broken rotor bar. Second, comparison of the experimental results for a "good" motor and a "broken rotor bar" motor can be used to make a quantitative decision regarding the feasibility of detecting broken rotor bars by monitoring the magnitude of the $(1-2s)f$ harmonic component of the stator phase current.

4.2 Description of Experimental Facility

The facilities used to conduct the experiments consists of four major components; a 208 V rms (line-to-line) 3-phase power supply, a dynamometer, a test motor, and a signal analyzer. A MAGTROL, Inc. model HD800-8 dynamometer is used to provide the load necessary to operate the test motor at various constant speeds (or rotor slips). Due to the kinetic power dissipation limit of the HD800-8, only small values of rotor slip (0-0.04) can be safely achieved. However, this range of rotor slips does cover the full load operating range of the test motors. For a rotor slip of 0.04, the test motor can be operated for approximately 10

minutes every two hours without exceeding the rating of the dynamometer. The control section for the HD800-8 provides digital read-outs for the following parameters:

stator phase current [A rms]

stator phase voltage [V rms]

stator phase power [W]

shaft speed [rpm]

shaft power [W]

shaft torque [N-m]

A Hewlett-Packard model HP-3561A dynamic signal analyzer is used to fast Fourier transform the stator phase current measurements and display the resulting frequency spectrum. The HP-3561A is a single-channel, multi-function signal analyzer. The analyzer was set-up to calculate and display the stator phase current frequency spectrum over a 20 Hz span centered at 60 Hz. For this setting, the frequency resolution of the analyzer is 0.05 Hz and a sample-time record length of 20 seconds is required to process the stator-current signal. Like the simulation program, a second-order Hanning window function is used to aid in distinguishing among frequency components which are relatively close. In order to increase the sig-nal-to-noise ratio of the input stator-current signal, a time averaging feature is used. Using this feature, five successive time records are averaged on a point-by-point

basis. Thus, for each test the analyzer requires approximately two minutes of stator phase current signals. The output units of the HP-3561A are volts rms squared. For the "typical" frequency spectrum plots included in this chapter (Figures 4-4, 4-8, 4-15, and 4-19), the following relation can be used to convert the analyzer output to amps rms

$$A \text{ rms} = 2.0\sqrt{(V \text{ rms})^2} \qquad (4-1)$$

where

$(V \text{ rms})^2$ = analyzer output reading

A major concern throughout the experimental portion of this research is the issue of data reproducibility. In an effort to increase the confidence level of the experimental data gathered, several tests were conducted for each rotor at each rotor slip value. For each test the magnitudes of the $(1-2s)f$ and fundamental components of the stator phase currents were recorded. These values were then averaged and the standard deviation was determined. The tests were continually repeated until the measured values were consistently within one standard deviation of the mean value. In addition to this, the averaging technique, number of averages, frequency span and resolution, etc. of the

118

HP-3561A were varied to ensure that the choice of analyzer settings was not introducing any error into the measurements.

4.3 Experimental Results and Analysis of a Motor With and Without a Broken Rotor Bar

The following sections provide a summary of the experimental data collected and corresponding analysis for each rotor. Appendix C contains tables of the measured data (the fundamental and (1-2s)f components of the stator phase current) for each rotor tested.

4.3.1 Experimental Results for a Motor Without a Broken Rotor Bar(ROTOR #1)

The averaged voltage and current data for ROTOR #1 is shown in Table 4-3. This is the baseline data. In addition to the fundamental and (1-2s)f components of the stator phase current, three other components were apparent, at frequencies (1+2s)f, (1-4s)f, and (1+4s)f. In general, the (1-4s)f and (1+4s)f components, when detected, were usually on the order of one-half the magnitude of the (1-2s)f component. As shown in Appendix D, these components could be produced by the third and fifth time-harmonics of the stator phase current. The (1+2s)f component is typically on the same order as the (1-2s)f component and is generally attributed to torque pulsations and the resulting speed oscillations at twice-the-slip

frequency [7,8,9,10,11]. In addition, this component could also be produced by the third time-harmonic of the stator phase current as shown in Appendix D. Table 4-4 lists the magnitudes of these components for a "typical" test at each each rotor slip value.

For all values of rotor slip, the non-fundamental harmonic components detected were less than 0.05% of the fundamental component of the stator phase current. From Table 4-3, the variation in the magnitude of the $(1-2s)f$ component is shown to be on the order of 25-30% of the mean value for this component. Figures 4-1 and 4-2 show the averaged data and raw data for the $(1-2s)f$ component. Figure 4-3 shows the averaged data for the fundamental component. Figure 4-4 shows the "typical" frequency spectrum for various rotor slip values.

SLIP	VOLTAGE V rms	I(60 Hz) MEAN A rms	I(60 Hz) STD. DEV. A rms	I(1-2s)f MEAN A rms	I(1-2s)f STD. DEV. A rms
0.01	123.3	4.76	0.06	0.0011	0.0003
0.02	123.1	6.00	0.15	0.0015	0.0005
0.03	122.7	7.37	0.11	0.0025	0.0005
0.04	122.5	8.98	0.12	0.0032	0.0009

Table 4-3. ROTOR #1 averaged data.

COMPONENT	s=0.01	s=0.02	s=0.03	s=0.04
(1-4s)f	<0.0001	<0.0001	0.0015	0.0022
(1-2s)f	0.0011	0.0014	0.0024	0.0026
60 Hz	4.940	5.926	7.642	8.626
(1+2s)f	0.0013	0.0016	0.0051	0.0035
(1+4s)f	<0.0001	0.0011	0.0020	0.0024
note: all values given in A rms				

Table 4-4. ROTOR #1 "typical" harmonic frequency data.

EXPERIMENTAL RESULTS
STATOR PHASE I(1−2s)f CURRENT
ROTOR #1
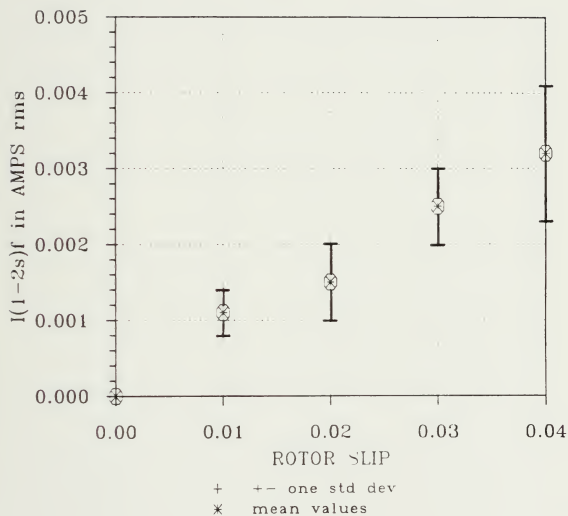
Figure 4-1. ROTOR #1 I(1-2s)f averaged results.

122

EXPERIMENTAL "RAW" RESULTS
STATOR PHASE I(1-2s)f CURRENT
ROTOR #1
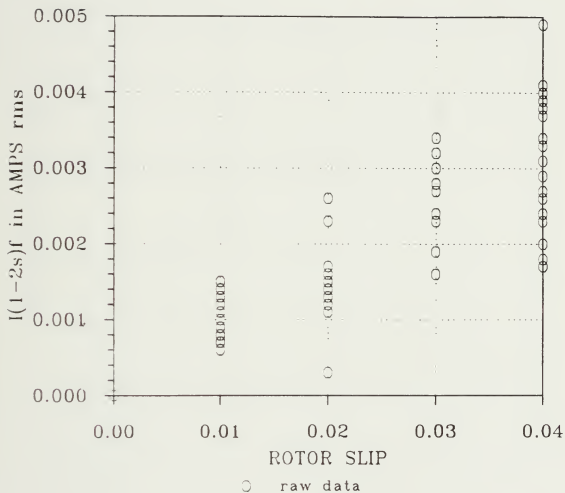
Figure 4-2. ROTOR #1 I(1-2s)f "raw" data.

123

EXPERIMENTAL RESULTS
STATOR PHASE 60 Hz CURRENT
ROTOR #1
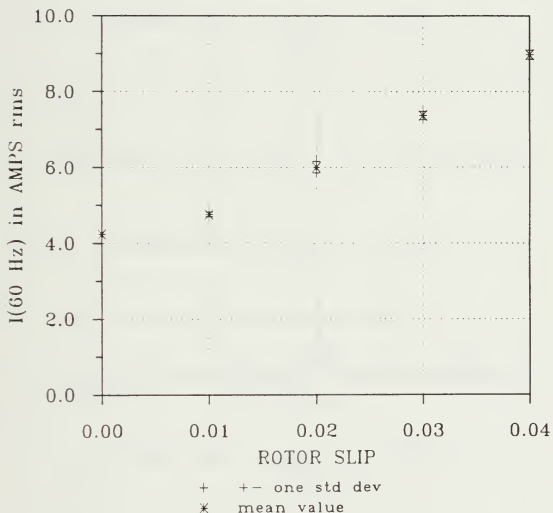
Figure 4-3. ROTOR #1 I(60 Hz) averaged results.
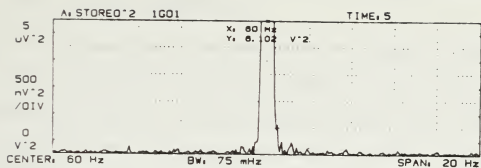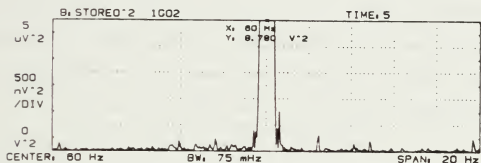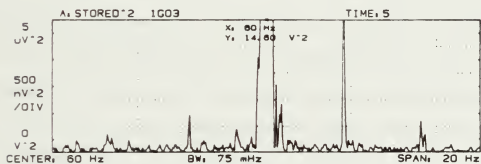
(a) slip=0.01
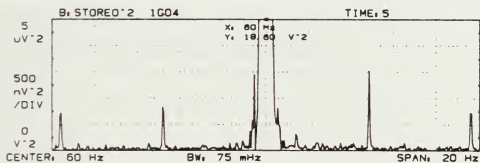
(b) slip=0.02

(c) slip=0.03

(d) slip=0.04

Figure 4-4. ROTOR #1 "typical" frequency spectrum.

4.3.2 Experimental Results for a Motor With a Broken Rotor Bar (one end open--ROTOR #2)

The averaged data for ROTOR #2 is shown in Table 4-5. Like the results obtained for ROTOR #1, the components at frequencies $(1+2s)f$, $(1-4s)f$, and $(1+4s)f$ were detected in addition to the fundamental and $(1-2s)f$ stator phase current harmonics. The $(1-4s)f$ and $(1+4s)f$ components, when detected, were usually on the order of one-half the magnitude of the $(1-2s)f$ component. The $(1+2s)f$ component was typically on the same order as the $(1-2s)f$ component. Table 4-6 lists the magnitudes of these components for a "typical" test at each rotor slip value.

For all values of rotor slip, the non-fundamental harmonic components detected were less than 0.05% of the fundamental component of the stator phase current. From Table 4-5, the variation in the magnitude of the $(1-2s)f$ component is shown to be on the order of 25-30% of the mean value for this component. Figures 4-5 and 4-6 show the averaged data and raw data for the $(1-2s)f$ component. Figure 4-7 shows the averaged data for the fundamental component. Figure 4-8 shows the "typical" frequency spectrum for various rotor slip values.

SLIP	VOLTAGE V rms	I(60 Hz) MEAN A rms	I(60 Hz) STD. DEV. A rms	I(1-2s)f MEAN A rms	I(1-2s)f STD. DEV. A rms
0.01	122.6	4.59	0.05	0.0013	0.0003
0.02	122.4	5.86	0.10	0.0018	0.0007
0.03	122.1	7.16	0.26	0.0023	0.0007
0.04	121.9	8.78	0.15	0.0023	0.0008

Table 4-5. ROTOR #2 averaged data.

COMPONENT	s=0.01	s=0.02	s=0.03	s=0.04
(1-4s)f	0.0016	0.0029	<0.0001	<0.0001
(1-2s)f	0.0013	0.0019	0.0019	0.0020
60 Hz	4.620	5.940	7.746	8.646
(1+2s)f	0.0012	0.0015	0.0018	0.0019
(1+4s)f	0.0029	0.0030	<0.0001	<0.0001
note: all values given in A rms				

Table 4-6. ROTOR #2 "typical" harmonic frequency data.

EXPERIMENTAL RESULTS
STATOR PHASE I(1-2s)f CURRENT
ROTOR #2
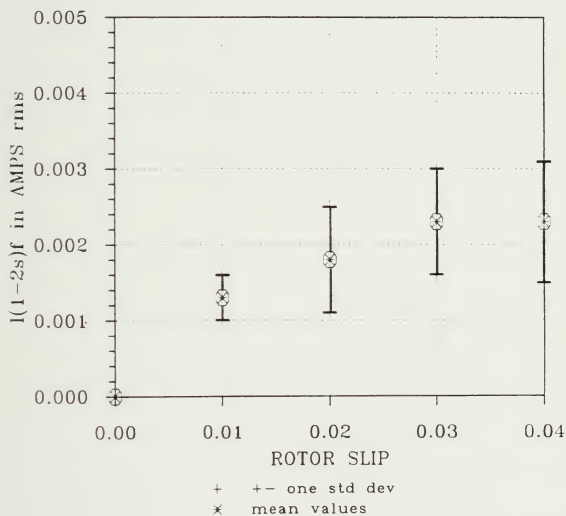
Figure 4-5. ROTOR #2 I(1-2s)f averaged results.

128

EXPERIMENTAL "RAW" RESULTS
STATOR PHASE I(1-2s)f CURRENT
ROTOR #2
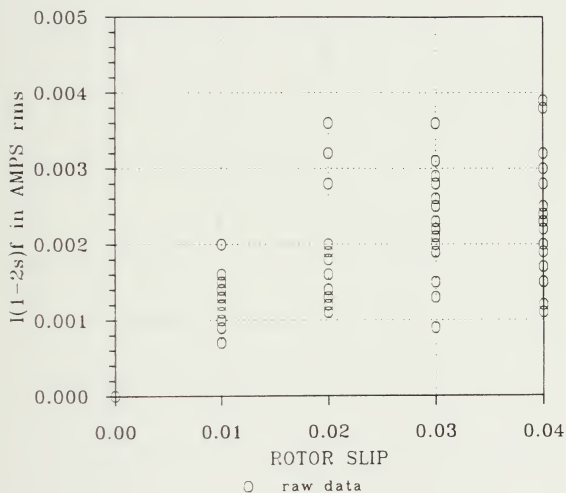
Figure 4-6. ROTOR #2 I(1-2s)f "raw" data.
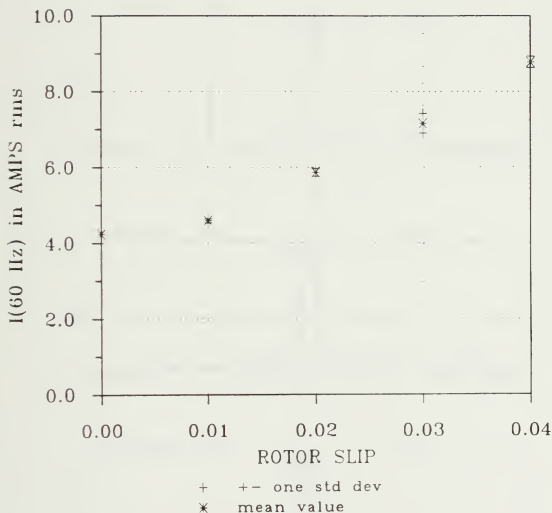
Figure 4-7. ROTOR #2 I(60 Hz) averaged results.
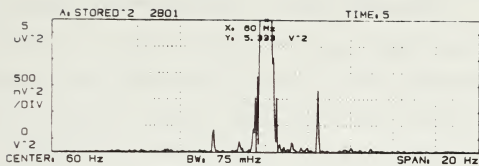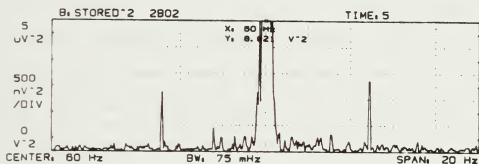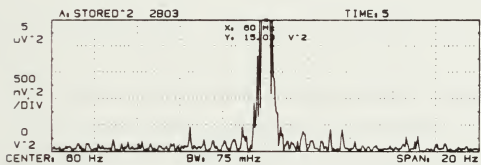
(a) slip=0.01
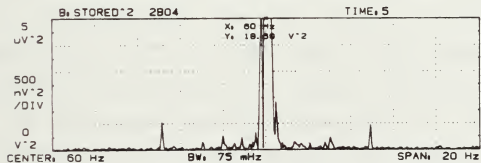
(b) slip=0.02

(c) slip=0.03

(d) slip=0.04

Figure 4-8. ROTOR #2 "typical" frequency spectrum.

4.3.3 Discussion of Simulation and Experimental Results for a Motor With and Without a Broken Rotor Bar

Tables 4-7 and 4-8 show the simulation results from Chapter 3 and experimental results of the fundamental and (1-2s)f harmonic components of the stator phase currents for a motor with and without a broken rotor bar. These tables show that the simulation program accurately solves for the fundamental component of the stator phase current for a motor with and without a broken rotor bar. This was expected since the input parameters for the simulation program are determined using the single-phase, equiv- alent-circuit model values for the test motors. However, for the (1-2s)f component, the simulation results and experimental results are significantly different. These unexpected differences raise two questions which must be answered.

First, why is the value of the (1-2s)f component of the stator phase current non-zero in a motor without a broken rotor bar? This question can be answered by considering the effect of manufacturing asymmetries on the stator phase current. From the analysis conducted by Kliman et al. [7], it was shown that manufacturing asymmetries (i.e., rotor out of round, rotating eccentric- ity, or non-uniform magnetic orientation of the rotor laminations) can also create airgap flux anomalies with a fundamental component on the same order as that of a

broken bar. This flux anomaly induces currents at a frequency of (1-2s)f in the stator phase windings. Thus, manufacturing asymmetries, which are present to some degree in all induction motors, can result in a non-zero (1-2s)f harmonic component of the stator phase current.

I(60 Hz) AMPS rms				
SLIP	"GOOD" MOTOR ROTOR #1	SIMULATION	"BROKEN BAR" MOTOR ROTOR #2	SIMULATION
0.01	4.76	4.79	4.59	4.65
0.02	6.00	5.95	5.86	5.87
0.03	7.37	7.41	7.16	7.24
0.04	8.98	8.96	8.78	8.79

Table 4-7. Simulation and experimental results I(60 Hz).

I(1-2s)f AMPS rms				
SLIP	"GOOD" MOTOR ROTOR #1	SIMULATION	"BROKEN BAR" MOTOR ROTOR #2	SIMULATION
0.01	0.0011	0	0.0013	0.0417
0.02	0.0015	0	0.0018	0.0870
0.03	0.0025	0	0.0023	0.1315
0.04	0.0032	0	0.0023	0.1761

Table 4-8. Simulation and experimental results I(1-2s)f.

The second question which must be answered is why are
the simulation results for the (1-2s)f component on the
order of 40 to 75 times greater than those measured for a
motor with a broken rotor bar. One possible mechanism is
that the bar was not completely broken. This could be the
case in the present experiments if the rotor bar was not
completely disconnected from the end ring during milling
so that path for current to flow still exists. In order to
demonstrate how this mechanism would result in a reduced
magnitude of the (1-2s)f component, the simulation program
was used to calculate the stator phase currents for a
motor with a rotor bar that has a higher series impedance
than the other rotor bars. For a rotor slip of 0.04, the
impedance (both the rotor bar resistance and leakage
inductance) of one rotor bar was varied (relative to the
impedance of a normal rotor bar) and the fundamental and
(1-2s)f components of the stator phase current was
calculated. These results are shown in Table 4-9 and
graphically in Figures 4-9 and 4-10. As expected, the
results show that the fundamental component of the stator
phase current remains approximately constant while the
magnitude of the (1-2s)f component increases as the rotor
bar impedance is increased. In addition, these results
indicate that only a 2% increase in the bar impedance is
required for the simulation program to predict the (1-2s)f
values measured for ROTOR #2. Certainly, the bar impedance

would increase by a substantially larger factor than 2% if a section of the rotor bar was removed (i.e., the broken bar on ROTOR #2).

After removing ROTOR #2 and visually inspecting the broken rotor bar, it was concluded that the rotor bar was completely cut away from the end ring. Thus it appears certain that current is not flowing into the broken bar across the break from the end ring.

RATIO OF BAR IMPEDANCE TO ALL OTHER BARS	I(60 Hz) AMPS rms	I(1-2s)f AMPS rms
1.0 ("good" motor)	8.78	0
1.1	8.77	0.0145
1.2	8.76	0.0269
1.5	8.74	0.0546
2.0	8.72	0.0834
5.0	8.68	0.1378
10.0	8.66	0.1566
infinity ("broken rotor bar motor")	8.65	0.1758
NOTE: all values for rotor slip=0.04		

Table 4-9. Bar impedance variation results.

BAR IMPEDANCE VARIATION RESULTS
SLIP=.04 1728 rpm
STATOR PHASE I(1−2s)f CURRENT
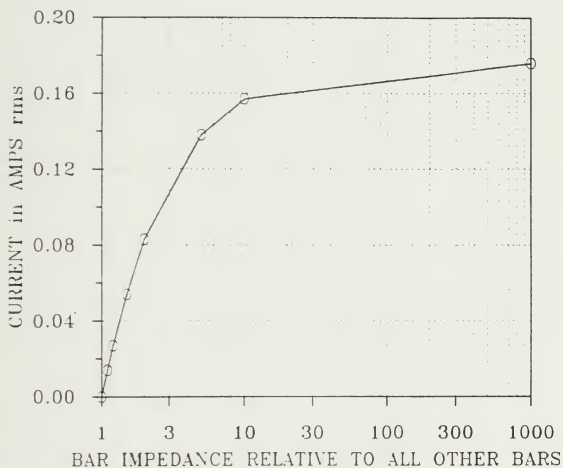
Figure 4-9. Bar impedance variation I(1-2s)f.

BAR IMPEDANCE VARIATION RESULTS
SLIP=.04 1728 rpm
STATOR PHASE 60 Hz CURRENT
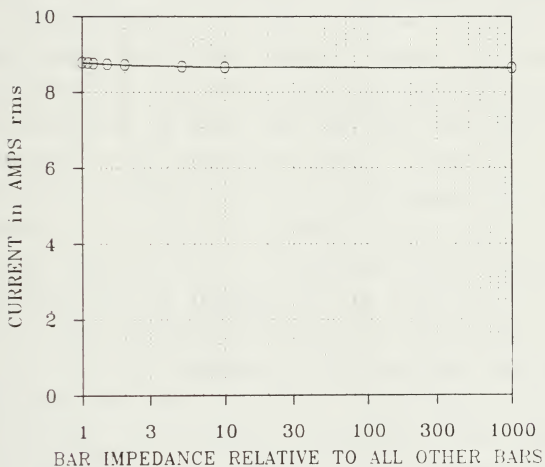
Figure 4-10. Bar impedance variation I(60 Hz).

137

Another mechanism that could result in a current flowing through a broken rotor bar is that of inter-bar currents. Inter-bar currents are currents which flow between a rotor bar and adjacent rotor bars through the rotor laminations. The presence of such currents could be expected to "short circuit" the effect of a break in a rotor bar, hence resulting in a current flow in the broken bar that would not be predicted by the simulation program.

The existence of large inter-bar currents in three-phase squirrel-cage induction motors with broken rotor bars has been analyzed and experimentally verified by Kerszenbaum and Landy [9]. They have shown that the magnitude of the inter-bar current is a function of the rotor-bar impedance and the distributed inter-bar impedance. The inter-bar impedance is the sum of the contact impedance of the rotor bar-to-rotor lamination interface and the impedance of the rotor core (i.e., laminations) between two adjacent rotor bars. As the ratio of the rotor-bar impedance to the inter-bar impedance increases, the magnitude of the current flowing into a broken rotor bar approaches the magnitude of the current which would flow into a "healthy" (i.e., not broken) rotor bar for the same operating conditions. This is shown in Figure 4-9 where

I_{bb} = current flowing in a broken bar

I_H = current flowing in a "healthy" bar

Z_b = rotor-bar impedance

R_c = inter-bar impedance
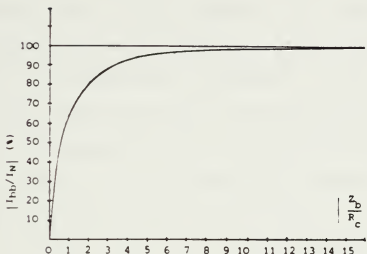
Figure 4-11. Ratio of current in a broken bar to a "healthy" bar [9].

4.4 Experimental Results for a Motor With a Broken Rotor Bar (both ends open--ROTOR #2.1)

In order to investigate the hypothesis that inter-bar currents were masking the effects of the break in the rotor bar during experiments with ROTOR #2, the opposite end of the broken rotor bar on ROTOR #2 was also cut away from the end ring, resulting in the rotor known as ROTOR #2.1. This was expected to result in a further decrease in the magnitude of the current flowing through the broken rotor bar thus, increasing the resulting magnitude of the (1-2s)f component of the stator phase current.

The averaged data for ROTOR #2.1 is shown in Table 4-10. Once again the (1-4s)f, (1+2s)f, and (1+4s)f harmonic components were detected. Table 4-11 lists the magnitudes of these components for a "typical" test at each each rotor slip value. For all values of rotor slip, the non-fundamental harmonic components detected were less than 0.25% of the fundamental component of the stator phase current. From Table 4-10, the variation in the magnitude of the (1-2s)f component is shown to be on the order of 10-25% of the mean value for this component. Figures 4-12 and 4-13 show the averaged data and raw data for the (1-2s)f component. Figure 4-14 shows the averaged data for the fundamental component. Figure 4-15 shows the "typical" frequency spectrum for various rotor slip values.

Tables 4-12 and 4-13 show the values of the fundamental and (1-2s)f components of the stator phase current measured for ROTOR #2 and ROTOR #2.1, and the simulation results for a broken rotor bar case. Comparison of the data shown in Table 4-12 shows that the fundamental component of the stator phase currents for both rotors and the simulation are approximately the same. For the (1-2s)f component shown in Table 4-13, the values for ROTOR #2.1 are significantly greater (by a factor of 4 to 8) than those for ROTOR #2. This result strengthens the hypothesis that inter-bar currents are present and that significant current is flowing through the broken rotor bar on ROTOR #2. The

simulation results for the (1-2s)f component indicates that current is still flowing in the broken rotor bar on ROTOR #2.1.

SLIP	VOLTAGE V rms	I(60 Hz)		I(1-2s)f	
		MEAN A rms	STD. DEV. A rms	MEAN A rms	STD. DEV. A rms
0.01	123.1	4.66	0.13	0.0041	0.0011
0.02	122.9	5.93	0.21	0.0073	0.0009
0.03	122.5	7.26	0.20	0.0128	0.0010
0.04	122.2	8.61	0.15	0.0172	0.0023

Table 4-10. ROTOR #2.1 averaged data.

COMPONENT	s=0.01	s=0.02	s=0.03	s=0.04
(1-4s)f	<0.0001	<0.0001	0.0041	0.0068
(1-2s)f	0.0041	0.0087	0.0121	0.0184
60 Hz	4.757	5.930	7.253	8.420
(1+2s)f	0.0032	0.0074	0.0105	0.0196
(1+4s)f	<0.0001	<0.0001	0.0054	0.0089
note: all values given in A rms				

Table 4-11. ROTOR #2.1 "typical" harmonic frequency data.

I(60 Hz) AMPS rms			
SLIP	ROTOR #2	ROTOR #2.1	SIMULATION
0.01	4.59	4.66	4.65
0.02	5.86	5.93	5.87
0.03	7.16	7.26	7.24
0.04	8.78	8.61	8.79

Table 4-12. Broken bar results I(60 Hz)

I(1-2s)f AMPS rms			
SLIP	ROTOR #2	ROTOR #2.1	SIMULATION
0.01	0.0013	0.0041	0.0417
0.02	0.0018	0.0073	0.0870
0.03	0.0023	0.0128	0.1315
0.04	0.0023	0.0172	0.1761

Table 4-13. Broken bar results I(1-2s)f

EXPERIMENTAL RESULTS
STATOR PHASE I(1−2s)f CURRENT
ROTOR #2.1
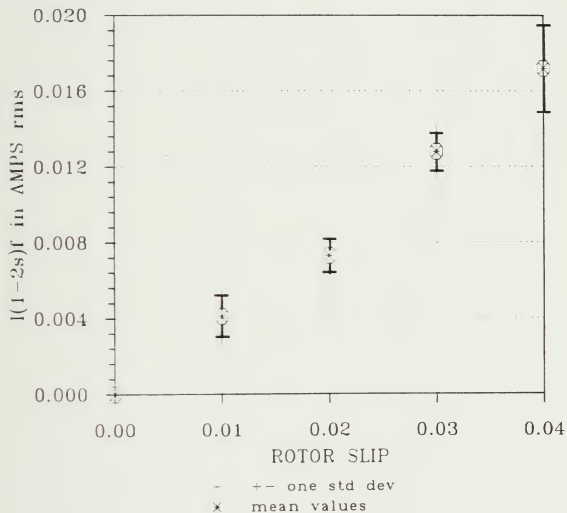
Figure 4-12. ROTOR #2.1 I(1−2s)f averaged results.

143

EXPERIMENTAL "RAW" RESULTS
STATOR PHASE I(1−2s)f CURRENT
ROTOR #2.1
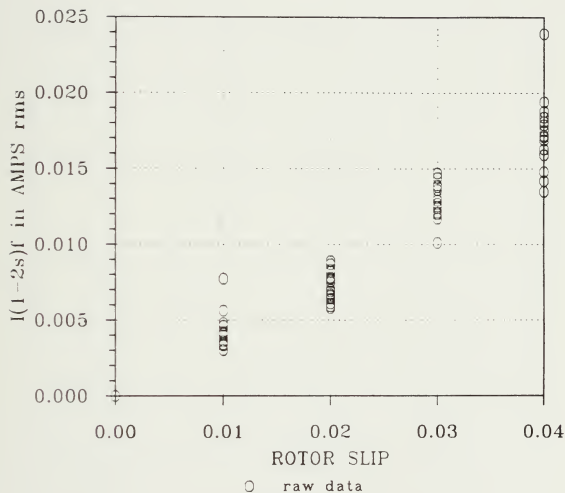
Figure 4-13. ROTOR #2.1 I(1-2s)f "raw" data.

EXPERIMENTAL RESULTS
STATOR PHASE 60 Hz CURRENT
ROTOR #2.1
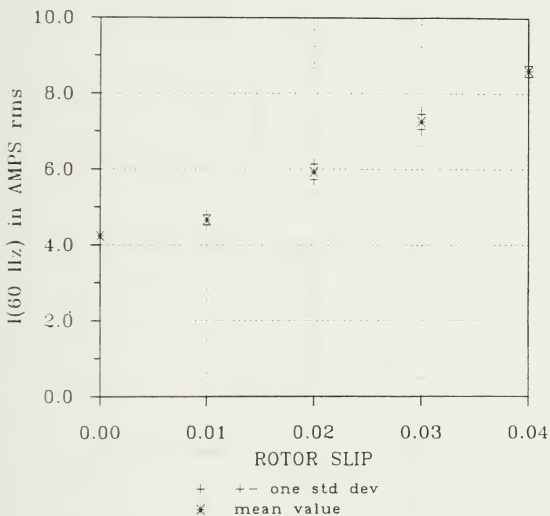
Figure 4-14. ROTOR #2.1 I(60 Hz) averaged results.
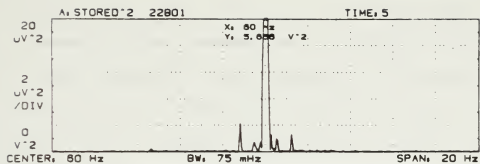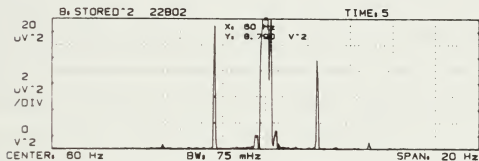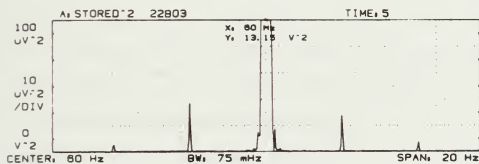
(a) slip=0.01
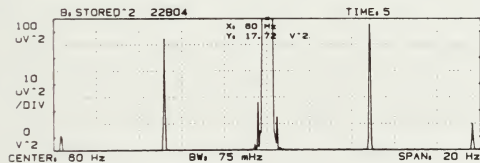
(b) slip=0.02

(c) slip=0.03

(d) slip=0.04

Figure 4-15. ROTOR #2.1 "typical" frequency spectrum.

4.5 <u>Additional</u> <u>Results</u> <u>for</u> <u>a</u> <u>"Good"</u> <u>Motor</u> <u>(ROTOR #3)</u>

In order to see the effects on the stator phase current due to manufacturing asymmetries, a second "as manufactured" rotor (ROTOR #3) was installed in the test motor. The averaged data for ROTOR #3 is shown in Table 4-14. Once again the $(1-4s)f$, $(1+2s)f$, and $(1+4s)f$ harmonic components were detected. Table 4-15 lists the magnitudes of these components for a "typical" test at each each rotor slip value. For all values of rotor slip, the non-fundamental harmonic components detected were less than 0.05% of the fundamental component of the stator phase current. From Table 4-14, the variation in the magnitude of the $(1-2s)f$ component is shown to be on the order of 20-30% of the mean value for this component. Figures 4-16 and 4-17 show the averaged data and raw data for the $(1-2s)f$ component. Figure 4-18 shows the averaged data for the fundamental component. Figure 4-19 shows the "typical" frequency spectrum for various rotor slip values.

Comparison of the data for ROTOR #1 (Table 4-3) and for ROTOR #3 (Table 4-14) shows that the fundamental component of the stator phase currents for both motors is approximately the same. For the $(1-2s)f$ component, the values for ROTOR #1 are approximately two times greater than those for ROTOR #3. This result indicates that the degree of manufacturing asymmetries in ROTOR #1 is somewhat larger than those in ROTOR #3.

147

SLIP	VOLTAGE V rms	I(60 Hz)		I(1-2s)f	
		MEAN A rms	STD. DEV. A rms	MEAN A rms	STD. DEV. A rms
0.01	122.7	4.63	0.07	0.0007	0.0003
0.02	122.4	5.84	0.07	0.0006	0.0002
0.03	122.1	7.18	0.18	0.0011	0.0003
0.04	121.8	8.65	0.05	0.0013	0.0002

Table 4-14. ROTOR #3 averaged data.

COMPONENT	s=0.01	s=0.02	s=0.03	s=0.04
(1-4s)f	<0.0001	<0.0001	0.0015	0.0023
(1-2s)f	0.0005	0.0006	0.0008	0.0016
60 Hz	4.630	5.930	7.156	8.646
(1+2s)f	0.0008	0.0005	0.0007	<0.0001
(1+4s)f	<0.0001	0.0015	0.0023	0.0028
note: all values given in A rms				

Table 4-15. ROTOR #3 "typical" harmonic frequency data.

148
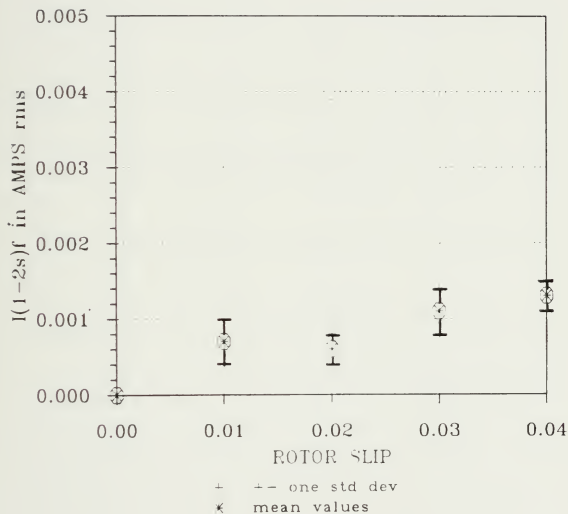
Figure 4-16. ROTOR #3 I(1-2s)f averaged results.
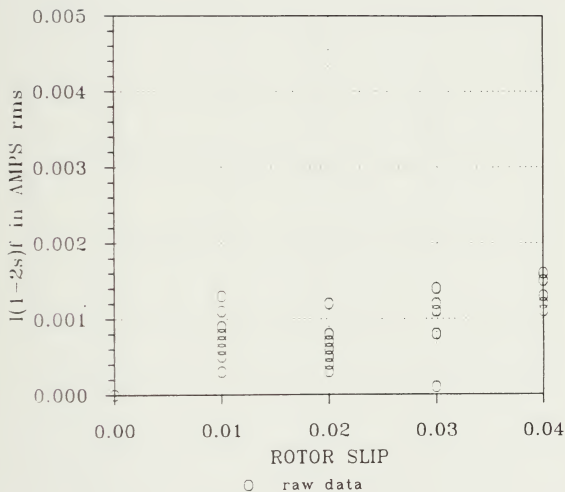
Figure 4-17. ROTOR #3 I(1-2s)f "raw" data.
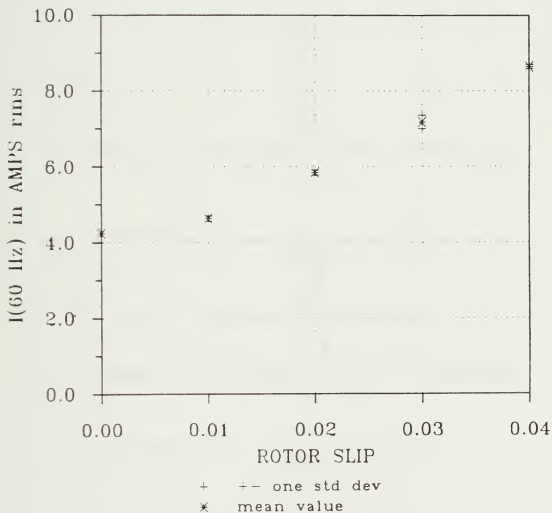
Figure 4-18. ROTOR #3 I(60 Hz) averaged results.

151
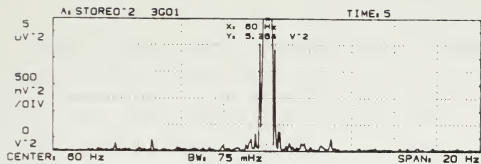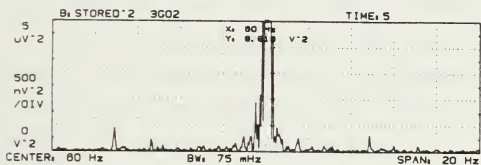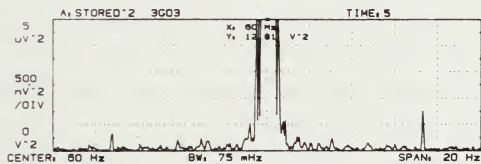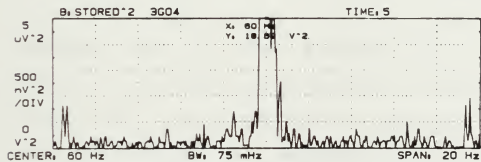
Figure 4-19. ROTOR #3 "typical" frequency spectrum.

4.6 Summary

The fundamental and (1-2s)f harmonic components of the stator phase current were recorded for an "off-the-shelf" 3-HP squirrel-cage induction motor with various rotors installed. Two "as manufactured" rotors with no broken rotor bars and a third rotor with a single rotor bar deliberately open-circuited were used for the experiments. The broken bar rotor was initially tested with only one end of the broken bar disconnected from the end ring. Subsequently, the opposite end of the broken bar was disconnected from the other end ring and a series of experiments were completed using this rotor.

For each rotor tested, in addition to the fundamental and (1-2s)f components of the stator phase current, significant components at the frequencies (1-4s)f, (1+2s)f, and (1+4s)f were detected. The (1-4s)f and (1+4s)f components can be produced by the third and fifth time-harmonic components of the stator phase currents as shown in Appendix D. The (1+2s)f component can be attributed to the torque pulsations and the resulting speed oscillations at twice-the-slip frequency [7,8,9,10,11]. This component can also be produced by the third time-harmonic of the stator phase current. In general, the magnitudes of the (1-4s)f and (1+4s)f components were on the order of one-half the magnitude of the (1-2s)f component. The magnitude of the (1+2s)f component is

approximately the same as the (1-2s)f component. For the two "good" rotors (ROTOR #1 and ROTOR #3) and the broken bar rotor with one end disconnected (ROTOR #2), the magnitude of these harmonic components was less than 0.05% of the fundamental component. For the broken rotor bar with both ends disconnected (ROTOR #2.1), the magnitude of these components increased five-fold.

Comparison of the experimental and simulation results for a motor with and without a broken rotor bar has shown that a more complex simulation model is required to accurately predict the (1-2s)f component of the stator phase current. In particular, the model must be able to account for manufacturing asymmetries which are present to some degree in all induction motors and it also must be able to model the effects of inter-bar currents.

The existence of inter-bar currents in a squirrel-cage induction motor of the type tested in this thesis effectively "masks" the effects of a broken rotor bar. These currents reduce the magnitude of the (1-2s)f component of the stator phase current to a value on the order of those present in a "good" rotor due to manufacturing asymmetries. Thus, distinguishing a broken rotor bar from a manufacturing asymmetry using only the (1-2s)f component of the stator phase current appears very difficult. This effect is illustrated in Figure 4-20, where the values of the (1-2s)f component for the four rotors

154

Figure 4-20. Simulation and experimental results I(1-2s)f.

155

tested and for the simulation program are plotted as a function of rotor slip. A distinction between a broken rotor bar and a manufacturing asymmetry is only possible after both ends of the broken rotor bar are disconnected from the end ring.

As a final note, if the single-test diagnostic algorithm of Kliman et al. [7] (see Chapter 1) were used, a motor with either ROTOR #1, ROTOR #2, or ROTOR #3 installed would be declared a "good" motor. For a motor with ROTOR #2.1 installed, the measured dB value (-54 dB) falls in the region between a "good" motor and a "broken rotor bar" motor and thus would be declared "suspect".

CHAPTER 5

CONCLUSIONS AND RECOMMENDATIONS FOR FUTURE RESEARCH

5.1 Summary of Thesis

The purpose of this thesis was to critically evaluate one method for the detection of broken rotor bars in induction motors using stator current and voltage measurements. This effort supported the ongoing development of a failure analysis system for electric machines by the M.I.T. Laboratory for Electromagnetic and Electronic Systems. The hypothesis of the method, given a sinusoidally applied voltage, was that the presence of certain harmonics in the stator currents could be used to detect the presence of broken rotor bars.

To support the evaluation, a system of first-order differential equations describing the electrical performance of a three-phase induction motor was developed using stator phase currents and rotor loop currents as state variables. Each stator phase and rotor loop was described in terms of a resistance and inductance. The stator phase voltages (assumed to be sinusoidal) were the driving functions for the system.

A relationship between the standard single-phase, equivalent-circuit model for an induction motor and the system of equations was derived (Equations 2-100 to 2-106). With this relationship, the electrical parameters needed to solve the system of equations were easily calculated from

157

the single-phase, equivalent-circuit parameter values which are often available from the manufacturer, or are easily measured in the laboratory. This relationship was useful in that the solution to the system of equations could be obtained without disassembling the motor, removing the rotor, and measuring the geometrical and material properties of the motor such as the rotor radius, the airgap length, and conductivity of the rotor bars. Thus, by performing the standard no-load, locked-rotor, and DC tests and knowing the number of rotor bars, the system of equations could be used to simulate a three-phase induction motor with an arbitrary number of rotor bars.

A FORTRAN simulation routine was developed to solve the system of equations describing the electrical performance of an induction motor with or without a broken rotor bar. The routine uses a fixed-step, fourth-order Runge-Kutta procedure to numerically integrate the system of equations. A matrix inversion routine, Cholesky's method with partial pivoting, was required to invert the time-varying inductance matrix for each value of time. In addition to the FORTRAN simulation program, two PRO-MATLAB routines were also employed. The PRO-MATLAB eigenvalue routine was used to aid in determining the fixed time step for the Runge-Kutta integration. A PRO-MATLAB FFT routine was used to transform the output data of the FORTRAN program from

the time domain to the frequency domain. Thus the fundamental and (1-2s)f frequency components of the stator phase currents could be determined.

The FORTRAN simulation program and PRO-MATLAB FFT routine were initially validated using a hypothetical 3-bar rotor induction motor. The errors between the simulation results and exact solutions for both the no-broken-bar and the one-broken-bar cases were less than 1%. The simulation program accurately solved the system of equations derived for the stator phase currents and rotor loop currents. Thus, the simulation permitted numerical experiments which were used to test the failure detection hypothesis.

For the numerical experiments, the single-phase, equivalent-circuit parameter values for an "off-the-shelf" 3-HP squirrel-cage induction motor were used as inputs to the simulation routine. Thus, the simulations represented the operation of the same motors which were used for the physical experiments. The results of the simulation for a no-broken-bar case showed only a fundamental component of the stator phase currents. However, for the one-broken-bar case, the simulation showed that an additional component at a frequency of (1-2s)f was also present in the stator phase current. The magnitude of this component was approximately 2% of the magnitude of the fundamental component for the full load operating speed of the motor. Thus, the failure detection hypothesis appeared plausible and physical

experiments were undertaken to verify that the $(1-2s)f$ component of the stator phase current could be used to detect the presence of a broken rotor bar.

The physical experiments were conducted with commercially-available induction motors. The fundamental and $(1-2s)f$ harmonic components of the stator phase current were recorded for an "off-the-shelf" 3-HP squirrel-cage induction motor with various rotors installed. Two "as manufactured" rotors with no broken rotor bars and a third rotor with a single rotor bar deliberately disconnected from the end ring by removing a small section of the rotor bar were used for the experiments. The broken-bar rotor was initially tested with only one end of the broken bar disconnected from the end ring. Subsequently, the opposite end of the broken bar was cut away from the other end ring and a series of experiments was completed using this rotor.

For the two "good" rotors tested, the $(1-2s)f$ component of the stator phase current was detected. The magnitude of this component was approximately 0.05% of the fundamental component. The $(1-2s)f$ component was present in a "good" rotor due to manufacturing asymmetries which are present to some degree in all machines. The measured values of the $(1-2s)f$ component for the broken bar rotor with one end disconnected were also only 0.05% of the fundamental component. Thus, using only the $(1-2s)f$ component of the stator phase current, the distinction between manufacturing

asymmetries and a broken rotor bar was impossible. This result was significantly different than that predicted by the simulation program.

In order to explain the differences between the simulation and experimental results, a hypothesis that current was still flowing through the broken rotor bar was investigated. One possible mechanism was that the bar was not completely broken. This could be the case in the present experiments if the rotor bar was not completely disconnected from the end ring during milling so that path for current to flow still exists. After removing the rotor and visually inspecting the broken rotor bar, it was concluded that the rotor bar was completely cut away from the end ring. Thus it appeared certain that current is not flowing into the broken bar across the break from the end ring.

Another mechanism that could result in a current flowing through a broken rotor bar was that of inter-bar currents. Inter-bar currents are currents which flow between a rotor bar and adjacent rotor bars through the rotor laminations. The presence of such currents could be expected to "short circuit" the effect of a break in a rotor bar, hence resulting in a current flow in the broken bar that would not be predicted by the simulation program.

In order to investigate the hypothesis that inter-bar currents were masking the effects of the break in the rotor

bar during experiments with the broken bar rotor, the opposite end of the broken rotor bar was also cut away from the end ring. This was expected to result in a further decrease in the magnitude of the current flowing through the broken rotor bar, thus increasing the resulting magnitude of the (1-2s)f component of the stator phase current. The measured values of the (1-2s)f component for this rotor were on the order of 4 to 8 times greater than the previous results. This strengthened the hypothesis that inter-bar currents were flowing and that significant current was flowing through the broken rotor bar with one end disconnected during the previous tests. In addition, the simulation results were still an order of magnitude greater than the measured results for the broken rotor bar with both ends disconnected, thus indicating that current was still flowing in the broken rotor bar.

5.2 Conclusion

The existence of inter-bar currents in a squirrel-cage induction motor of the type tested in this thesis effectively "masks" the effects of a broken rotor bar. These currents reduce the magnitude of the (1-2s)f component of the stator phase current to a value on the order of those already present in a "good" rotor due to manufacturing asymmetries. The distinction between a broken rotor bar and a manufacturing asymmetry is only possible after both ends of a rotor bar are cut away from the end

ring. Thus, distinguishing a broken rotor bar from a manufacturing asymmetry using only the (1-2s)f component of the stator phase current appears highly improbable.

5.3 Recommendations for Future Work

Although the results of this thesis show that the detection of a broken rotor bar in a squirrel-cage induction motor of the type tested is highly improbable using only the (1-2s)f component of the stator phase current, examination of the higher-order stator phase current harmonics may provide a basis for distinguishing between a broken rotor bar and manufacturing asymmetries. Kliman et al. [7] has shown that the higher-order harmonic components of the airgap flux resulting from a broken rotor bar are typically much larger than those resulting from manufacturing asymmetries. Thus, an investigation of the effects on the higher-order stator phase current harmonics due to a broken rotor bar is needed if the failure analysis system is to be based solely on the measurements of terminal voltages and currents. In addition, the effects of inter-bar currents would have to be modeled in detail.

In order to use the simulation program developed in this thesis in a failure analysis system for electrical machines, the program must be modified to include the effects of inter-bar currents. This requires an in-depth analysis on the existence of and effects of inter-bar currents in squirrel-cage induction motors. In addition to

modifying the simulation program, changes in the current manufacturing process for squirrel-cage rotors may be recommended based on this analysis (e.g., insulation between the rotor bars and laminations).

Axial flux monitoring [11] is another method which has been successful in detecting broken rotor bars, as well as various other faults, in operating induction machines. Although this method requires that an external sensing coil be attached to a machine, it appears to be very promising and can be implemented into a failure analysis system. This method is currently being investigated at the M.I.T. Laboratory for Electromagnetic and Electronic Systems [21].

REFERENCES

1. P. E. Albrecht, et al., "Assessment of the reliability of motors in utility applications", <u>IEE-IAS</u> <u>Annual Meeting Conference Record</u>, Chicago, 1984, pp. 364-366.

2. C. R. Heising and P. O'Donnell, "Summary of results from IEEE survey of the reliability of large motors in industrial and commercial installations", <u>Proceedings of the 12TH INTER-RAM Conference for the Electric Power Industry</u>, 1985, pp. 386-392.

3. IEEE Committee Report, P. O'Donnell, coordinating author, "Report of large motor reliability survey of industrial and commercial installations-- parts 1-3", <u>Industrial and Commercial Power Systems Technical Conference</u>, May 1983,84,85.

4. J. H. Lang and G. C. Verghese, "A proposal to study the reliability improvement of electrical machines", Unpublished research proposal, MIT Laboratory for Electromagnetic and Electronic Systems, July 1986.

5. J. L. Kirtley, J. H. Lang, F. C. Schweppe, and S. D. Umans, "Ship service power system development", Unpublished research proposal, MIT Laboratory for Electromagnetic and Electronic Systems, June 1986.

6. J. R. Smith, "Editorial on plant condition monitoring", <u>IEE Proceedings</u>, vol. 133, part B, no. 3, May 1986, pp. 142-148.

7. G. B. Kliman, R. A. Koegl, J. Stein, R. D. Endicott, and M. W. Madden, "Noninvasive detection of broken rotor bars in operating induction motors", Paper presented at IEEE/PES 1988 Winter Meeting, New York, February 1988.

8. C. Hargis, B. G. Gaydon, and K. Kamash, "The detection of rotor defects in induction motors", <u>IEE Electric Machinery Design and Application Conference Record</u>, London, July 1982, pp. 216-220.

9. I. Kerszenbaum and C. F. Landy, "The existence of large inter-bar currents in three phase squirrel cage motors with rotor-bar and/or end-ring faults", <u>IEEE Transaction on Power Apparatus and Systems</u>, vol. PAS-103, no. 7, July 1984, pp. 1854-1862.

10. S. Williamson and A. C. Smith, "Steady-state analysis of 3-phase cage motors with rotor-bar and end-ring faults", _IEE Proceedings_, vol. 129, part B, no. 3, May 1982, pp. 93-100.

11. J. Penman, M. N. Dey, A. J. Tait, and W. E. Bryan, "Condition monitoring of electrical drives", _IEE Proceedings_, vol. 133, part B, no. 3, May 1986, pp. 142-148.

12. A. E. Fitzgerald, C. Kingsley, Jr., and S. D. Umans, _Electric Machinery_. New York, NY: McGraw-Hill, 1983.

13. M. L. James, G. M. Smith, and J. C. Wolford, _Applied Numerical Methods for Digital Computation with Fortran and CSMP_. New York: Harper and Row, 1977.

14. G. E. Forsythe, M. A. Malcolm, and C. B. Moler, _Computer Methods for Mathematical Computations_. Englewood Cliffs, NJ: Prentice Hall, 1977.

15. J. M. McCormick and M. G. Salvadori, _Numerical Methods in FORTRAN_. Englewood Cliffs, NJ: Prentice Hall, 1964.

16. A. R. Miller, _FORTRAN Programs for Scientists and Engineers_. Berkeley, CA: Sybex, 1982.

17. T. E. Shoup, _Numerical Methods for the Personal Computer_. Englewood Cliffs, NJ: Prentice Hall, 1983.

18. F. J. Harris, "On the use of windows for harmonic analysis with the discrete fourier transform", _Proceedings of the IEEE_, vol. 66, no. 1, January 1978, pp. 51-83.

19. G. D. Bergland, "A guided tour of the fast fourier transform", _IEEE Spectrum_, vol. 6, no. 7, July 1969, pp. 41-52.

20. R. Cho, S. M. Thesis in progress, MIT Department of EECS, March 1988.

21. S. Neville, "Axial leakage-flux measurements on polyphase induction motors", S. B. Thesis, MIT Department of EECS, May 1988.

APPENDIX A

ELEMENTS FOR SYSTEM MATRICES

The following sections give the expressions for the elements of the voltage, inductance, and effective resistance matrices derived in Chapter 2 (NOTE: m=row, n=column). Refer to the List of Symbols given in section 2.2 for a definition of symbols.

A-1 Voltage Matrix [v]

for m=1,2,3

$$v_1 = v_a \tag{A-1}$$

$$v_2 = v_b \tag{A-2}$$

$$v_3 = v_c \tag{A-3}$$

for m=4,5,...N_{sa}+3

$$v_m = 0 \tag{A-4}$$

A-2 Inductance Matrix [L]

for m=n=1,2,3

$$L_{m,n} = L_l + L_{ss} \tag{A-5}$$

where L_s is given by equation 2-26.

for m≠n   m,n=1,2,3

$$L_{m,n} = \frac{-L_s}{2} \tag{A-6}$$

167

for $m = 1, 2, 3$ $n = 4, 5, \ldots N_{RB}+3$

$$L_{m,n} = M \sin\left(p\left(\frac{(2(n-3)-1)\pi}{N_{RB}} + \omega_m t + \theta_o \right) - (m-1)\frac{2\pi}{3} \right) \qquad (A-7)$$

where M is given by equation 2-52.

for $m = 4, 5, \ldots N_{RB}+3$ $n = 1, 2, 3$

$$L_{m,n} = M \sin\left(p\left(\frac{(2(m-3)-1)\pi}{N_{RB}} + \omega_m t + \theta_o \right) - (n-1)\frac{2\pi}{3} \right) \qquad (A-8)$$

for $m = n = 4, 5, \ldots N_{RB}+3$

$$L_{m,n} = L_P + L_{Lrb(m-3)} + L_{Lrb(m-2)} \qquad (A-9)$$

(note: for $m = N_{RB}+3$ $L_{Lrb(m-2)} = L_{Lrb1}$)

where L_P is given by equation 2-42.

for $n = m+1$ $m = 4, 5, \ldots N_{RB}+3$

$$L_{m,n} = \frac{-L_P}{(N_{RB}-1)} - L_{Lrb(m-2)} \qquad (A-10)$$

(note: for $m = N_{RB}+3$, $n = 4$ $L_{Lrb(m-2)} = L_{Lrb1}$)

for $n = m-1$ $m = 4, 5, \ldots N_{RB}+3$

$$L_{m,n} = \frac{-L_P}{(N_{RB}-1)} - L_{Lrb(m-3)} \qquad (A-11)$$

(note: for $m = 4$, $n = N_{RB}+3$ $L_{Lrb(m-3)} = L_{Lrb1}$)

for $n \neq m, m+1, m-1$ $n, m = 4, 5, \ldots N_{RB} + 3$

$$L_{m,n} = \frac{-L_R}{(N_{RB} - 1)} \tag{A-12}$$

A-3 Effective Resistance Matrix [RR]

for $m = n = 1, 2, 3$

$$RR_{m,n} = R_s \tag{A-13}$$

for $m \neq n$ $m, n = 1, 2, 3$

$$RR_{m,n} = 0 \tag{A-14}$$

for $m = 1, 2, 3$ $n = 4, 5, \ldots N_{RB} + 3$

$$RR_{m,n} = p \, \omega_m M \cos\left(p\left(\frac{(2(n-3)-1)\pi}{N_{RB}} + \omega_m t + \theta_o \right) - (m-1)\frac{2\pi}{3} \right) \tag{A-15}$$

(note: this expression assumes the mechanical speed of the rotor is a constant)

for $m = 4, 5, \ldots N_{RB} + 3$ $n = 1, 2, 3$

$$RR_{m,n} = p \, \omega_m M \cos\left(p\left(\frac{(2(m-3)-1)\pi}{N_{RB}} + \omega_m t + \theta_o \right) - (n-1)\frac{2\pi}{3} \right) \tag{A-16}$$

(note: this expression assumes the mechanical speed of the rotor is a constant)

for $m = n = 4, 5, \ldots N_{RB} + 3$

$$RR_{m,n} = R_{rb(m-3)} + R_{rb(m-2)} \tag{A-17}$$

(note: for $m = N_{RB} + 3$ $R_{rb(m-2)} = R_{rb1}$)

169

for n=m+1 m=4,5,...N_{RB}+3

$$RR_{m,n} = -R_{rb(m-2)}$$ (A-18)

(note: for m=N_{RB}+3, n=4 $R_{rb(m-2)} = R_{rb1}$)

for n=m-1 m=4,5,...N_{RB}+3

$$RR_{m,n} = -R_{rb(m-3)}$$ (A-19)

(note: for m=4, n=N_{RB}+3 $R_{rb(m-3)} = R_{rb1}$)

for n≠m,m+1,m-1 n,m=4,5,...N_{RB}+3

$$RR_{m,n} = 0$$ (A-20)

SIMULATION PROGRAMS AND DATA FILES

B-1 FORTRAN SIMULATION PROGRAM

The FORTRAN simulation program can be used to solve the system of equations describing the electrical performance of an induction motor derived in Chapter 2 for the time-varying stator phase and rotor loop currents. A fixed-step, fourth-order Runge-Kutta procedure is used to numerically integrate the system of equations. The time-varying inductance matrix is inverted for each value of time using Cholesky's method with partial pivoting. The program can be used to simulate an induction motor with either no broken rotor bars or one broken rotor bar. A flowchart for the program is shown in Figure 3-1. The program is divided into six parts, a main program and five subroutines. The following paragraphs describe the purpose of each part of the simulation program.

Main program: The main program performs several functions. The primary function is to act as a buffer and pass data between the subroutines. In addition, the main program keeps track of the simulation time, calculates the value of the current vector at the end of each time step, and writes the results to an external file.

Subroutine INPUT: This subroutine is called once by the main program. It performs two functions. First, it reads the data contained in an external input file. The external input file provides a description of the machine being simulated. It includes the single-phase, equivalent-circuit model values, number of rotor bars, and number of pole-pairs for the machine, the rotor slip, and the supply voltage and frequency. The simulation time parameters (i.e., step-size and stop time) and a broken bar flag are also included in the input file. Second, using the relations derived in section 2.3, the coefficients for the inductance and effective resistance matrix elements are calculated and passed to the main program.

Subroutine MOTOR: This subroutine is called for each value of time. It performs two functions; it calculates the elements of the voltage, inductance, and effective resistance matrices, and it reduces the system of equations. For the voltage vector, a balanced

171

three-phase supply is assumed. The inductance and effective resistance elements are calculated using the relations given in Appendix A. For both a "no broken bar" simulation and a "one broken bar" simulation, the system of equations can be reduced from $N_{RB}+3$ to $N_{RB}+2$ since the sum of the rotor loop currents equals zero. This condition is imposed on the system of equations by eliminating rotor loop N_{RB} current. Column $N_{RB}+3$ is subtracted from columns 4 through $N_{RB}+2$ and column $N_{RB}+3$ is deleted from the inductance and effective resistance matrices. Next, row $N_{RB}+3$ is deleted from each matrix to complete the reduction. In addition, for a "one broken bar" simulation (assume rotor bar $N_{RB}-1$ is broken), the system of equations can be reduced again by setting rotor loop $N_{RB}-1$ current equal to rotor loop $N_{RB}-2$ current. For this condition, column $N_{RB}+2$ is added to column $N_{RB}+1$ and column $N_{RB}+2$ is deleted from the inductance and effective resistance matrices. Faraday's law is satisfied by adding row $N_{RB}+2$ to row $N_{RB}+1$ and deleting row $N_{RB}+2$ from each matrix to complete the reduction.

Subroutine <u>CURRENT:</u> This subroutine is used to calculate the intermediate values of the current vector for the Runge-Kutta method.

$$[EST] = [I] + \frac{d[I]}{dt} \Delta t$$

where:

[EST] = intermediate value of current vector

[I] = initial current vector

Subroutine <u>DRIVE:</u> The purpose of this subroutine is to calculate the "driving function" for each value of time and current, i.e.,

driving function = $[V] - [RR][I]$

Subroutine <u>CHLSKY:</u> This subroutine performs the inductance matrix inversion to calculate the derivative

of the current vector for each time value. For the
fourth-order Runge-Kutta procedure, this calculation is
performed four times per time step.

a. PROGRAM LISTING

```
        PROGRAM INDUCTION MOTOR
C
C       FILENAME: MARK.FOR
C       AUTHOR: MARK S. WELSH
C       REFERENCES: CHAPTERS 2 AND 3 OF THESIS
C                   SECTIONS 3-4 AND 6-5 OF REFERENCE [13]
C
C       THIS PROGRAM SIMULATES THE ELECTRICAL OPERATION OF A
C       3-PHASE SQUIRREL-CAGE INDUCTION MOTOR WITH NRB ROTOR
C       BARS. THE PROGRAM SOLVES THE SYSTEM OF EQUATIONS IN
C       THE FORM OF
C               [V]=[L]d/dt[I]+[RR][I]
C       FOR THE STATOR PHASE AND ROTOR LOOP CURRENTS. A
C       FIXED-STEP, FOURTH-ORDER, RUNGE-KUTTA INTEGRATION
C       ROUTINE IS USED. IN ADDITION CHOLESKY'S METHOD WITH
C       PARTIAL PIVOTING IS USED TO SOLVE FOR THE VALUES OF
C       d/dt[I] FOR EACH TIME VALUE (I.E., INVERTS [L] FOR
C       EACH TIME VALUE). THE PROGRAM IS BROKEN DOWN INTO
C       SIX SECTIONS (MAIN PROGRAM AND FIVE SUBROUTINES).
C       THE PROGRAM WILL ALLOW FOR SIMULATION OF EITHER NO
C       BROKEN ROTOR BARS OR ONE BROKEN ROTOR BAR.
C
C       LIST OF VARIABLES FOR MAIN PROGRAM
C
C       NAMOUT     OUTPUT FILE NAME
C       BRN        FLAG FOR A BROKEN ROTOR BAR
C       NRB        NO. OF ROTOR BARS
C       K          NO. OF SYSTEM EQUATIONS (NRB+3)
C       K1         NO. OF SYSTEM EQUATIONS FOR THE NO BROKEN
C                  BAR CASE (NRB+2)
C       K2         NO. OF SYSTEM EQUATIONS FOR THE ONE BROKEN
C                  BAR CASE (NRB+1)
C       LS         STATOR PHASE SELF INDUCTANCE
C       LSL        STATOR PHASE LEAKAGE INDUCTANCE
C       RS         STATOR PHASE RESISTANCE
C       MSR        STATOR PHASE-ROTOR LOOP MUTUAL INDUCTANCE
C                  COEFFICIENT
C       LR         ROTOR LOOP SELF INDUCTANCE
C       LRLB       ROTOR BAR LEAKAGE INDUCTANCE
C       RRB        ROTOR BAR RESISTANCE
C       E          INPUT VOLTAGE AMPLITUDE
C       W          INPUT VOLTAGE ELECTRICAL FREQUENCY
C       WM         ROTOR MECHANICAL SPEED
C       T          SIMULATION TIME
C       INC        TIME STEP FOR INTEGRATION
C       TSTOP      SIMULATION STOP TIME
C       TOUT       SIMULATION TIME TO BEGIN WRITING OUTPUT
C       FACTOR     INTERMEDIATE TIME STEP FOR INTEGRATION
C       TIME       INTERMEDIATE SIMULATION TIME
C       PP         NO. OF MACHINE POLE-PAIRS
C       AMPS       CURRENT VECTOR
```

174

```
C        V            VOLTAGE VECTOR
C        L            INDUCTANCE MATRIX
C        R            EFFECTIVE RESISTANCE MATRIX
C        VRI          DRIVE VECTOR (VRI=[V]-[RR][I])
C        EST          INTERMEDIATE CURRENT ESTIMATE
C        RK1          INITIAL VALUE OF d/dt[I] FOR EACH STEP
C        RK2          INTERMEDIATE VALUE d/dt[I] FOR EACH STEP
C        RK3          INTERMEDIATE VALUE d/dt[I] FOR EACH STEP
C        RK4          LAST VALUE OF d/dt[I] FOR EACH STEP
C
C        VARIABLE DECLARATIONS
C
         CHARACTER*20 NAMOUT
         INTEGER BKN,NRB,K,K1,K2
         DOUBLE PRECISION LS,LSL,RS,MSR,LR,LRLB,RRB,E,W,WM,T,
        *INC,TSTOP,TOUT,FACTOR,TIME,PP,AMPS(100,1),V(100,100),
        *L(100,100),R(100,100),VRI(100,1),EST(100,1),
        *RK1(100,1),RK2(100,1),RK3(100,1),RK4(100,1)
C
C        GET INPUT PARAMETERS
C
         CALL INPUT(LS,LSL,RS,MSR,LR,LRLB,RRB,BKN,E,W,WM,NRB,
        *TSTOP,TOUT,INC,PP)
C
C        SET UP OUTPUT FILE
C
         PRINT *,'ENTER OUTPUT FILE NAME'
         READ *,NAMOUT
         OPEN(UNIT=7,FILE=NAMOUT,STATUS='UNKNOWN')
C
C        DETERMINE NUMBER OF SYSTEM EQUATIONS
C
         K=NRB+3
         K1=K-1
         IF(BKN.LE.0) THEN
             K2=K1
         ELSE
             K2=K1-1
         ENDIF
C
C        INITIALIZE SIMULATION TIME AND CURRENTS
C
         DO 10 J=1,K2
             AMPS(J,1)=0.
10       CONTINUE
         T=0.
C
C        SET UP SYSTEM MATRICES FOR TIME=T
C
         CALL MOTOR(V,L,R,K,K1,K2,T,LS,LSL,RS,MSR,LR,LRLB,RRB,
        *BKN,E,W,WM,NRB,PP)
C
C        START SIMULATION LOOP
```

175

```
C
C         WRITE OUTPUT TO DATA FILE (TIME, PHASE A CURRENT,
C         AND ROTOR LOOP 1 CURRENT)
C
1         IF(T.GE.TOUT) THEN
              WRITE(7,999)T,AMPS(1,1),AMPS(4,1)
          ENDIF
C
C         CALCULATE RK1 (d/dt[I]) FOR TIME=T
C
C         CALCULATE VRI FOR TIME=T, I=AMPS
C
          CALL DRIVE(R,K2,AMPS,V,VRI)
C
          CALL CHLSKY(L,K2,K2+1,VRI,RK1)
C
C         CALCULATE RK2 (d/dt[I]) FOR TIME=T+INC/2
C
          TIME=T+INC/2.0
          FACTOR=INC/2.0
C
C         ESTIMATE CURRENT FOR TIME=T+INC/2 USING RK1
C
          CALL CURRENT(AMPS,RK1,FACTOR,K2,EST)
C
C         SET UP SYSTEM MATRICES FOR TIME=T+INC/2
C
          CALL MOTOR(V,L,R,K,K1,K2,TIME,LS,LSL,RS,MSR,LR,LRLB,
         *RRB,BKN,E,WM,NRB,PP)
C
C         CALCULATE VRI FOR TIME=T+INC/2, I=EST
C
          CALL DRIVE(R,K2,EST,V,VRI)
C
          CALL CHLSKY(L,K2,K2+1,VRI,RK2)
C
C         CALCULATE RK3 (d/dt[I]) FOR TIME=T+INC/2
C
C         ESTIMATE CURRENT FOR TIME=T+INC/2 USING RK2
C
          CALL CURRENT(AMPS,RK2,FACTOR,K2,EST)
C
C         CALCULATE VRI FOR TIME=T+INC/2, I=EST
C
          CALL DRIVE(R,K2,EST,V,VRI)
C
          CALL CHLSKY(L,K2,K2+1,VRI,RK3)
C
C         CALCULATE RK4 (d/dt[I]) FOR TIME=T+INC
C
          TIME=T+INC
C
C         ESTIMATE CURRENT FOR TIME=T+INC USING RK3
```

```
C
      CALL CURRENT(AMPS,RK3,INC,K2,EST)
C
C     SET UP SYSTEM MATRICES FOR TIME=T+INC
C
      CALL MOTOR(V,L,R,K,K1,K2,TIME,LS,LSL,RS,MSR,LR,LRLB,
     *RRB,BKN,E,W,WM,NRB,PP)
C
C     CALCULATE VRI FOR TIME=T+INC, I=EST
C
      CALL DRIVE(R,K2,EST,V,VRI)
C
      CALL CHLSKY(L,K2,K2+1,VRI,RK4)
C
C     CALCULATE NEW CURRENT VALUES AND INCREMENT TIME
C
      DO 20 J=1,K2
        AMPS(J,1)=AMPS(J,1)+(INC/6.0)*(RK1(J,1)+2*RK2(J,1)+
     *  2*RK3(J,1)+RK4(J,1))
20    CONTINUE
      T=TIME
C
C     CONTINUE SIMULATION IF T<TSTOP ELSE STOP
C
      IF(T.LE.TSTOP) GO TO 1
C
      CLOSE(UNIT=7)
      STOP
C
999   FORMAT(3(3X,F12.7))
      END
```

```fortran
      SUBROUTINE INPUT(LS,LSL,RS,MSR,LR,LRLB,RRB,BKN,E,W,
     *WM,NRB,TSTOP,TOUT,INC,PP)
C
C     THIS SUBROUTINE IS THE INPUT INTERFACE FOR THE
C     SIMULATION PROGRAM. REQUIRED INPUT VALUES ARE READ
C     IN FROM AN EXISTING INPUT DATA FILE AND THE VALUES
C     OF INDUCTANCES,RESISTANCES,ETC. ARE CALCULATED FROM
C     THE RELATIONS DERIVED IN SECTION 2.3 AND PASSED TO
C     THE MAIN PROGRAM
C
C     LIST OF VARIABLES
C
C     NAMEIN    INPUT DATA FILENAME
C     STEPS     NO. OF TIME STEPS PER SECOND
C     S         ROTOR SLIP
C     PI        RADIANS IN A HALF CIRCLE
C     K         CONSTANT FACTOR FOR CALCULATIONS
C     R1        CIRCUIT MODEL STATOR PHASE RESISTANCE
C     L1        CIRCUIT MODEL STATOR PHASE LEAKAGE INDUCTANCE
C     L12       CIRCUIT MODEL MUTUAL INDUCTANCE
C     L2        CIRCUIT MODEL ROTOR LEAKAGE INDUCTANCE
C     R2        CIRCUIT MODEL ROTOR RESISTANCE
C
C     VARIABLE DECLARATIONS
C
      CHARACTER *20 NAMEIN
      INTEGER BKN,NRB,PP,STEPS
      DOUBLE    PRECISION TSTOP,TOUT,LS,LSL,RS,MSR,LR,
     *LRLB,RRB,E,W,WM,S,PI,INC,K,R1,L1,L12,L2,R2
C
C     READ IN INPUT DATA FILE
C
      PRINT *,'ENTER INPUT FILENAME'
      READ *,NAMEIN
      OPEN(UNIT=8,FILE=NAMEIN,STATUS='UNKNOWN')
      READ(8,*)R1,L1,L12,L2,R2
      READ(8,*)NRB,BKN
      READ(8,*)E,W,S,PP
      READ(8,*)STEPS,TSTOP,TOUT
      CLOSE(UNIT=8)
C
C     DEFINE PARAMETERS
C
      PI=4*ATAN(1.0)
      K=PI*PP/NRB
      LSL=L1
      RS=R1
      LS=2*L12/3.0
      MSR=8*SIN(K)*L12/(3*PI)
      LRLB=(L2-(K**2/(SIN(K)**2)-1)*L12)*4*NRB/(3*PI**2)
      RRB=4*NRB/(3*PI**2)*R2
      LR=16*(NRB-1)*PP**2*L12/(3*NRB**2)
```

178

```
INC=1.0/STEPS
WM=W*(1-S)/PP
RETURN
END
```

```fortran
      SUBROUTINE MOTOR(V2,L2,R2,K,K1,K2,TIME,LS,LSL,RS,MSR,
     *LR,LRLB,RRB,BKN,E,W,WM,NRB,PP)
C
C     THIS SUBROUTINE CALCULATES THE ELEMENTS IN
C     EACH MATRIX OF THE SYSTEM OF EQUATIONS FOR A GIVEN
C     VALUE OF TIME. THE MATRICES ARE SET-UP AND THEN
C     REDUCED FOR THE CONDITION THAT THE SUM OF THE ROTOR
C     LOOP CURRENTS IS ZERO. FOR A BROKEN BAR THE SYSTEM IS
C     AGAIN REDUCED BY ONE SINCE THE ROTOR LOOP CURRENTS
C     ASSOCIATED WITH A BROKEN BAR ARE SET EQUAL. FOR THIS
C     SIMULATION ROTOR BAR NRB-1 IS THE BROKEN BAR.
C
C     LIST OF VARIABLES
C
C     V1,R1,L1  MATRICES V,R,L REDUCED FOR SUM OF ROTOR
C               LOOP CURRENT=0 CONDITION
C     V2,R2,L2  MATRICES V1,R1,L1 REDUCED FOR BROKEN ROTOR
C               BAR CONDITION
C
C     VARIABLE DECLARATIONS
C
      INTEGER K,K1,K2,BKN,NRB,PP
      DOUBLE PRECISION V(100,1),R(100,100),L(100,100),
     *V1(100,1),R1(100,100),L1(100,100),V2(100,1),
     *R2(100,100),L2(100,100),TIME,LS,LSL,RS,MSR,LR,LRLB,
     *RRB,E,W,WM,PI
C
      PI=4*ATAN(1.0)
C
C     CALCULATE VOLTAGE VECTOR
C
      DO 10 J=1,K
          IF(J.GT.3) THEN
              V(J,1)=0.0
          ELSE
              V(J,1)=E*COS(W*TIME-(J-1)*2*PI/3.0)
          ENDIF
10    CONTINUE
C
C     CALCULATE INDUCTANCE AND EFFECTIVE RESISTANCE MATRIX
C     ELEMENTS
C
      DO 20 I=1,K
          DO 30 J=I,K
              IF(I.LE.3.AND.J.LE.3) THEN
                  IF(I.EQ.J) THEN
                      L(I,J)=LS+LSL
                      R(I,J)=RS
                  ELSE
                      L(I,J)=-LS/2.0
                      R(I,J)=0.0
                  ENDIF
```

```
                ELSEIF(I.LE.3.AND.J.GT.3) THEN
                    L(I,J)=MSR*SIN(PP*WM*TIME+(2*(J-3)-1)*
     *                  PI/NRB-(I-1)*2*PI/3.0)
                    R(I,J)=PP*WM*MSR*COS(PP*WM*TIME+(2*(J-3)
     *                  -1)*PI/NRB-(I-1)*2*PI/3.0)
                ELSE
                    IF(I.EQ.J) THEN
                        L(I,J)=LR+2*LRLB
                        R(I,J)=2*RRB
                    ELSEIF(J.EQ.(I+1))THEN
                        L(I,J)=-LR/(NRB-1)-LRLB
                        R(I,J)=-RRB
                    ELSE
                        L(I,J)=-LR/(NRB-1)
                        R(I,J)=0.0
                    ENDIF
                ENDIF
            R(J,I)=R(I,J)
            L(J,I)=L(I,J)
30          CONTINUE
20      CONTINUE
        L(4,K)=-LR/(NRB-1)-LRLB
        L(K,4)=L(4,K)
        R(4,K)=-RRB
        R(K,4)=R(4,K)
C
C       REDUCE EQUATIONS FOR SUM OF ROTOR LOOP CURRENTS
C       EQUAL ZERO CONDITION
C
        DO 40 I=1,K1
            DO 50 J=1,K1
                IF(J.LE.3) THEN
                    R1(I,J)=R(I,J)
                    L1(I,J)=L(I,J)
                ELSE
                    R1(I,J)=R(I,J)-R(I,K)
                    L1(I,J)=L(I,J)-L(I,K)
                ENDIF
50          CONTINUE
            V1(I,1)=V(I,1)
40      CONTINUE
C
C       FOR A BROKEN BAR REDUCE EQUATIONS AGAIN ELSE
C       SET V2=V1,R2=R1,L2=L1 AND RETURN TO MAIN PROGRAM
C
        IF(BKN.LE.0) GO TO 1000
C
C       REDUCING EQUATIONS FOR BROKEN BAR
C
        DO 60 I=1,K1
            R1(I,K2)=R1(I,K2)+R1(I,K1)
            L1(I,K2)=L1(I,K2)+L1(I,K1)
60      CONTINUE
```

181

```
      DO 70 I=1,K1
          R1(K2,I)=R1(K2,I)+R1(K1,I)
          L1(K2,I)=L1(K2,I)+L1(K1,I)
70        CONTINUE
C
C     SETTING FINAL VALUES FOR V,R,L MATRICES
C
1000  DO 80 I=1,K2
          DO 90 J=1,K2
              R2(I,J)=R1(I,J)
              L2(I,J)=L1(I,J)
90        CONTINUE
          V2(I,1)=V1(I,1)
80    CONTINUE
      RETURN
      END
```

```fortran
      SUBROUTINE CURRENT(A,B,C,N,RESULT)
C
C     THIS SUBROUTINE CALCULATES THE INTERMEDIATE
C     VALUES OF CURRENT FOR THE INTEGRATION ROUTINE.
C        [I(EST)]=[I(start)]+d/dt[I]*dt
C
C     LIST OF VARIABLES
C
C     N        NO. OF EQUATIONS
C     A        INITIAL VALUE OF CURRENTS
C     B        d/dt[I]
C     C        dt (INCREMENTAL TIME)
C     RESULT   ESTIMATED CURRENT (A+B*C)
C
C     VARIABLE DECLARATIONS
C
      INTEGER N
      DOUBLE PRECISION A(100,1),B(100,1),RESULT(100,1),C
C
C     CALCULATE CURRENT ESTIMATE
C
      DO 10 J=1,N
         RESULT(J,1)=A(J,1)+B(J,1)*C
10    CONTINUE
      RETURN
      END
```

183

```
      SUBROUTINE DRIVE(A,K2,B,C,RESULT)
C
C     THIS SUBROUTINE CALCULATES THE VALUE OF
C     [V]-[RR][I] FOR EACH VALUE OF TIME.
C
C     LIST OF VARIABLES
C
C     A        EFFECTIVE RESISTANCE MATRIX [RR]
C     B        CURRENT VECTOR [I]
C     C        VOLTAGE VECTOR [V]
C     RESULT   [V]-[RR][I]
C
C     VARIABLE DECLARATIONS
C
      INTEGER K2
      DOUBLE PRECISION A(100,100),B(100,1),C(100,1),
     *RESULT(100,1)
C
C     CALCULATE RESULT
C
      DO 10 I=1,K2
          RESULT(I,1)=0.0
C
C     DETERMINE [RR][I]
C
          DO 20 J=1,K2
              RESULT(I,1)=RESULT(I,1)+A(I,J)*B(J,1)
20        CONTINUE
C
C     DETERMINE [V]-[RR][I]
C
          RESULT(I,1)=C(I,1)-RESULT(I,1)
10    CONTINUE
      RETURN
      END
```

```
          SUBROUTINE CHLSKY(A1,N,M,B,RESULT)
C
C         THIS SUBROUTINE CALCULATES THE VALUES OF d/dt[I]
C         FOR EACH VALUE OF TIME USING CHOLESKY'S METHOD WITH
C         PARTIAL PIVOTING. THE EQUATIONS ARE IN THE FORM:
C                   [L]d/dt[I]=[V]-[RR][I]
C
C         LIST OF VARIABLES
C
C         A        WORKING MATRIX [L¦V-RR I]
C         A1       INDUCTANCE MATRIX [L]
C         B        DRIVE VECTOR [V]-[RR][I]
C         RESULT   CURRENT DERIVATIVES d/dt[I]
C         PIVOT    VALUE OF PIVOT ELEMENT
C         SWAP     DUMMY VARIABLE FOR CHANGING ROWS
C         SUM      VARIABLE FOR MULTIPLICATION OPERATIONS
C
C         VARIABLE DECLARATIONS
C
          INTEGER N,M
          DOUBLE PRECISION A(100,101),A1(100,100),B(100,1),
         *RESULT(100,1),PIVOT,SWAP,SUM
C
C         SET UP A MATRIX [A]=[A1¦B]
C         (ADD DRIVE COLUMN TO INDUCTANCE MATRIX)
C
          DO 1 I=1,N
              DO 2 J=1,M
                  IF(J.NE.M) THEN
                      A(I,J)=A1(I,J)
                  ELSE
                      A(I,J)=B(I,1)
                  ENDIF
2             CONTINUE
1         CONTINUE
C
C         PERFORM PARTIAL PIVOTING
C
          DO 10 I=1,N
C
C         FIND LARGEST PIVOT
C
              PIVOT=A(I,I)
              IL=I
              DO 20 J=I+1,N
                  IF(ABS(A(J,I)).LE.ABS(PIVOT)) GO TO 20
                  PIVOT=A(J,I)
                  IL=J
20            CONTINUE
              IF(IL.EQ.I) GO TO 10
C
C         INTERCHANGE ROWS TO PUT PIVOT ON DIAGONAL


                              185
```

```
C
            DO 30 K=1,M
                SWAP=A(I,K)
                A(I,K)=A(IL,K)
                A(IL,K)=SWAP
30          CONTINUE
10      CONTINUE
C
C       CALCULATE FIRST ROW OF UPPER TRIANGULAR MATRIX
C
        DO 40 J=2,M
            A(1,J)=A(1,J)/A(1,1)
40      CONTINUE
C
C       DETERMINE ALL OTHER ELEMENTS OF UPPER AND LOWER
C       TRIANGULAR MATRICES
C
        DO 50 I=2,N
C
C       LOWER TRIANGULAR MATRIX ELEMENTS
C
            DO 60 J=I,N
                SUM=0.0
                DO 70 K=1,I-1
                    SUM=SUM+A(J,K)*A(K,I)
70              CONTINUE
                A(J,I)=A(J,I)-SUM
60          CONTINUE
C
C       UPPER TRIANGULAR MATRIX ELEMENTS
C
            DO 80 J=I+1,M
                SUM=0.0
                DO 90 K=1,I-1
                    SUM=SUM+A(I,K)*A(K,J)
90              CONTINUE
                A(I,J)=(A(I,J)-SUM)/A(I,I)
80          CONTINUE
50      CONTINUE
C
C       USE BACK SUBSTITUTION TO FIND d/dt[I]
C
        RESULT(N,1)=A(N,M)
        DO 100 I=1,N-1
            J=N-I
            SUM=0.0
            DO 110 K=J+1,N
                SUM=SUM+A(J,K)*RESULT(K,1)
110         CONTINUE
            RESULT(J,1)=A(J,M)-SUM
100     CONTINUE
        RETURN
        END
```

b. SAMPLE INPUT FILE

The following input file is for a 45-bar rotor with a
broken rotor bar at s=0.04. The values are in the following
format (i.e., refer to subroutine input above):

equivalent-circuit values (R_1,L_1,L_{12},L_2,R_2)
no. of rotor bars, broken bar flag
input voltage, electrical frequency, slip, pole-pairs
no. of steps/sec, stop time, start print time

```
.859,.0046,.0704,.0046,.5612
45,1
169.71,377,.04,2
1536,4.3334,1.0
```

Table B-1. Sample simulation input file.

c. SAMPLE OUTPUT FILE

The following output file is for a 45-bar rotor with a broken rotor bar. This is a portion of the output file generated from the simulation program using the input file given in section 1.1.1. Plots of stator phase a current and rotor loop 1 current are included.

TIME (sec)	STATOR PHASE A CURRENT (amps)	ROTOR LOOP 1 CURRENT (amps)
1.0000	9.388	2.926
1.0007	10.963	2.902
1.0013	11.878	2.878
1.0020	12.080	2.854
1.0026	11.556	2.830
1.0033	10.340	2.805
1.0039	8.503	2.780
1.0046	6.158	2.754
1.0052	3.444	2.729
1.0059	0.525	2.703
1.0065	-2.424	2.676
1.0072	-5.225	2.650
1.0078	-7.711	2.623
1.0085	-9.733	2.596
1.0091	-11.169	2.569
1.0098	-11.933	2.542
1.0104	-11.980	2.514
1.0111	-11.308	2.486
1.0117	-9.957	2.458
1.0124	-8.008	2.430
1.0130	-5.580	2.401
1.0137	-2.817	2.372
1.0143	0.114	2.343
1.0150	3.036	2.314
1.0156	5.775	2.284
1.0163	8.165	2.254
1.0169	10.064	2.224
1.0176	11.357	2.194
1.0182	11.968	2.164
1.0189	11.858	2.133
1.0195	11.037	2.102
1.0202	9.552	2.071
1.0208	7.494	2.040
1.0215	4.986	2.009
1.0221	2.179	1.977
1.0228	-0.758	1.945
1.0234	-3.648	1.913
1.0241	-6.319	1.881

Table B-2. Sample simulation output file.

TIME (sec)	STATOR PHASE A CURRENT (amps)	ROTOR LOOP 1 CURRENT (amps)
1.0247	-8.609	1.849
1.0254	-10.380	1.816
1.0260	-11.528	1.783
1.0267	-11.982	1.751
1.0273	-11.716	1.718
1.0280	-10.745	1.684
1.0286	-9.129	1.651
1.0293	-6.964	1.617
1.0299	-4.380	1.584
1.0306	-1.534	1.550
1.0313	1.404	1.516
1.0319	4.258	1.482
1.0326	6.855	1.447
1.0332	9.040	1.413
1.0339	10.682	1.378
1.0345	11.681	1.344
1.0352	11.977	1.309
1.0358	11.554	1.274
1.0365	10.435	1.239
1.0371	8.689	1.204
1.0378	6.421	1.168
1.0384	3.766	1.133
1.0391	0.885	1.097
1.0397	-2.050	1.062
1.0404	-4.862	1.026
1.0410	-7.382	0.990
1.0417	-9.458	0.954
1.0423	-10.966	0.918
1.0430	-11.815	0.882
1.0436	-11.953	0.846
1.0443	-11.373	0.810
1.0449	-10.109	0.773
1.0456	-8.237	0.737
1.0462	-5.869	0.700
1.0469	-3.147	0.664
1.0475	-0.236	0.627
1.0482	2.691	0.591
1.0488	5.456	0.554
1.0495	7.895	0.517
1.0501	9.859	0.480
1.0508	11.232	0.443
1.0514	11.930	0.406
1.0521	11.910	0.369
1.0527	11.175	0.332
1.0534	9.768	0.295
1.0540	7.773	0.258

Table B-2. (cont.) Sample simulation output file.

TIME (sec)	STATOR PHASE A CURRENT (amps)	ROTOR LOOP 1 CURRENT (amps)
1.0547	5.310	0.221
1.0553	2.526	0.184
1.0560	-0.410	0.147
1.0566	-3.324	0.110
1.0573	-6.038	0.072
1.0579	-8.392	0.035
1.0586	-10.242	-0.002
1.0592	-11.477	-0.039
1.0599	-12.024	-0.076
1.0605	-11.848	-0.113
1.0612	-10.960	-0.151
1.0618	-9.413	-0.188
1.0625	-7.300	-0.225
1.0632	-4.746	-0.262
1.0638	-1.906	-0.299
1.0645	1.050	-0.336
1.0651	3.945	-0.373
1.0658	6.604	-0.410
1.0664	8.869	-0.447
1.0671	10.602	-0.484
1.0677	11.700	-0.521
1.0684	12.095	-0.558
1.0690	11.765	-0.594
1.0697	10.727	-0.631
1.0703	9.045	-0.668
1.0710	6.819	-0.704
1.0716	4.181	-0.741
1.0723	1.291	-0.777
1.0729	-1.679	-0.813
1.0736	-4.551	-0.850
1.0742	-7.151	-0.886
1.0749	-9.323	-0.922
1.0755	-10.938	-0.958
1.0762	-11.897	-0.994
1.0768	-12.143	-1.030
1.0775	-11.660	-1.066
1.0781	-10.477	-1.101
1.0788	-8.665	-1.137
1.0794	-6.331	-1.172
1.0801	-3.616	-1.207

Table B-2. (cont.) Sample simulation output file.

TIME (sec)	STATOR PHASE A CURRENT (amps)	ROTOR LOOP 1 CURRENT (amps)
1.0807	-0.681	-1.243
1.0814	2.297	-1.278
1.0820	5.139	-1.313
1.0827	7.675	-1.347
1.0833	9.752	-1.382
1.0840	11.246	-1.417
1.0846	12.067	-1.451
1.0853	12.165	-1.485
1.0859	11.533	-1.519
1.0866	10.209	-1.553
1.0872	8.272	-1.587
1.0879	5.838	-1.621
1.0885	3.051	-1.654
1.0892	0.080	-1.688
1.0898	-2.899	-1.721
1.0905	-5.706	-1.754
1.0911	-8.173	-1.787
1.0918	-10.152	-1.820
1.0924	-11.524	-1.852
1.0931	-12.207	-1.884
1.0938	-12.158	-1.917
1.0944	-11.381	-1.949

Table B-2. (cont.) Sample simulation output file.

SIMULATION STATOR PHASE CURRENT
SLIP=.04 1728 rpm
ONE BROKEN ROTOR BAR
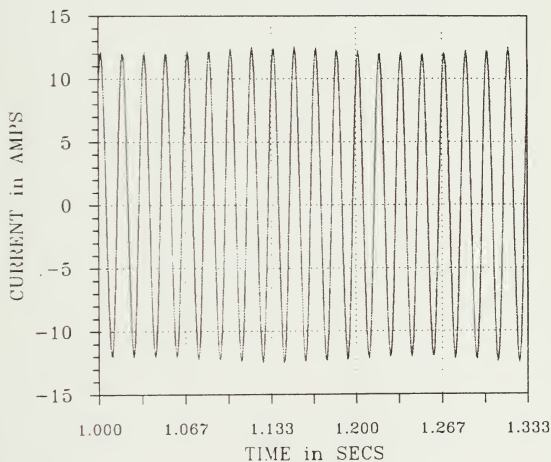
Figure B-1. Stator phase a current vs. time for sample
simulation.

SIMULATION ROTOR LOOP CURRENT
SLIP=.04 1728 rpm
ONE BROKEN ROTOR BAR
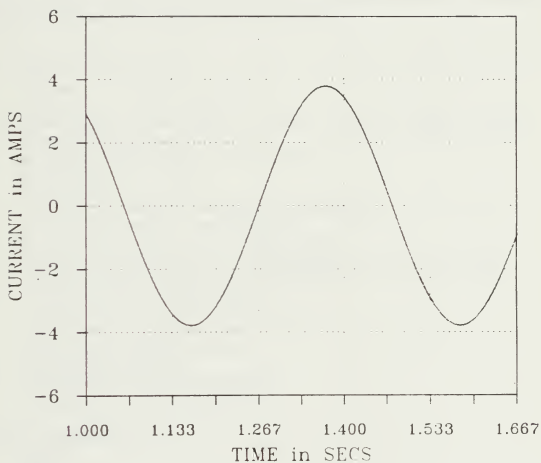
Figure B-2. Rotor loop 1 current vs. time for sample
simulation.

B-2 PRO-MATLAB EIGENVALUE ROUTINE

PRO-MATLAB is a matrix computation software package
developed by The MathWorks, Inc. of Sherborn, MA. This
PRO-MATLAB script file calculates the eigenvalues of the
[RR]/[L] matrix. The eigenvalues are computed for rotor
slip=1.0 (i.e., the rotor is stationary).

a. PROGRAM LISTING

```
% program EIGENVALUES
%
% filename: root.m
% author: Mark S. Welsh
% references: PRO-MATLAB user's guide
%
% PRO-MATLAB routine to calculate eigenvalues for induction
% motor system of equations ([r]/[l]).
%
% variable list
%    sf=rotor slip
%    t=time
%    nrb=no. of rotor bars
%    r1eq,l1eq,l12eq,l2eq,r2eq=eq. circuit model values
%    pp=machine pole-pairs
%    w=input electrical frequency
%    wm=mechanical speed
%    k=constant
%    lsl=stator phase leakage inductance
%    rs=stator phase resistance
%    ls=stator phase self inductance
%    m=mutual inductance coefficient for stator-rotor
%    lrl=rotor bar leakage inductance
%    rr=rotor bar resistance
%    lr=rotor loop self inductance
%    l,ll=inductance matrix
%    r,rl=resistance matrix
%    meig=eigenvalues
%    t1=smallest time constant
%    t2=longest time constant
%
% input parameters
      sf=0;
      t=0;
      nrb=45;
      r1eq=.859;
      l1eq=.0046;
      l12eq=.0704;
      l2eq=.0046;
      r2eq=.5612;
      pp=2;
      w=377;
% calculate electrical and mechanical parameters
```

194

```
        wm=w*(1-sf)/pp;
        k=pi*pp/nrb;
        lsl=lleq;
        rs=rleq;
        ls=2*ll2eq/3;
        m=8*sin(k)*ll2eq/(3*pi);
        lrl=(l2eq-(k^2/(sin(k)^2)-1)*ll2eq)*4*nrb/(3*pi^2);
        rr=4*nrb/(3*pi^2)*r2eq;
        lr=16*(nrb-1)*pp^2*ll2eq/(3*nrb^2);
% calculate elements of r and l matrix
        for i=1:3;
            for j=1:3;
                r(i,j)=0;
                l(i,j)=-ls/2;
            end
            r(i,i)=rs;
            l(i,i)=ls+lsl;
            for j=4:nrb+3;
                l(i,j)=m*sin(pp*wm*t+(2*(j-3)-1)*pi*pp/nrb-(i-1)*
                    2*pi/3);
                r(i,j)=pp*wm*m*cos(pp*wm*t+(2*(j-3)-1)*pi*pp/nrb-
                    (i-1)*2*pi/3);
            end
        end
        for i=4:nrb+3;
            for j=i:nrb+3;
                r(i,j)=0;
                l(i,j)=-lr/(nrb-1);
                if j==i+1;
                    l(i,j)=-lr/(nrb-1)-lrl;
                    r(i,j)=-rr;
                end
            end
            r(i,i)=2*rr;
            l(i,i)=lr+2*lrl;
        end
        l(4,nrb+3)=-lr/(nrb-1)-lrl;
        r(4,nrb+3)=-rr;
        for i=1:nrb+3;
            for j=i:nrb+3;
                r(j,i)=r(i,j);
                l(j,i)=l(i,j);
            end
        end
% reduce system for sum of rotor loop currents=0
        for i=1:nrb+2;
            for j=1:nrb+2;
                if j<4;
                    r1(i,j)=r(i,j);
                    l1(i,j)=l(i,j);
                else;
                    r1(i,j)=r(i,j)-r(i,nrb+3);
                    l1(i,j)=l(i,j)-l(i,nrb+3);
```

```
                end
            end
        end
% calculate eigenvalues
        meig=eig(-ll\rl);
% determine smallest time constant
        t1=1/max(abs(meig));
% determine largest time constant
        t2=1/min(abs(meig));
% save values
        save eigs.mat;
```

b. EIGENVALUES FOR 3-BAR ROTOR

The following values are the eigenvalues calculated for the 3-bar rotor discussed in Chapter 3.

```
          -186.740
          -154.590
          -154.590
            -4.662
            -4.662
```

Table B-3. 3-bar rotor eigenvalues.

c. EIGENVALUES FOR 45-BAR ROTOR

The following values are the eigenvalues calculated for the 45-bar rotor (i.e., experimental motor) discussed in Chapter 3.

-186.740	-80.344
-154.590	-80.344
-4.662	-84.698
-154.590	-88.364
-4.662	-88.364
-1.961	-93.992
-1.961	-91.436
-15.636	-91.436
-15.636	-93.992
-25.273	-96.101
-25.273	-96.101
-35.354	-97.817
-35.354	-97.817
-45.124	-99.185
-45.124	-99.185
-54.129	-101.010
-54.129	-101.510
-62.161	-101.010
-62.161	-101.510
-69.171	-100.240
-69.171	-100.240
-75.203	-101.760
-75.203	-101.760
-84.698	

Table B-4. 45-bar rotor eigenvalues.

B-3 PRO-MATLAB FFT ROUTINE

This PRO-MATLAB script file computes the fast Fourier transform of the stator phase and rotor loop current outputs of the FORTRAN simulation program. The magnitude of the FFT values are converted to dB and written to a file for future plotting if desired.

a. PROGRAM LISTING

```
% program FFT
%
% filename: fast.m
% author: Mark S. Welsh
% references: PRO-MATLAB user's guide
%             references [18],[19]
%
% PRO-MATLAB procedure to calculate the FFT of the stator
% phase and rotor loop current outputs from the FORTRAN
% simulation program. The input data is sampled at a
% frequency of 153.6 Hz (or 512 data points are taken).
% A second-order Hanning window is used to aid in
% resolution of harmonic frequency components present.
% The power spectral density function is computed and
% converted to a dB scale.
%
% variable list
%    a=input signals array (t,ia,ir1)
%    t=time
%    ia=stator current
%    ir=rotor loop 1 current
%    s=FFT of ia
%    r=FFT of ir
%    ps=power spectral density of ia
%    pr=power spectral density of ir
%    w=hanning weight factors
%
% sample data at 153.6 hz
     t=a(1:10:5120,1);
     ia=a(1:10:5120,2);
     ir=a(1:10:5120,3);
% calculate window function
     w=.5*(ones(1:512)-cos(2*pi*(0:511)/512));
% weight inputs using window function
     iaw=ia.*w';
     irw=ir.*w';
% determine ffts
     s=FFT(iaw);
     r=FFT(irw);
% determine spectral densities
     ps=s.*conj(s);
     pr=r.*conj(r);
% convert to dB
```

199

```
      ps=10*log10(ps);
      pr=10*log10(pr);
% determine frequencies
      f=153.6*(0:255)/512;
% save values and put in plot format
      b=[f' ps(1:256)];
      c=[f' pr(1:256)];
      save ffts.mat;
```

b. SAMPLE FFT OUTPUT FILE

The following table is the output from the PRO-MATLAB FFT routine. The values given are the power spectral densities for the FORTRAN simulation program output currents of section 1.1.2 above. Plots of the frequency spectrum for stator phase a and rotor loop 1 currents are included.

FREQUENCY (Hz)	STATOR PHASE A CURRENT PSD (dB)	ROTOR LOOP 1 CURRENT PSD (dB)
0.0	-120.490	-48.451
0.3	-117.140	-53.454
0.6	-121.350	-68.221
0.9	-117.370	-63.254
1.2	-117.610	-56.369
1.5	-119.050	-48.357
1.8	-115.980	-36.333
2.1	-120.710	47.687
2.4	-118.420	53.710
2.7	-117.390	47.692
3.0	-120.740	-36.337
3.3	-120.190	-48.388
3.6	-117.220	-56.358
3.9	-118.840	-62.401
4.2	-117.980	-67.268
4.5	-120.120	-71.393
4.8	-117.740	-74.918
5.1	-120.040	-78.041
5.4	-118.100	-80.848
5.7	-118.700	-83.388
6.0	-117.840	-85.617
6.3	-118.500	-87.782
6.6	-116.340	-89.849
6.9	-119.570	-91.454
7.2	-117.290	-93.317
7.5	-118.280	-94.946
7.8	-115.270	-96.140
8.1	-119.600	-98.164
8.4	-116.090	-98.824
8.7	-116.310	-100.810
9.0	-119.770	-101.670
9.3	-113.980	-102.490
9.6	-118.430	-104.630
9.9	-116.180	-104.240
10.2	-117.560	-106.670
10.5	-115.430	-106.870

Table B-5. FFT output file.

FREQUENCY (Hz)	STATOR PHASE A CURRENT PSD (dB)	ROTOR LOOP 1 CURRENT PSD (dB)
10.8	-115.520	-107.940
11.1	-116.440	-109.460
11.4	-114.510	-108.920
11.7	-118.390	-111.340
12.0	-114.800	-112.150
12.3	-113.590	-110.150
12.6	-116.000	-116.330
12.9	-114.220	-111.390
13.2	-114.280	-115.520
13.5	-116.640	-115.190
13.8	-113.160	-115.720
14.1	-113.980	-115.860
14.4	-114.900	-119.660
14.7	-114.180	-118.010
15.0	-113.710	-116.340
15.3	-113.610	-118.070
15.6	-113.860	-125.450
15.9	-113.600	-119.010
16.2	-111.620	-117.840
16.5	-113.520	-124.520
16.8	-112.260	-120.970
17.1	-112.840	-121.440
17.4	-112.180	-122.970
17.7	-112.190	-124.910
18.0	-112.020	-121.540
18.3	-111.010	-125.780
18.6	-112.460	-120.890
18.9	-110.760	-120.280
19.2	-112.040	-115.820
19.5	-110.670	-124.750
19.8	-109.900	-121.160
20.1	-111.180	-125.260
20.4	-111.230	-124.470
20.7	-108.920	-142.480
21.0	-110.990	-122.410
21.3	-99.670	-131.490
21.6	-98.796	-123.640
21.9	-99.621	-127.000
22.2	-109.030	-129.970
22.5	-109.380	-128.540
22.8	-108.480	-125.770
23.1	-108.520	-126.560
23.4	-107.810	-135.920
23.7	-108.910	-125.290

Table B-5. (cont.) Sample FFT output file.

FREQUENCY (Hz)	STATOR PHASE A CURRENT PSD (dB)	ROTOR LOOP 1 CURRENT PSD (dB)
24.0	-107.210	-129.800
24.3	-107.170	-127.430
24.6	-108.180	-132.510
24.9	-107.020	-130.390
25.2	-106.790	-133.600
25.5	-106.530	-129.600
25.8	-107.180	-124.460
26.1	-105.870	-126.050
26.4	-105.780	-125.480
26.7	-105.290	-131.720
27.0	-106.050	-132.720
27.3	-105.470	-140.190
27.6	-104.450	-122.270
27.9	-105.650	-129.900
28.2	-104.010	-135.800
28.5	-104.180	-125.730
28.8	-104.100	-134.130
29.1	-103.810	-134.500
29.4	-103.620	-124.620
29.7	-102.930	-125.320
30.0	-103.550	-126.870
30.3	-102.190	-125.760
30.6	-102.490	-119.520
30.9	-102.120	-123.740
31.2	-102.120	-129.180
31.5	-101.730	-124.990
31.8	-101.060	-132.810
32.1	-101.390	-135.670
32.4	-100.340	-129.790
32.7	-100.610	-126.290
33.0	-100.460	-132.600
33.3	-99.795	-130.500
33.6	-99.354	-126.870
33.9	-99.584	-137.510
34.2	-98.968	-136.360
34.5	-98.627	-144.390
34.8	-98.221	-131.530
35.1	-98.288	-145.710
35.4	-97.658	-126.560
35.7	-97.524	-76.744
36.0	-96.991	-70.852
36.3	-96.985	-76.980
36.6	-96.150	-128.330
36.9	-96.247	-128.480
37.2	-95.819	-124.140

Table B-5. (cont.) Sample FFT output file.

FREQUENCY (Hz)	STATOR PHASE A CURRENT PSD (dB)	ROTOR LOOP 1 CURRENT PSD (dB)
37.5	-95.310	-129.900
37.8	-95.145	-148.670
38.1	-94.592	-128.070
38.4	-94.500	-131.560
38.7	-94.062	-129.210
39.0	-93.424	-130.500
39.3	-93.278	-123.870
39.6	-92.801	-133.130
39.9	-92.563	-127.250
40.2	-92.018	-136.670
40.5	-91.743	-110.170
40.8	-91.323	-104.290
41.1	-90.756	-110.790
41.4	-90.485	-126.750
41.7	-89.964	-133.240
42.0	-89.702	-128.000
42.3	-89.106	-129.450
42.6	-88.737	-129.520
42.9	-88.230	-133.660
43.2	-87.867	-139.180
43.5	-87.242	-128.160
43.8	-86.899	-144.760
44.1	-86.351	-127.010
44.4	-85.971	-127.780
44.7	-85.277	-129.190
45.0	-84.879	-135.890
45.3	-84.398	-140.460
45.6	-83.763	-128.750
45.9	-83.270	-128.910
46.2	-82.767	-132.750
46.5	-82.112	-132.010
46.8	-81.559	-131.580
47.1	-81.015	-131.070
47.4	-80.360	-138.210
47.7	-79.759	-125.470
48.0	-79.152	-129.590
48.3	-78.467	-137.420
48.6	-77.825	-130.090
48.9	-77.168	-135.140
49.2	-76.467	-132.980
49.5	-75.738	-131.590
49.8	-75.034	-136.100
50.1	-74.285	-148.390
50.4	-73.528	-136.750
50.7	-72.760	-131.330

Table B-5. (cont.) Sample FFT output file.

FREQUENCY (Hz)	STATOR PHASE A CURRENT PSD (dB)	ROTOR LOOP 1 CURRENT PSD (dB)
51.0	-71.924	-141.820
51.3	-71.151	-136.470
51.6	-70.303	-157.810
51.9	-69.445	-133.010
52.2	-68.565	-129.240
52.5	-67.630	-132.530
52.8	-66.607	-127.240
53.1	-65.291	-134.450
53.4	-63.277	-131.820
53.7	-59.719	-136.240
54.0	-53.913	-134.880
54.3	-45.531	-130.020
54.6	-33.052	-128.300
54.9	23.979	-131.300
55.2	30.056	-134.000
55.5	24.092	-135.190
55.8	-32.168	-123.950
56.1	-41.944	-124.990
56.4	-44.745	-130.200
56.7	-44.090	-121.450
57.0	-42.096	-123.830
57.3	-39.464	-126.810
57.6	-36.775	-123.950
57.9	-33.185	-125.870
58.2	-29.069	-132.570
58.5	-24.232	-138.080
58.8	-18.225	-134.530
59.1	-10.281	-134.520
59.4	1.728	-133.890
59.7	57.809	-129.160
60.0	63.892	-135.130
60.3	57.932	-137.680
60.6	1.878	-129.910
60.9	-10.194	-131.000
61.2	-18.165	-129.220
61.5	-24.193	-127.560
61.8	-29.059	-126.040
62.1	-33.145	-123.560
62.4	-36.669	-134.160
62.7	-39.769	-132.280
63.0	-42.536	-136.570
63.3	-45.037	-128.000
63.6	-47.316	-124.010
63.9	-49.412	-127.040
64.2	-51.350	-134.290

Table B-5. (cont.) Sample FFT output file.

FREQUENCY (Hz)	STATOR PHASE A CURRENT PSD (dB)	ROTOR LOOP 1 CURRENT PSD (dB)
64.5	-53.152	-130.420
64.8	-54.841	-130.330
65.1	-56.422	-133.160
65.4	-57.911	-145.320
65.7	-59.326	-135.670
66.0	-60.656	-125.890
66.3	-61.930	-127.300
66.6	-63.138	-139.560
66.9	-64.300	-128.220
67.2	-65.392	-132.960
67.5	-66.459	-125.600
67.8	-67.466	-127.090
68.1	-68.455	-128.730
68.4	-69.369	-143.340
68.7	-70.296	-135.280
69.0	-71.153	-128.240
69.3	-71.998	-128.200
69.6	-72.792	-133.360
69.9	-73.598	-127.150
70.2	-74.317	-121.150
70.5	-75.079	-123.520
70.8	-75.729	-128.960
71.1	-76.456	-137.850
71.4	-77.050	-149.120
71.7	-77.736	-134.230
72.0	-78.304	-132.220
72.3	-78.885	-135.290
72.6	-79.435	-139.460
72.9	-79.952	-126.330
73.2	-80.441	-127.550
73.5	-80.928	-131.900
73.8	-81.307	-129.540
74.1	-81.752	-136.740
74.4	-82.122	-129.350
74.7	-82.474	-132.450
75.0	-82.672	-131.340

Table B-5. (cont.) Sample FFT output file.

STATOR PHASE FREQUENCY SPECTRUM
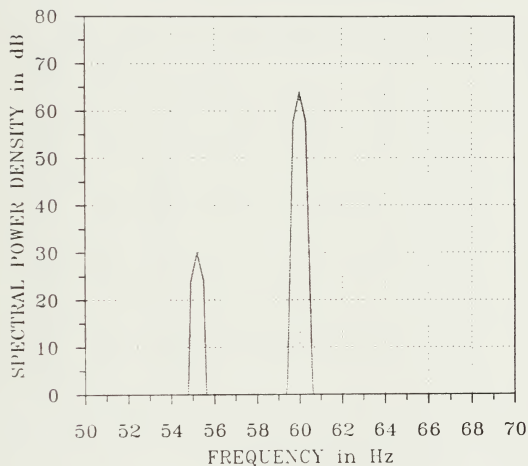SLIP=.04 1728 rpm
ONE BROKEN BAR

Figure B-3. Stator phase a frequency spectrum for sample
simulation.

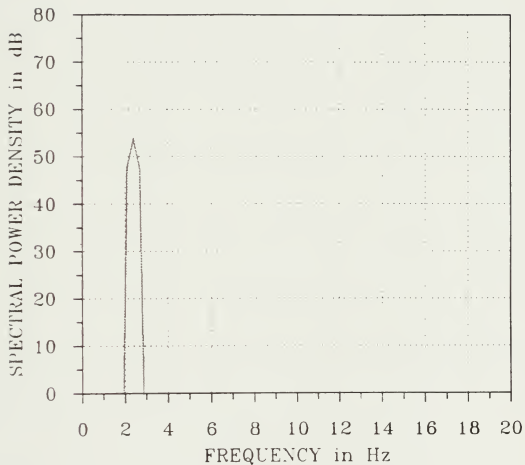ROTOR LOOP FREQUENCY SPECTRUM
SLIP=.04 1728 rpm
ONE BROKEN BAR

Figure B-4. Rotor loop 1 frequency spectrum for sample
simulation.

APPENDIX C

EXPERIMENTAL DATA

The following sections contain tables of the measured data (the fundamental and (1-2s)f components of the stator phase current) for the four rotors tested. This is the data recorded using the HP-3561A dynamic spectrum analyzer as discussed in section 4.2. Included in each table is the average value and standard deviations for each data set. In addition, the average stator phase voltage is included in the tables for the fundamental component of the stator phase current. An analysis of the data presented below is included in Chapter 4.

ROTOR #1 I(1-2s)f COMPONENT OF STATOR CURRENT AMPS rms				
TEST NO.	s=0.01	s=0.02	s=0.03	s=0.04
1	0.0014	0.0026	0.0027	0.0031
2	0.0010	0.0017	0.0019	0.0034
3	0.0009	0.0013	0.0027	0.0041
4	0.0012	0.0023	0.0032	0.0027
5	0.0008	0.0013	0.0030	0.0049
6	0.0011	0.0017	0.0034	0.0017
7	0.0006	0.0016	0.0019	0.0041
8	0.0007	0.0013	0.0016	0.0033
9	0.0012	0.0013	0.0019	0.0024
10	0.0006	0.0011	0.0028	0.0037
11	0.0010	0.0015	0.0024	0.0018
12	0.0007	0.0003	0.0019	0.0040
13	0.0013	0.0013	0.0027	0.0039
14	0.0012	0.0015	0.0024	0.0020
15	0.0014	0.0016	0.0023	0.0029
16	0.0014	0.0012	0.0023	0.0023
17	0.0015	0.0012	0.0030	0.0038
18	0.0012	0.0014	0.0027	0.0026
MEAN	0.0011	0.0015	0.0025	0.0032
STD DEV.	0.0003	0.0005	0.0005	0.0009

Table C-1. ROTOR #1 I(1-2s)f raw data.

ROTOR #1 FUNDAMENTAL COMPONENT OF STATOR CURRENT AMPS rms				
TEST NO.	s=0.01	s=0.02	s=0.03	s=0.04
1	4.68	5.97	7.50	8.96
2	4.87	6.26	7.20	9.17
3	4.74	5.86	7.38	8.94
4	4.81	6.13	7.51	8.77
5	4.75	5.91	7.30	9.02
6	4.71	5.87	7.30	9.02
MEAN	4.76	6.00	7.37	8.98
STD DEV.	0.06	0.15	0.11	0.12
AVG INPUT VOLTAGE (V rms)	123.3	123.1	122.7	122.5

Table C-2. ROTOR #1 I(60 Hz) raw data.

ROTOR #2 I(1-2s)f COMPONENT OF STATOR CURRENT AMPS rms				
TEST NO.	s=0.01	s=0.02	s=0.03	s=0.04
1	0.0020	0.0018	0.0029	0.0012
2	0.0012	0.0011	0.0013	0.0030
3	0.0009	0.0036	0.0015	0.0019
4	0.0011	0.0014	0.0020	0.0011
5	0.0009	0.0028	0.0036	0.0023
6	0.0013	0.0032	0.0009	0.0038
7	0.0015	0.0011	0.0023	0.0020
8	0.0015	0.0013	0.0020	0.0032
9	0.0010	0.0019	0.0022	0.0015
10	0.0010	0.0016	0.0029	0.0017
11	0.0016	0.0012	0.0021	0.0028
12	0.0014	0.0013	0.0019	0.0024
13	0.0007	0.0028	0.0026	0.0020
14	0.0014	0.0016	0.0028	0.0017
15	0.0012	0.0020	0.0031	0.0022
16	0.0013	0.0013	0.0025	0.0028
17	0.0015	0.0019	0.0019	0.0025
18	0.0011	0.0013	0.0020	0.0039
MEAN	0.0013	0.0018	0.0023	0.0023
STD DEV.	0.0003	0.0007	0.0007	0.0008

Table C-3. ROTOR #2 I(1-2s)f raw data.

ROTOR #2 FUNDAMENTAL COMPONENT OF STATOR CURRENT AMPS rms				
TEST NO.	s=0.01	s=0.02	s=0.03	s=0.04
1	4.53	5.83	7.40	8.81
2	4.65	5.71	6.97	8.84
3	4.53	5.85	6.79	8.71
4	4.58	6.03	7.04	8.56
5	4.62	5.94	7.57	8.70
6	4.64	5.79	7.22	9.06
MEAN	4.59	5.86	7.16	8.78
STD DEV.	0.05	0.10	0.26	0.15
AVG INPUT VOLTAGE (V rms)	122.6	122.4	122.1	121.9

Table C-4. ROTOR #2 I(60 Hz) raw data.

ROTOR #2.1 I(1-2s)f COMPONENT OF STATOR CURRENT AMPS rms			
TEST NO.	s=0.01	s=0.02	s=0.03	s=0.04
1	0.0034	0.0083	0.0101	0.0169
2	0.0036	0.0082	0.0117	0.0169
3	0.0042	0.0070	0.0121	0.0184
4	0.0056	0.0067	0.0120	0.0175
5	0.0040	0.0064	0.0129	0.0188
6	0.0077	0.0075	0.0125	0.0194
7	0.0046	0.0078	0.0131	0.0135
8	0.0048	0.0087	0.0147	0.0148
9	0.0034	0.0070	0.0131	0.0159
10	0.0034	0.0089	0.0127	0.0172
11	0.0041	0.0077	0.0144	0.0239
12	0.0030	0.0078	0.0124	0.0163
13	0.0036	0.0066	0.0129	0.0181
14	0.0033	0.0058	0.0138	0.0188
15	0.0036	0.0059	0.0124	0.0179
16	0.0030	0.0061	0.0124	0.0142
17	0.0042	0.0069	0.0136	0.0171
18	0.0041	0.0077	0.0139	0.0145
MEAN	0.0041	0.0073	0.0128	0.0172
STD DEV.	0.0011	0.0009	0.0010	0.0023

Table C-5. ROTOR #2.1 I(1-2s)f raw data.

ROTOR #2.1 FUNDAMENTAL COMPONENT OF STATOR CURRENT AMPS rms				
TEST NO.	s=0.01	s=0.02	s=0.03	s=0.04
1	4.87	6.33	7.66	8.67
2	4.76	5.93	7.25	8.42
3	4.67	5.93	7.28	8.64
4	4.60	5.71	7.21	8.87
5	4.57	5.72	7.13	8.58
6	4.48	5.98	7.03	8.46
MEAN	4.66	5.93	7.26	8.61
STD DEV.	0.13	0.21	0.20	0.15
AVG INPUT VOLTAGE (V rms)	123.1	122.9	122.5	122.2

Table C-6. ROTOR #2.1 I(60 Hz) raw data.

ROTOR #3 I(1-2s)f COMPONENT OF STATOR CURRENT AMPS rms			
TEST NO.	s=0.01	s=0.02	s=0.03	s=0.04
1	0.0008	0.0003	0.0011	0.0013
2	0.0007	0.0006	0.0014	0.0013
3	0.0011	0.0012	0.0012	0.0013
4	0.0005	0.0006	0.0012	0.0016
5	0.0009	0.0006	0.0011	0.0016
6	0.0005	0.0008	0.0001	0.0013
7	0.0013	0.0005	0.0012	0.0012
8	0.0005	0.0008	0.0014	0.0012
9	0.0006	0.0006	0.0012	0.0011
10	0.0005	0.0006	0.0011	0.0013
11	0.0006	0.0006	0.0012	0.0015
12	0.0003	0.0008	0.0014	0.0015
13	0.0009	0.0006	0.0012	0.0016
14	0.0008	0.0006	0.0008	0.0011
15	0.0009	0.0006	0.0012	0.0012
16	0.0007	0.0004	0.0008	0.0015
17	0.0003	0.0007	0.0014	0.0013
18	0.0005	0.0007	0.0011	0.0012
MEAN	0.0007	0.0006	0.0011	0.0013
STD DEV.	0.0003	0.0002	0.0003	0.0002

Table C-7. ROTOR #3 I(1-2s)f raw data.

ROTOR #3 FUNDAMENTAL COMPONENT OF STATOR CURRENT AMPS rms				
TEST NO.	s=0.01	s=0.02	s=0.03	s=0.04
1	4.60	5.80	7.40	8.61
2	4.54	5.73	6.84	8.74
3	4.63	5.94	7.16	8.65
4	4.72	5.92	7.34	8.64
5	4.72	5.80	7.19	8.57
6	4.59	5.82	7.13	8.67
MEAN	4.63	5.84	7.18	8.65
STD DEV.	0.07	0.07	0.18	0.05
AVG INPUT VOLTAGE (V rms)	122.7	122.4	122.1	121.8

Table C-8. ROTOR #3 I(60 Hz) raw data.

APPENDIX D

INDUCTION MOTOR STATOR PHASE CURRENT HARMONICS

D-1 <u>Introduction</u>

In addition to the fundamental and $(1-2s)f$ frequency components of the stator phase current, components at frequencies $(1-4s)f$, $(1+2s)f$, and $(1+4s)f$ were also detected for each rotor tested as shown in Chapter 4. In order to examine the source of these additional frequency components, an expression for the frequency components which can exist in the stator phase currents due to both time- and space-harmonic components of the airgap flux is derived.

D-2 <u>Derivation</u>

Assume initially that the airgap flux density due to currents flowing in the stator phase windings is given by the following expression

$$B_s = \sum_{m-odd} \sum_{n-odd} \{ B_{mn}^+ \sin(m\omega t + np\theta)$$
$$+ B_{mn}^- \sin(m\omega t - np\theta) \} \tag{D-1}$$

where

B_{mn}^+, B_{mn}^- = Fourier coefficents

$m = m^{th}$ stator time-harmonic

$n = n^{th}$ stator space-harmonic

Using the transformation relation given by equation 2-5, in the rotor reference frame equation D-1 becomes

$$B_s = \sum_{m-odd} \sum_{n-odd} \{ B_{mn}^+ \sin(m\omega t + np\theta' + n(1-s)\omega t)$$
$$+ B_{mn}^- \sin(m\omega t - np\theta' - n(1-s)\omega t) \} \tag{D-2}$$

218

From equation D-2, it can be seen that airgap flux will couple with the rotor loops and induce currents of frequencies

$$(m \pm n(1-s))\omega \quad \text{for m,n odd} \tag{D-3}$$

These induced rotor currents also produce an airgap flux which can be expressed in the following form

$$B_r = \sum_{q-\text{odd}} \sum_{m-\text{odd}} \sum_{n-\text{odd}} \{ B_{qmn}^{..} \sin((m+n(1-s))\omega t + qp\theta')$$

$$+ B_{qmn}^{..} \sin((m+n(1-s))\omega t - qp\theta')$$

$$+ B_{qmn}^{..} \sin((m-n(1-s))\omega t + qp\theta')$$

$$+ B_{qmn}^{..} \sin((m-n(1-s))\omega t - qp\theta')\} \tag{D-4}$$

where

$B_{qmn}^{..}, B_{qmn}^{..}, B_{qmn}^{..}, B_{qmn}^{..} =$ Fourier coefficients

$q = q^{th}$ rotor space-harmonic

In the stator reference frame this becomes

$$B_r = \sum_{q-\text{odd}} \sum_{m-\text{odd}} \sum_{n-\text{odd}} \{ B_{qmn}^{..} \sin((m+n(1-s)-q(1-s))\omega t + qp\theta)$$

$$+ B_{qmn}^{..} \sin((m+n(1-s)+q(1-s))\omega t - qp\theta)$$

$$+ B_{qmn}^{..} \sin((m-n(1-s)-q(1-s))\omega t + qp\theta)$$

$$+ B_{qmn}^{..} \sin((m-n(1-s)+q(1-s))\omega t - qp\theta)\} \tag{D-5}$$

This component of the airgap flux will couple with the stator phase windings and induce currents with the following frequencies

$$(m + n(1-s) - q(1-s))\omega \quad \text{for m,n,q odd} \qquad (D-6)$$

$$(m + n(1-s) + q(1-s))\omega \quad \text{for m,n,q odd} \qquad (D-7)$$

$$(m - n(1-s) - q(1-s))\omega \quad \text{for m,n,q odd} \qquad (D-8)$$

$$(m - n(1-s) + q(1-s))\omega \quad \text{for m,n,q odd} \qquad (D-9)$$

Thus for each combination of m, n, and q there can be as many as four distinct frequencies of currents induced in a stator phase winding. Table D-1 shows the possible stator phase current harmonics for m,n,q=1,3,5. This table shows that the $(1-4s)f$ and the $(1+2s)f$ components are produced by the third time-harmonic and that the $(1+4s)f$ component is produced by the fifth time-harmonic component of the stator phase current.

For the experimental motor with ROTOR #3 installed and operating at a slip of 0.0011, the stator phase current frequency spectrum measured using the HP-3561A signal analyzer is shown in Figure D-1. This spectrum shows that the magnitudes of the third and fifth time-harmonics are approximately the same and that they are larger than all other harmonic components except the fundamental component of the stator phase current. This would indicate that for the motors tested, the $(1-4s)f$, $(1+2s)f$, and $(1+4s)f$ components can be attributed to the third and fifth time-harmonics of the stator phase current.

time/space component			STATOR PHASE CURRENT HARMONICS normalized to the fundamental frequency			
m	n	q	(eqn D-6)	(eqn D-7)	(eqn D-8)	(eqn D-9)
1	1	1	1	3-2s	-1+2s	1
1	1	3	-1+2s	5-4s	-3+4s	3-2s
1	1	5	-3+4s	7-6s	-5+6s	5-4s
1	3	1	3-2s	5-4s	-3+4s	-1+2s
1	3	3	1	7-6s	-5+6s	1
1	3	5	-1+2s	9-8s	-7+8s	3-2s
1	5	1	5-4s	7-6s	-5+6s	-3+4s
1	5	3	3-2s	9-8s	-7+8s	-1+2s
1	5	5	1	11-10s	-9+10s	1
3	1	1	3	5-2s	1+2s	3
3	1	3	1+2s	7-4s	-1+4s	5-2s
3	1	5	-1+4s	9-6s	-3+6s	7-4s
3	3	1	5-2s	7-4s	-1+4s	1+2s
3	3	3	3	9-6s	-3+6s	3
3	3	5	1+2s	11-8s	-5+8s	5-2s
3	5	1	7-4s	9-6s	-3+6s	-1+4s
3	5	3	5-2s	11-8s	-5+8s	1+2s
3	5	5	3	13-10s	-7+10s	3
5	1	1	5	7-2s	3+2s	5
5	1	3	3+2s	9-4s	1+4s	7-2s
5	1	5	1+4s	11-6s	-1+6s	9-4s
5	3	1	7-2s	9-4s	1+4s	3+2s
5	3	3	5	11-6s	-1+6s	5
5	3	5	3+2s	13-8s	-3+8s	7-2s
5	5	1	9-4s	11-6s	-1+6s	1+4s
5	5	3	7-2s	13-8s	-3+8s	3+2s
5	5	5	5	15-10s	-5+10s	5

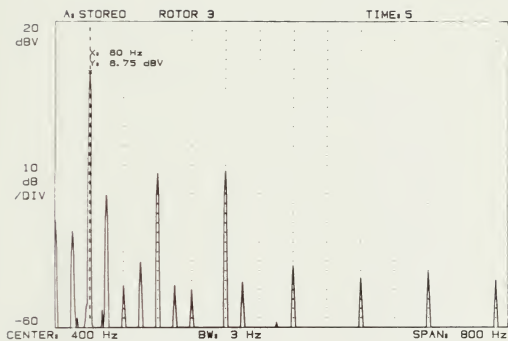Table D-1. Predicted stator current harmonics.

221

Figure D-1. Stator current time-harmonics.